Investigation of 160 Gbit/s optical communication systems

Xu, Zhenbo

Publication date:
2006

Document Version
Publisher's PDF, also known as Version of record

Investigation of 160 Gbit/s optical communication systems

Zhenbo Xu
徐 振 波

January 2006

Research Center COM
Technical University of Denmark
Building 343V
Kgs.Lyngby, DK-2800
Denmark

Resumé (in Danish)

Afhandlingen drejer sig om transmission i optiske fibre ved den meget høje datahastighed 160 Gbit/s på en enkelt optisk bølgelængde. Formålet med arbejdet er at forudsige den længst mulige transmissionsafstand ved brug af Raman forstærkning og at undersøge nye modulationsformater, som er særligt velegnede. Et stort antal computer simulationer og nogle eksperimenter er blevet udført.

De grundlæggende fysiske processer bag Raman forstærkning i optiske fibre resumeres, og dernæst gives en oversigt over den numeriske løsning af de partielle differentialligninger, som beskriver Raman forstærkning. Skadelige lineære og ulineære effekter og også støj fra Raman forstærkningen beskrives. Særlig vægt er lagt på kodning og dekodning i forbindelse med modulationsformaterne DPSK (differential-phase-shift-keying) og DQPSK (differential-quadrature-phase-shift-keying).

To forskellige former for Raman forstærkning analyseres numerisk ud fra et transmissionssynspunkt. Den første form er diskret (lokaliseret) forstærkning med fire forskellige pumpemetoder. For den bedste metode forudsiges en transmissionsafstand på 1800 km. Desuden diskuteres signal pulsbredde samt dispersion og effektivt kerneareal af fibrene i forhold til systempræstationer.

Den anden form er fordelt Raman forstærkning; her kan forudsiges en forbedret afstand på op til 2500 km. Den optimale fordeling af signaleffekt langs fiberen samt input effekt bestemmes for tre forskellige pumpemetoder. I simuleringerne anvendes fibre med stort kerneareal i næsten alle undersøgte systemer for på denne måde at mindske den forstyrrende indflydelse fra ulinearitet i fiberen.

Baseret på SSMF & DCF strækninger analyseres tolerancer overfor dispersion og ulinearitet for modulationsformaterne RZ, CSRZ, RZ-DPSK, CSRZ-DPSK og DQPSK. Dispersionskontrol diskuteres også for disse formater.

Et eksperiment med 160 Gbit/s på SSMF beskrives også i afhandlingen. Optimal Raman pumpemetode til opretholdelse af OSNR hen langs fiberforbindelsen bestemmes, og 174 km fejlfri transmissionsafstand opnås. I et andet 160 Gbit/s enkeltkanal eksperiment undersøges to dispersionskonfigurationer, nemlig symmetrisk og post-dispersionskompensation, idet der samtidigt drages fordel af Raman forstærkning. Post-dispersionskompensation giver den største tolerance overfor variationer i signaleffekt på indgangen af fiberen.

WDM (wavelength division multiplex) systemer baseret på fordelt Raman forstærkning og forskelllige modulationsformater er også blevet undersøgt. Systemrækkevidden for forskellige kanalafstande diskuteres. CSRZ-DPSK (carrier suppressed return to zero-DPSK) overgår RZ-DPSK med en transmissionsafstand på 1800 km med høj spektral tæthed og næsten fordoblet dispersionstolerance.

Dispersionskontrol diskuteres, hvad angår optimering af pre-, post og indlinie dispersionskompensering hen langs fiberforbindelsen. En sammenligning mellem driftsbetingelserne for enkeltkanal og 5-kanal WDM systemer gives for forskellige modulationsformater.

Abstract

In this thesis 160 Gbit/s per-channel transmission systems are investigated in the form of both single channel systems and WDM systems. The aim of the research is to identify the longest possible transmission distance, employing Raman amplification and to study advanced modulation formats. Numerous computer simulations and some experiments have been performed.

The principle mechanism of Raman amplification inside fiber is introduced, followed by the numerical solution of the detailed coupled equations governing Raman amplification. Detrimental linear and nonlinear effects and also Raman noise terms are described. Several modulation format generation methods are introduced. Special emphasis is given to analyses of encoding and decoding methods of differential-phase-shift-keying (DPSK) and differential quadrature phase-shift-keying (DQPSK).

Two kinds of Raman amplification are numerically analysed from a transmission system standpoint. The first section focuses on the discrete Raman amplification with estimation of system performance using four kinds of Raman pumping schemes. An optimal transmission distance of 1800 km is predicted. Moreover, signal pulse width, dispersion and effective core area of fibers are discussed with respect to system performance.

In the following section three schemes with distributed Raman amplification are discussed. The system performance is improved reaching a transmission distance of 2500 km. The optimal signal power evolution and span input power for the three pumping schemes are determined. In the simulation research large core area fibers are adopted in almost all systems to better mitigate the nonlinearities compared with SSMFs.

Based on SSMF & DCF spans, the dispersion and nonlinear system tolerances of the RZ, CSRZ, RZ-DPSK, CSRZ-DPSK and DQPSK

modulation formats are analysed. Dispersion management is also discussed for these formats.

A SSMF based 160 Gbit/s single channel transmission experiment is demonstrated. Optimum Raman pumping operation conditions are identified to maintain the OSNR in the transmission link, and 174 km error free transmission is obtained. In another 160 Gbit/s single channel experiment, two dispersion maps are investigated in transmission spans, namely symmetrical and post dispersion compensation maps taking advantage of the benefit from Raman amplification. The post compensation map offers best power tolerance.

WDM systems based on distributed Raman amplification and various modulation formats are investigated. The system reach for different channel spacing is discussed. CSRZ-DPSK outperforms RZ-DPSK with 1800 km transmission distance at high spectral efficiency and nearly doubled dispersion tolerance.

Dispersion management is discussed with regard to optimizing pre, post and in-line dispersion compensation along the fiber link. A comparison of optimal operating conditions for single channel systems and 5-channel WDM systems are given for various modulation formats.

Publication list

1. **Zhenbo Xu,** P. Jeppesen, “Dispersion Tolerance in 160 Gbit/s Modulation Systems”, submitted to CLEO 2006.

2. **Zhenbo Xu,** K. Rottwitt and P. Jeppesen, "Analyses of spectral efficiency and nonlinear tolerance of DPSK formats in 160 Gbit/s Raman amplified systems," IEEE Photonics Technology Letters, Vol 17, No.7, July, 2005, pp.1552-1554.

3. **Zhenbo Xu,** K. Rottwitt, C. Peucheret, P. Jeppesen, “Optimization of Pumping Schemes for 160-Gb/s Single-Channel Raman Amplified Systems”, IEEE Photonics Technology Letters, Vol. 16, Jan. 2004, pp. 329-331.

4. **Zhenbo Xu,** K. Rottwitt, P. Jeppesen, “Spectral Efficiency and Nonlinear Tolerance of DPSK Formats in 160 Gb/s Raman Amplified Systems”, CLEO 2005, paper JThE79, Baltimore, Maryland, 2005.

5. **Zhenbo Xu,** K. Rottwitt, P. Jeppesen, “Evaluation of Modulation Formats for 160 Gb/s Transmission Systems using Raman Amplification”, LEOS 2004, paper WR5, Puerto Rico, November, 2004.

6. **Zhenbo Xu,** J. Seoane, A. I. Siahlo, L. K. Oxenløwe, A. T. Clausen P. Jeppesen, “Experimental characterization of dispersion maps with Raman gain in 160 Gb/s transmission systems”, CLEO/IQEC 2004, paper CWA 20, San Francisco, CA, May, 2004.

7. **Zhenbo Xu,** C. Peucheret, A. I. Siahlo, K. Rottwitt, P. Jeppesen, “Dispersion and nonlinearity tolerance of modulation

formats for 160 Gb/s systems", CLEO/IQEC 2004, paper CWA 21, San Francisco, CA, May, 2004.

8. **Zhenbo Xu,** L. K. Oxenløwe, A. I. Siahlo, K. S. Berg, A. T. Clausen, Q. N. T. Le, C. Peucheret, K. Rottwitt and P. Jeppesen, "Experimental characterisation of distributed Raman amplification in a standard single mode fibre based 160 Gbit/s transmission system", ECOC'03, paper Tu4.7.2, vol. 2, pp. 344-345, Rimini, Italy, September, 2003.

9. **Zhenbo Xu,** K. Rottwitt, P. Jeppesen, "An investigation of different Raman amplification configurations in 160 Gbit/s OTDM transmission lines", CLEO/Europe 2003, Munich, Germany, June 2003.

10. **Zhenbo Xu,** C. Peucheret, Q. Le and P. Jeppesen, "Short period dispersion management of 160 Gb/s single channel fiber system", in Proc. European Conference on Optical Communication, ECOC'2002, paper P3.15, vol. 3, Copenhagen, Denmark, September 2002.

11. A. I. Siahlo, A. T. Clausen, L. K. Oxenløwe, J. Seoane, K. S. Berg, **Z. Xu,** J. Zeng and P. Jeppesen, "Phase nodulation for postcompensation of dispersion in 160 Gb/s systems", IEEE Photonics Technology Letters, vol. 17, Feb. 2005, pp. 498-500.

12. J. Seoane, A. I. Siahlo, A. T. Clausen, L. K. Oxenløwe, **Z. Xu** and P. Jeppesen"All optical 160 to 10 Gbit/s demultiplexing using co-propagating optical clock", CLEO 2004, paper CThQ4.

13. A. I. Siahlo, A. T. Clausen, L. K. Oxenløwe, J. Seoane, **Z. Xu** and P. Jeppesen, "Tunable dispersion compensation using phase modulation in receiver part", OFC 2004, Paper ThU4.

Acknowledgements

I would like to start by extending my great thanks to my supervisor Palle Jeppesen for all the support, advice and motivation during my study time here in COM. I would like to express my deep gratitude for his close guidance on my research by providing inspiration and comprehensible insight throughout the entire project.

I would also like to express my appreciation of my co-supervisors Christophe Peucheret and Karsten Rottwitt for great help on performing simulations and obtaining precise theoretical understanding.

I also thank the colleges who stood by me and supported me. In particular, I am grateful to Andrei Siahlo who gave me advice on simulations and experiments; many thanks should go to Leif Oxenløwe for instructions on experiments and I especially thank Jorge Seoane for warm-hearted help and altruistic support.

In addition, I would also like to thank Henning Christiansen for solving occasional network problems and Janne Witt Bengtsen for arranging my travels during all three years. Many thanks go to Lone Bjørnstjerne for always providing in time help.

Last but not least, I thank my husband for his great effort to support me and take care of the family during my Ph.D. study.

Zhenbo Xu

January 2006

List of Acronyms

ABA	symmetrical dispersion map
ASE	amplified spontaneous emission
BER	bit error rate
CS-RZ	carrier suppressed return-to-zero
CW	continuous wave
DCF	dispersion compensation fiber
DEMUX	demultiplexer / demultiplexing
DM	dispersion management
DPSK	differential phase shift keying
DQPSK	differential quadrature phase shift keying
EDFA	erbium doped fiber amplifier
ENF	effective noise figure
FEC	forward error correction
FWHM	full width half maximum
FWM	four-wave mixing
GVD	group-velocity dispersion
HNLF	highly nonlinear fiber
IDF	inversed dispersion fiber
IFWM	inter-four-wave-mixing

ISI	inter-symbol interference
IXPM	inter-cross phase modulation
LPF	low bandpass filter
MML	mode locked laser
MPI	multi-path interference
MUX	multiplexer / multiplexing
MZI	Mach-Zehnder interferometer
MZM	Mach-Zehnder modulator
NF	noise figure
NOLM	nonlinear optical loop mirror
NRZ	non-return-to-zero
OBPF	optical bandpass filter
OOK	on-off-keying
OSA	optical spectrum analyser
OSNR	optical signal to noise ratio
OTDM	optical time division multiplexing
PC	polarisation control
PDF	power density function
PMD	polarisation mode dispersion
PRBS	pseudo random bit sequence
Rx	receiver
RZ	return-to-zero
SLA	super large effective core area fiber
SSMF	standard single mode fiber
SPM	self-phase modulation
SRS	stimulated Raman scattering

Tx	transmitter
WDM	wavelength division multiplexing
XPM	cross-phase modulation

Table of Contents

Chapter 1

Introduction

Towards 160 Gbit/s transmission systems

The explosive increase in number of Internet users boosts the demand for high-speed data capacity in LANs (local-area-networks), WANs (wide-area-networks) and especially backbone networks. In order to provide enough capacity for the huge data traffic, data rates must be upgraded from Mbit/s in access networks to Gbit/s and even Tbit/s in the backbone network. In the latter type of network, the combination of WDM technique and high data rate on each wavelength makes it feasible to accommodate the huge network traffic requirements; and new OTDM technology still at the research stage could be taken into use in the future to overcome the bottleneck in electronic multiplexers and demultiplexers.

In recent years, field trials have been performed in order to demonstrate the feasibility of upgrading from 10 Gbit/s to 40 Gbit/s systems. Impressive laboratory record-breaking results on 40 Gbit/s WDM systems have also been demonstrated with huge bandwidth accommodating hundreds of channels [1,2]. As the demand for capacity in the optical backbone network grows, increasing per channel capacity becomes of strong interest. The main motivation is to reduce the number of required wavelength channels, thus reducing the cost of managing too many channels, and to overcome the nonlinear crosstalk between many channels. As the next foreseeable scenario, 160 Gbit/s per channel systems have become of great research interest and several impressive transmission experiments have been demonstrated [3,4].

However, the signal at 160 Gbit/s will induce more intra-channel nonlinear impairments because of a quicker pulse broadening and will impose very challenging speed requirements on electronic components, consequently inducing new technical problems to be solved. Hence finding feasible approaches to implement optimal cost-saving 160 Gbit/s per channel systems is very meaningful.

Recently, new components have emerged in experiments such as tunable dispersion compensators [5], polarisation multiplexers [2] and forward error correction coding (FEC) equipment [6] to give a bigger tolerance in received bit-error rate. Raman amplification [1], DPSK (differential-phase-shift-keying) [6] and use of new fiber types such as super large area fiber (SLA) [4] in the span are also promising to improve system performance. In addition, optimal design of dispersion management becomes another critical issue to mitigate the nonlinearities along the link [7].

Motivation and purpose of this project

The research on 160 Gbit/s per channel systems is at the onset of a new era. Solid and detailed numerical simulations of different system configurations are very necessary and will pave the way to field trials and applications. Furthermore, through extensive simulations, the optimal conditions can be predicted for various system configurations and the best system configuration can be identified.

Primarily based on computer simulations, the purpose of this project is to explore 160 Gbit/s per channel transmission both in single channel and WDM systems. The focus is on potential benefits from Raman amplification and advanced modulation formats; the goals are to predict longest system reach under various conditions, to determine system margins for dispersion, nonlinearities, signal power and pump power and finally to investigate optimal dispersion management.

Structure of the thesis

In this thesis, three approaches towards ultra high-speed optical transmission systems are studied and the physical principles behind are discussed. The first approach is to employ Raman amplification to balance the intrinsic fiber loss and maintain the OSNR (optical signal-to-noise ratio) along the fiber link, thus significantly increasing the system reach. The second approach is to employ new modulation

formats such as carrier suppressed (CS) formats or differential-phase-shift-keying (DPSK) format and differential-quadrature-phase-shift-keying (DQPSK) format. The advantages of narrower spectrum width, smooth spectrum without sharp peaks and higher receiver sensitivity related to PSK formats can improve the transmission systems and reduce the nonlinear distortion. The third approach is to employ optimal dispersion maps as in high-speed systems the short pulse width leads to large dispersive pulse broadening and results in increased intra-channel nonlinear distortion such as intra-cross-phase modulation (IXPM) and intra-four-wave-mixing (IFWM). During our simulation research, large core area fiber instead of standard single mode fiber (SSMF) is adopted in most of the systems in order to mitigate nonlinearities.

The thesis is organised as follows. Chapter 2 provides an overview of the principle mechanism of stimulated Raman scattering. The coupled equations for Raman amplification are discussed including linear and nonlinear terms, followed by the introduction of detrimental effects. The numerical solution of the detailed coupled equations is presented separately. We also discuss the noise characteristics and derive the effective noise figure mathematically. At last, applications of the Raman amplifier are described.

Chapter 3 deals with the generation principles of the modulation formats RZ, CSRZ, DPSK and DQPSK. The encoding and decoding methods of DPSK and DQPSK are illustrated in detail, followed by analyses of modulation and demodulation schemes. In addition, a mathematical derivation is presented to explain the different spectra for different modulation formats. The BER estimation model is also discussed to give a clarification of the special features of the noise density distributions for the DPSK format at the receiver.

In Chapter 4, two kinds of Raman amplification are analysed by simulation from a systems standpoint. The first section focuses on discrete Raman amplification for four kinds of pumping schemes. The dispersion and effective core area of the fibers are discussed in terms of system performance. The following section compares three different distributed Raman amplification schemes. We find the system distance reach is even better compared to discrete pumping schemes. In the third section, we investigate the dispersion and nonlinear tolerances of the RZ, CSRZ, RZ-DPSK, CSRZ-DPSK and DQPSK formats using

SSMF & DCF spans. Dispersion management is also studied with respect to different formats.

Chapter 5 presents two experiments dealing with single channel 160 Gbit/s transmission systems. The first experiment is concerned with distributed Raman amplification in SSMF. 174 km error-free transmission is obtained, and optimum Raman pumping conditions are investigated to maintain the required OSNR in the transmission link, thus potentially increasing the system reach. In the second experiment, we characterize dispersion maps in the 160 Gbit/s transmission system. Two dispersion compensation maps, namely symmetrical and post dispersion compensation are discussed based on Raman amplification in the SSMF transmission span. We find the post compensation map offers better power tolerance.

Chapter 6 presents the simulation results for WDM systems based on distributed Raman amplification and various modulation formats. In the first section, the system reach for different channel spacing is discussed. RZ-DPSK and CSRZ-DPSK are compared in terms of dispersion tolerance and spectral efficiency. The following section deals with the dispersion management issue by investigating pre, post and in-line dispersion compensation. The optimal conditions with regard to modulation format are given. Comparisons of single channel systems and 5-channel WDM systems on optimal dispersion arrangement are given.

Finally, Chapter 7 summarises and discusses the main results of the thesis.

Chapter 2

Raman amplification

Raman amplification has been extensively studied for use in long-haul WDM systems because of the capability of amplification at any wavelength, broad-band flatten gain, higher OSNR (Optical signal to noise ratio) maintained compared to using EDFA, distributed Raman amplification and lower span launched signal power which is helpful to mitigate nonlinearities. Raman amplification compensates the intrinsic fiber loss, thus significantly increasing the system reach.

In this Chapter, the physical mechanism of Raman amplification is described. The coupled equations for Raman amplification are discussed including linear and nonlinear effects. The noise characteristics are discussed and the concept of effective noise figure is introduced. The numerical solution of the coupled equations is presented separately. Finally applications of the Raman amplifier are described.

2.1 Principle of Raman amplification

2.1.1 Physical background

The Raman process is strongly related to vibrational modes of the molecules of the material. It can be described quantum mechanically as a molecular transition between two vibrational energy states accompanied by absorbing energy and scattering photons [8,9]. During this process, the molecule scatters a photon of high frequency into a new photon of low frequency. However, unlike the Er-doped fiber amplifiers with specific excited energy levels, the Raman scattering process can amplify photons in a broad range of wavelengths characteristic to the specific fiber. The most likely scattered photons fall onto a specific frequency and a Raman gain peak is built up around this frequency. The Stokes frequency can vary for different materials [9]. The scattered photons are classified into two main categories as shown in Figure 2.1. One is spontaneous Raman scattering, which appears within the whole Raman gain spectrum as intrinsic Raman noise. In this case, the phase, propagation direction and polarisation of the emitted photons are completely random.

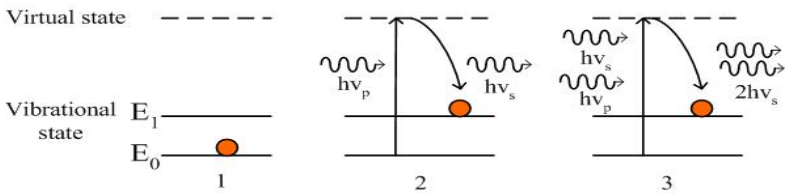

Figure 2.1. Photon emission by molecular transition between vibrational states. 1) Initial state, 2) spontaneous Raman scattering, 3) stimulated Raman scattering.

The process in which the molecule transition at the virtual state is stimulated by a Stokes photon to emit another Stokes photon is called stimulated Raman scattering as shown in Figure 2.1. In this case, an incident photon of frequency υ_s stimulates the molecule being in the virtual transition state accompanied by an incident pump photon of frequency υ_p, generates a new photon with identical frequency, phase,

propagation direction and polarisation as the incident photon υ_s. This stimulated Raman scattering is responsible for the amplification of a communication signal.

Amorphous silica has a wide Raman gain spectrum bandwidth up to 6 THz as shown in Figure 2.2 [10]. The maximum Raman gain occurs at 13 THz downshifted from the pump frequency and it is highly polarisation dependent. Figure 2.2 illustrates the measured gain profile in standard fibers, pure silica fibers, dispersion compensating fibers (DCF) and true wave (TW) fibers for unpolarized pump. The gain coefficient g_R depends on the fiber effective core area A_{eff} and parameter γ as $g_R \propto \gamma / A_{eff}$ [9]. Here γ is a coefficient mainly determined by the silica material and the germanium dopant.

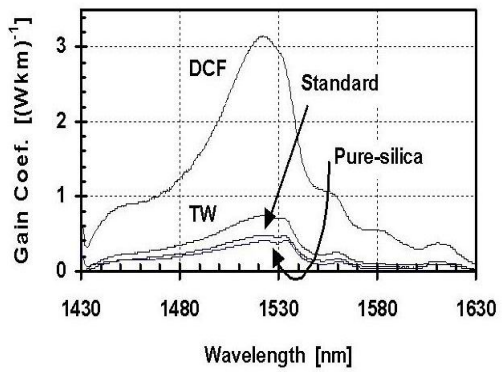

Figure 2.2 Gain coefficients for standard fibers, pure silica fibers, DCF and TW fibers [10].

2.1.2 Basic coupled equations

In principle, when the signal wave and the pump wave propagate along the fiber, the power evolution of each wave is mainly determined by three factors, namely the fiber loss, stimulated Raman scattering and pump depletion as in equations 2.1 and 2.2 [8]. The symbols P_S and P_P denote signal and pump power, respectively. α_S and α_P denote loss of signal and pump. In the pump power equation, the second term is responsible for energy transfer from the high frequency pump power with angular frequency ω_P to the low frequency signal power with

angular frequency ω_S , i.e. pump depletion. Here the equations represent forward signal and pump.

$$\frac{dP_S}{dz} = -\alpha_S P_S + g_R P_P P_S \tag{2.1}$$

$$\frac{dP_P}{dz} = -\alpha_P P_P - (\omega_P / \omega_S) g_R P_S P_P \tag{2.2}$$

Raman on-off gain, defined as the gain obtained by the signal when the Raman pump is on compared to when it is off, is the key quantity that characterizes Raman amplification. If we neglect the pump depletion term above, the Raman gain is determined by the launched pump power P_p^{Launch}, the gain coefficient g_R and the effective fiber length L_{eff} . The Raman on-off gain G_{on-off} is given by

$$G_{on-off} = \exp(g_R L_{eff} P_p^{Launch}) \tag{2.3}$$

Where L_{eff} is

$$L_{eff} = \frac{1 - \exp(-\alpha_p L)}{\alpha_p} \tag{2.4}$$

2.1.3 Raman Noise and nonlinear impairments

The coupled equations presented above don't take any Raman generated noise into account. Furthermore, in high-speed systems, for instance 160 Gbit/s systems, the wide signal spectrum suffers nonlinear impairments not only from SPM, but also intra cross-phase modulation (IXPM) and intra four-wave-mixing (IFWM). Furthermore, in WDM systems inter-XPM and inter-FWM become significant and can't be neglected.

Noise from Raman amplification

The noise comes from spontaneous Raman scattering, Rayleigh backscattering and multi-path interference (MPI). It should be kept in mind that the Rayleigh scattering as an elastic process causes a fundamental fiber loss mechanism, the Rayleigh scattered photons will also be taken as intrinsic Raman noise. Figure 2.3 illustrates the three

kinds of generated noise photons except incident photon (black) and stimulated new photons (green). Photons with yellow colour represent spontaneous Raman scattering that spans over the whole Raman gain spectra. Red colour photons represent Rayleigh scattering. Blue photons represent MPI, where the noise is backscattered multiple times and amplified in the same propagation direction as the signal.

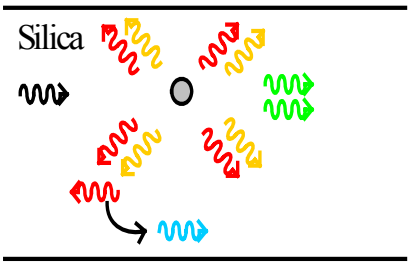

Figure 2.3 Noise terms from Raman pumping in silica fiber.

Raman noise figure

Noise figure (NF) as a basic parameter of an amplifier, is defined as $NF = \frac{SNR_{in}}{SNR_{out}}$. SNR_{in} denotes input signal-to-noise ratio (SNR) before the amplifier. SNR_{out} denotes output SNR after the amplifier. Since with Raman amplification, the signal power evolves along the fiber, as if there is an extra EDFA working along the fiber, the NF of a Raman amplifier is not the same as for an EDFA as described in Appendix A. Therefore the concept of effective noise figure (ENF) is introduced as shown in Figure 2.4.

Figure 2.4 a) shows constellations of two cases without and with Raman amplification. Figure 2.4 b) illustrates the signal power evolution along the fiber without Raman pump and with backward Raman pumping. From Figure 2.4 b) we define the ENF in dB as [11].

$$ENF_{dB} = NF_{netdB} - Loss_{dB} \tag{2.5}$$

Here the fiber loss can be expressed as

$$Loss_{dB} = G_{on-offdB} - G_{netdB} \tag{2.6}$$

So $$ENF_{dB} = NF_{netdB} - G_{on-offdB} + G_{netdB} \tag{2.7}$$

In the linear scale the parameters are described as follows

$$NF_{net} = \frac{1}{G_{net}}\left(\frac{P_{ASE}}{h\nu B} + 1\right) \tag{2.8}$$

Here P_{ASE} is the noise power from amplified spontaneous emission. B is the bandwidth and $h\upsilon$ is the photon energy. So the linear conversion of above is

$$10\log_{10} ENF = 10\log_{10} \frac{NF_{net} G_{net}}{G_{on-off}} \tag{2.9}$$

Therefore, the linear ENF is as

$$ENF = \frac{NF_{net} G_{net}}{G_{on-off}} = \frac{1}{G_{on-off}}\left(\frac{P_{ASE}}{h\nu B} + 1\right) \tag{2.10}$$

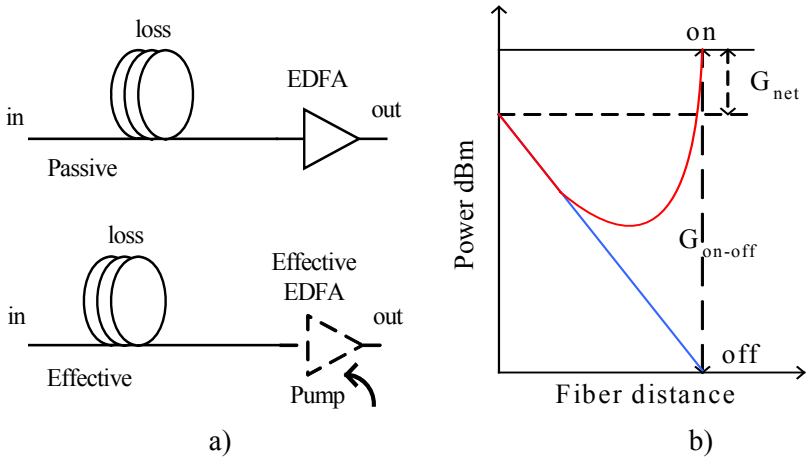

Figure 2.4 Comparison of span with and without Raman amplification. a) Schematics of effective noise figure, b) signal power distribution along fiber.

From the derivation above, it is clear that the NF of the span can be designed by the Raman on-off gain. What's more, when the ENF is designed to be less than 1, then the ENF in dB scale is negative, which can not be realized by EDFA and that is believed to be one of the merits from using Raman amplification.

Inter Raman effects

The inter channel Raman amplification also deteriorates to the signal quality as shown in Figure 2.5. Figure 2.5 a) is the initial power spectrum of multiple signal channels. After 10 km transmission, the power of the channels is shown in Figure 2.5 b). We can see power depletion in high frequency channels and power being transferred to low frequency channels.

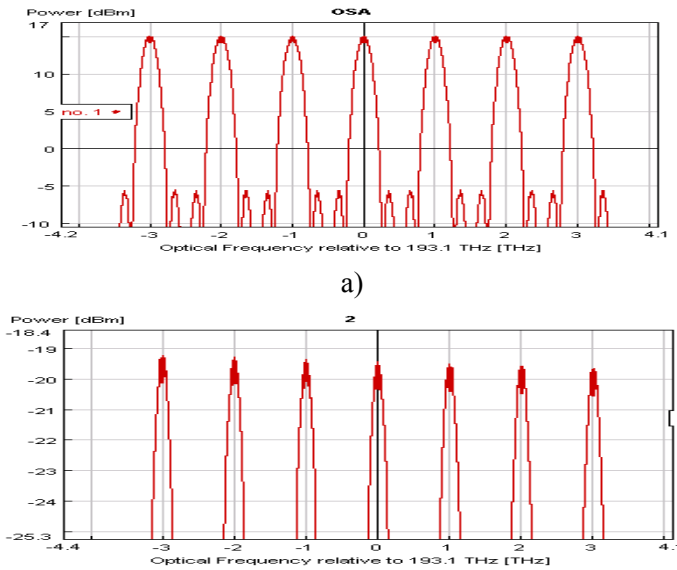

Figure 2.5 Inter pump depletion and inter signal interaction. a) Initial signal channels, b) signals after 10 km fiber span.

Nonlinear impairments

The signal power can induce temporal variations of the fiber refractive index. When the signal passes through the fiber, the signal phase can be modulated due to the nonlinear refractive index, resulting in different time-dependent phase change [8]. Self-phase modulation (SPM) and cross-phase modulation (XPM) originate from the principle of intensity dependence of the refractive index.

SPM is a self-induced phase shift. The phase shift ϕ_{NL} is accumulated with signal propagation along the fiber and is proportional to launched signal power $P(z)$ and fiber length L

according to $\phi_{NL} = \int_0^l \gamma P(z)dz$. Multiple peaks in the signal spectrum can be generated. The time dependent phase shift ϕ_{NL} is converted to frequency chirp and affects the pulse shape when it combines with linear chirp induced by fiber group velocity dispersion (GVD). The pulse can't be recovered as in a linear system.

XPM arises when two pulses are moving across each other. XPM phase shift depends not only on the power P_j in the channel considered but also on power in other co-propagating signals P_m at different frequencies [8]. As the signal propagates along the fiber, the variation of signal intensity changes the refractive index of the fiber, thus producing an intensity-dependent phase shift $\phi_j^{NL} = \gamma L_{eff}(P_j + 2\sum_{m \neq j} P_m)$. The time dependent phase shift of XPM can be converted into frequency chirp. The XPM will affect the system when it works together with dispersion in the transmission fiber, thus producing signal distortion and consequently a reduced OSNR. So in WDM systems, decreasing the fiber dispersion is helpful to mitigate XPM impairment.

The four-wave-mixing (FWM) process can be viewed as photons from one or more wavelengths being annihilated while new photons are created at different frequencies. FWM is a nonlinear impairment occurring among several optical waves when phase matching is satisfied as $\kappa = \Delta k_M + \Delta k_W + \Delta k_{NL} = 0$. Here Δk_M, Δk_W, Δk_{NL} represent the phase mismatch occurring from material dispersion, waveguide dispersion and nonlinear effects, respectively [8]. At least one term must be negative. The new FWM frequency component, dependent on whether the channel spacing is equidistant or not, coincides with the signal channels or falls into the margin between channels; in either case it emerges as noise and is deleterious to WDM systems. One way to eliminate the phase match is to use dispersion map with large local dispersion and nearly zero average dispersion along the link.

2.2 Two-stage numerical module structure

In our numerical simulation, the approach is based on both signal frequency decomposition and split-step method along the fiber [12].

2.2.1 Power analysis

As the first stage, a bidirectional power analysis using an iterative algorithm is performed by frequency decomposition not only of signal, but also of pump and generated noise. The whole simulation bandwidth is divided into discrete small frequency slots as shown in Figure 2.6 b). A single value represents the power at that frequency slot. In the power analysis, attenuation, stimulated Raman scattering, Raman spontaneous scattering, pump depletion and Rayleigh backscattering are considered. Furthermore, noise stemming from inter-Raman amplification related energy transferred to lower frequency signals and energy transferred to lower frequency pumps are also considered.

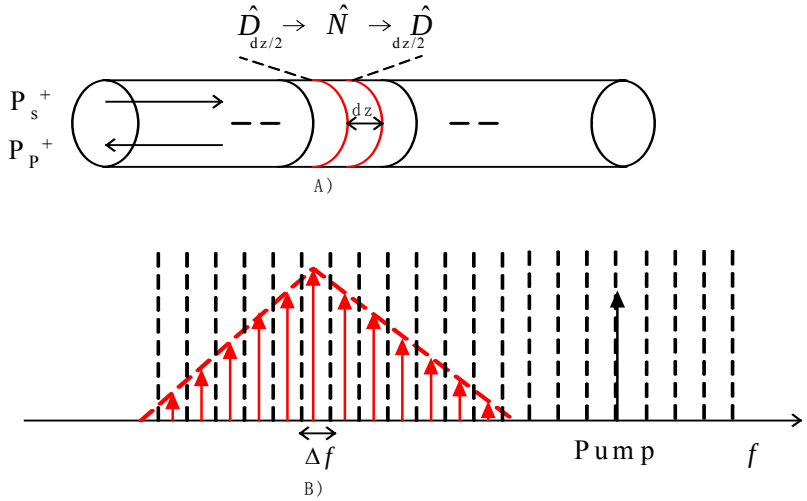

Figure 2.6 a) Split-step method along fiber and b) signal spectrum discretization for power analysis.

Below are given the coupled power equations 2.11) and 2.12) representing forward propagating signal power P_S and noise power

P_n. The pump power equation is analysed in the same way as the signal power component at a certain frequency slot. Here the '+' and '-' represents power in the forward direction and backward direction, respectively. η is the Rayleigh backscattering coefficient. The $g(f_k, f_j)$ and $N(f_k, f_j)$ denote the gain and spontaneous emission factor with regard to two frequency components f_k, f_j, respectively.

$$\frac{dP_S^+(f_i)}{dz} = \underbrace{-\alpha(f_i)P_S^+(f_i)}_{Attenuation} + \underbrace{\eta(f_i)P_S^-(f_i)}_{Rayleigh backscattering} + \underbrace{\sum_{k\neq i} g(f_k, f_i)\left[P_S^+(f_k) + P_n^+(f_k) + P_S^-(f_k) + P_n^-(f_k)\right]P_S^+(f_i)}_{Stimulated\ Raman scattering - bidirection} \tag{2.11}$$

$$\frac{dP_n^+(f_i)}{dz} = \underbrace{-\alpha(f_i)P_n^+(f_i)}_{Attenuation} + \underbrace{\eta(f_i)P_n^-(f_i)}_{Rayleigh backscattering} + \underbrace{\sum_{k\neq i} g(f_k, f_i)\left[P_S^+(f_k) + P_n^+(f_k) + P_S^-(f_k) + P_n^-(f_k)\right]P_n^+(f_i)}_{Stimulated\ Raman scattering - bidirection} + \underbrace{\sum_{k\neq i} g(f_k, f_i)N(f_k, f_i)\left[P_S^+(f_k) + P_n^+(f_k) + P_S^-(f_k) + P_n^-(f_k)\right]}_{Spontaneous\ Raman scattering - bidirection} \tag{2.12}$$

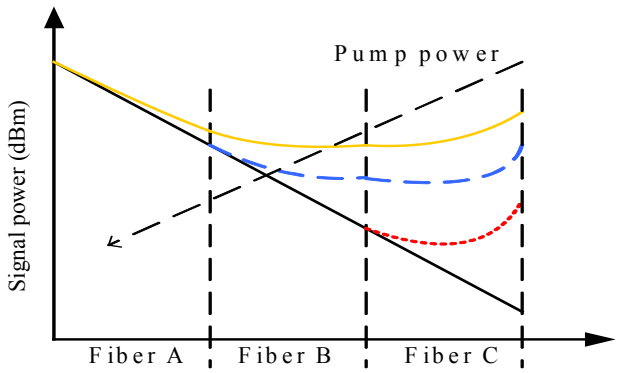

Figure 2.7 Iteration of the signal power along fiber section A, B and C.

The goal of the numerical algorithm for power analysis is to solve the boundary problem given at the end of the fiber, namely the signal power can't be obtained finally before the pump power has been

calculated through all the effective fibers with Raman effect. Figure 2.7 presents three fiber sections with backward pumping.

The fiber section C gets Raman amplification when backward pump power propagates across it as shown in red curve. The remaining pump power keeps propagating inside the fiber section B and amplifies the signal again as in blue curve. Then the signal power calculated in section C should be rescaled. When remaining pump power go to the section A, the signal is amplified again; hence, the signal power level of section B and C will be rescaled again to give a continuous signal power evolution. Finally, a correct signal power distribution along the fiber is given in orange curve. The iteration approach will attack this problem until the difference in signal power at the end of section C obtained after two consecutive iterations becomes less than the desired accuracy, which can be set in the simulation arbitrarily [12].

2.2.2 Field analysis

In the second stage, the field analysis is performed based on the power solution above. The full nonlinear Schrödinger equation (NLSE) is solved numerically by split-step Fourier method [12] which treats the fiber as concatenated sections of short fiber length as shown in Figure 2.6 a).

$$\frac{\partial}{\partial z}A_i^+(t) = -\frac{\alpha}{2}A_i^+(t) + \hat{D}A_i^+(t) + \hat{N}A_i^+(t) \qquad (2.13)$$

Here $\hat{D}$ and $\hat{N}$ represent linear and nonlinear operators, respectively. In the split-step Fourier method, the dispersion and nonlinearities are treated in corresponding domains respectively as shown in Figure 2.6 a). The frequency decomposition approach is still used to take nonlinear effects into account.

The dispersion operator includes the second order dispersion β_2 and third order dispersion β_3 and is defined as:

$$\hat{D} = j\frac{\beta_2}{2}\frac{\partial^2}{\partial t^2} + \frac{\beta_3}{6}\frac{\partial^3}{\partial t^3} \qquad (2.14)$$

Nonlinear effects are all included in the fiber model. The nonlinear operator include SPM, XPM, inter and intra Raman effects and is presented in (2.15).

Here γ_{ik} is a nonlinear coefficient representing interactions of propagating bands f_k and f_i and is given by $\gamma_{ki} = \frac{2\pi n_2 f_i}{CA_{eff}(f_k, f_i)}$. C is vacuum light speed, n_2 is the nonlinear refractive index, $A_{eff}(f_{k,} f_i)$ is the effective core area corresponding to f_k and f_i . $h(\tau)$ is the normalized Raman response function and ρ is the coefficient that describes the fractional contribution of the delayed Raman response function [8]. P_{RD} is the Rayleigh scattering power. ζ_1 , ζ_2, ζ_3, ζ_4 and ζ_5 is the coefficient of the nonlinear effects.

$$\hat{N}A_i^+(t) = -j\left[\begin{array}{l}\underbrace{\zeta_1(1-\rho)\gamma_{ii}\left|A_i^+(t)\right|^2 A_i^+(t)}_{SPM} + \underbrace{\zeta_2 2(1-\rho)A_i^+(t)\sum_{k\neq i}\gamma_{ki}\left|A_k^+(t)\right|^2}_{XPM-EC} \\ \underbrace{+\zeta_3\rho A_i^+(t)\sum_{k\neq i}\gamma_{ki}\int_0^\infty h(\tau)\left|A_k^+(t-\tau)\right|^2 d\tau}_{XPM-MC} + \underbrace{\zeta_4\rho\gamma_{ii}A_i^+(t)\int_0^\infty h(\tau)\left|A_i^+(t-\tau)\right|^2 d\tau}_{IntrabandRaman} + \\ \underbrace{\zeta_5\rho A_i^+(t)\sum_{k\neq j}\gamma_{kj}\int_0^\infty h(\tau)A_i^+(t-\tau)A_k^+(t-\tau)e^{2\pi j(f_i-f_k)\tau}d\tau}_{InterbandRaman} + \\ \underbrace{\rho\sum_{k\neq i}\gamma_{ki}\int_0^\infty h(\tau)A_i^+(t-\tau)\left[\varepsilon P_S^\pm(f_k)+\varepsilon_2 P_{RD}^\pm(f_k)\right]}_{InterbandRaman-noise}\end{array}\right] \quad (2.15)$$

2.3 Design and application of Raman amplifier

Raman application features a much larger bandwidth than that of EDFA. The most attractive advantage is the ultra broad-band Raman spectrum that can accommodate hundreds of signal channels. There are two types of Raman amplifier design, namely discrete and distributed Raman amplifier. Figure 2.8 presents the discrete amplifier schematically. It can be packed into an independent amplifier with high fixed gain and low NF. Furthermore, it can offer spectral bands that are not covered by EDFAs. DCF is used for not only dispersion compensation but also amplification at the same time. A Raman amplifier module made of a single DCF has been demonstrated compensating C+L band [13]. A 100 nm seamless bandwidth discrete

Raman repeater was realized with DCF by two-stage amplification [14].

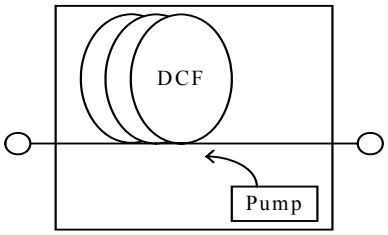

Figure 2.8 Discrete Raman amplifier set-up

Distributed Raman amplification uses the transmission fiber as amplification media. The signal is amplified when it propagates along the transmission fiber, thus mitigating the reduction of OSNR. So to obtain the same output signal power, less launched signal power is needed compared with an EDFA span, thus giving less nonlinearity.

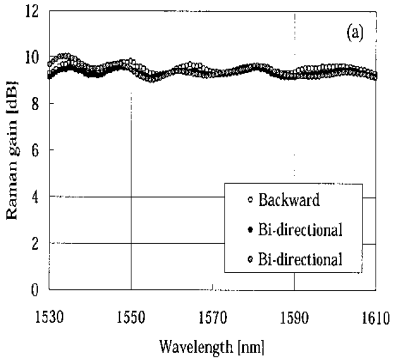

Figure 2.9 Flat gain by multiple pumps across the whole bandwidth.

However, WDM gain tilt arises by power transfer from high frequency pumps to low frequency pumps. The gain tilt is a deleterious effect that imposes different amplification on channels. To solve this problem, a gain equalizer function (GEF) is used to experimentally flatten the gain after each fiber loop [1].

Another solution is to employ multiple pumps with proper power allocation to achieve flat Raman gain across the demanded bandwidth [16-18]. It can be realized by a combination of forward pumps and backward pumps [16] as show in Figure 2.9.

The distributed Raman amplification is extensively used in high-speed and wide band WDM transmission systems because of the benefit of lower NF and better OSNR. Distributed multiple pump designs with respect to a specific fiber span are advantageous in WDM systems. Second order pump experiments were also demonstrated for amplification of the first order pump power, thus increasing the Raman gain in long fiber lengths [15].

2.4 Summary

A description of the basic physical mechanism of Raman amplification is given. In addition, the main noise terms and nonlinear effects are discussed. For accurate numerical simulation, the coupled equations that include noise processes and nonlinear impairments are discussed in detail. With the merit of Raman amplification, the system can potentially be improved largely, which is very important for ultra-high speed systems such as 160 Gbit/s systems.

Chapter 3

Modulation format

The adoption of new modulation formats such as carrier suppressed (CS) formats or DPSK (differential-phase-shift-keying) and DQPSK (differential-quadrature-phase-shift-keying) provides the advantages of narrower spectrum width or smooth spectrum without sharp peaks in addition to higher receiver sensitivity. Such formats can improve the transmission systems and reduce the nonlinear distortion.

Table 3.1 presents an overview of the outstanding experimental records on capacity and distance achieved in 40 Gbit/s WDM systems. It is noteworthy that all of these state-of-the-art experiments employ more advanced modulation formats than simple on-off keying. In these experiments the DPSK format is extensively employed as an advantageous modulation format offering better nonlinear resilience and consequently larger capacity and longer system reach [19-24]. The DQPSK format has emerged as a new modulation format that can largely increase the spectral efficiency [25-28], thus accommodating more channels within the available fiber bandwidth as listed in Table 3.2.

In this chapter, the generation method of each modulation format is illustrated. The encoding and decoding principles of DPSK and DQPSK are presented. Balanced detection and a noise estimation model are also discussed.

Table 3.1 Experiment record on 40 Gbit/s WDM systems

Authors	Capacity	Distance	Modulation format	Spectral efficiency	Fiber
Y. Frignac[19]	10.2Tb/s (256*42.7 Gb/s)	300km	VSB-NRZ	0.64 b/s/Hz	SSMF
G. Charlet[20]	6 Tb/s (149*42.7 Gb/s)	6120km	DPSK	0.8 b/s/Hz	SLA+ IDF
B.Zhu[21]	6.4 Tb/s (160*42.7 Gb/s)	3,200km	CSRZ-DPSK	0.8 b/s/Hz	SLA+ IDF
A. Agarwal[24]	5.12 Tb/s (128*42.7 Gb/s)	1,280km	CSRZ	0.8 b/s/Hz	SSMF
C.Rasmussen [23]	1.6Tb/s (40*42.7 Gb/s)	10,000km	CSRZ-DPSK	0.4 b/s/Hz	SLA+ IDF
I.Morita[22]	2.7Tb/s (64*42.7 Gb/s)	8200km	CSRZ-DPSK	0.8 b/s/Hz	

Table 3.2 WDM systems employing DQPSK

Authors	Capacity Gb/s	Distance	Modulation format	Spectral efficiency	Fiber
N. Yoshikane [25]	50*85.4	300 km	CS-RZ-DQPSK	1.14 b/s/Hz	NZDSF
Y. Zhu [26]	8×40	320 km	CS-RZ-DQPSK	1.6 bit/s/Hz	NZDSF
N. Yoshikane[27]	64*85.4	320km	RZ-DQPSK	1.6 bit/s/Hz	SSMF
A. H. Gnauck [28]	25*42.7	2800km	RZ-DQPSK	0.8b/s/Hz	SSMF

3.1 Generation of the RZ and CSRZ formats

A Mach Zenhder modulator (MZM) is usually used as a pulse carver made possible by the transfer function of such a modulator. Simple modulation formats such as RZ (Return-to-zero) and CSRZ (Carrier-suppressed-return-to-zero) can be generated by a Mach Zenhder modulator by choosing a proper bias point and applying a suitable electrical voltage swing as shown in Figure 3.1. An RZ signal of duty

cycle 50 % is generated by biasing on the quadrature point of the MZM and using a voltage swing of v_π (the voltage that dive the modulator from the maximum transmission point to minimum transmission point). When the electrical clock runs at half the bit rate with a peak-to-peak voltage of $2\,v_\pi$ and the MZM is biased at maximum transmission point, an RZ signal with duty cycle of 33% can be obtained.

The CSRZ format is generated by a clock that runs at half the bit rate and with full swing of $2\,v_\pi$, similar to the 33% RZ format, but the difference is that it is biased at minimum transmission point, which gives a broad pulse width with a duty cycle of 67%. Furthermore, it gives the output pulse a π phase shift between adjacent bits. Figure 3.2 shows the spectra of the RZ with 50% duty cycle and CSRZ formats. CSRZ has half the bandwidth due to half frequency modulation.

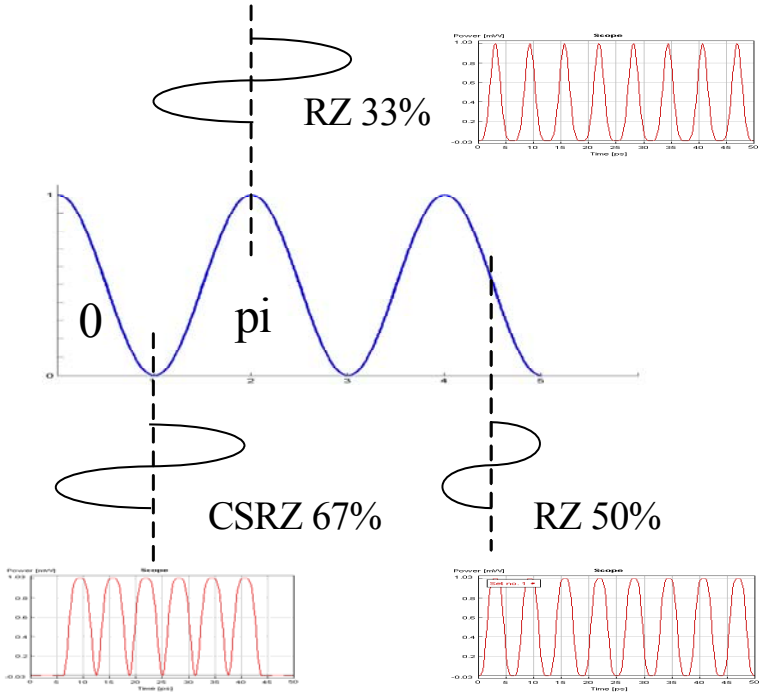

Figure 3.1. Mach Zenhder modulation for generation of RZ format with duty cycle of 33% and 50% and of CSRZ format with duty cycle of 67%. Corresponding pulse shapes are also shown.

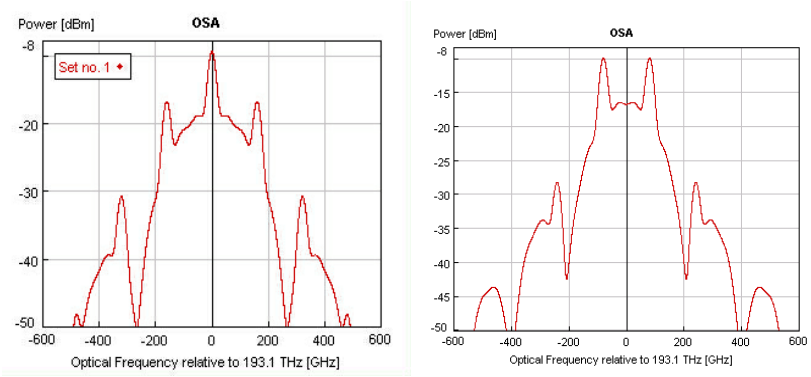

a) b)

Figure 3.2 Spectra of RZ and CSRZ formats at 160 Gbit/s.

3.2 Principle and application of DPSK

It is well known that the PSK format has higher sensitivity than OOK but the synchronous demodulation condition imposes strict demands on phase fluctuations [29]. In DPSK the information is encoded as phase difference between adjacent bits and can then be demodulated by delayed detection; this is a form of asynchronous demodulation and it poses relaxed requirements to low phase noise. It also offers 3 dB higher receiver sensitivity by balanced detection compared with OOK. Consequently, the launched signal power can be reduced and less nonlinearity is generated during propagation in the fiber.

3.2.1 Principle of encoding and decoding DPSK

Encoding

There are two methods to generate a DPSK signal. One approach is to drive a phase modulator by an electrical DPSK data voltage as shown in Figure 3.3 a). The refractive index is changed with δn by the applied voltage and this causes a certain phase shift after length L. The phase shift is determined by $\delta\phi = (2\pi/\lambda)(\delta n)L$. When the phase shift is accurately controlled and changed between 0 and π according to the output bit value ‘1’ or ‘0’, the DPSK signal is generated. In this case the phase modulator can provide constant optical output power

while some chirp might be induced due to the rise time of the electrical data.

Another approach is to drive a MZM by an electrical DPSK data signal as shown in Figure 3.3 b). The MZM is operated at the minimum transmission point and can give complete π phase shift between output bit '1' and '0'. However, the drawback is that some residual amplitude modulation occurs when there is a change in the adjacent bit values.

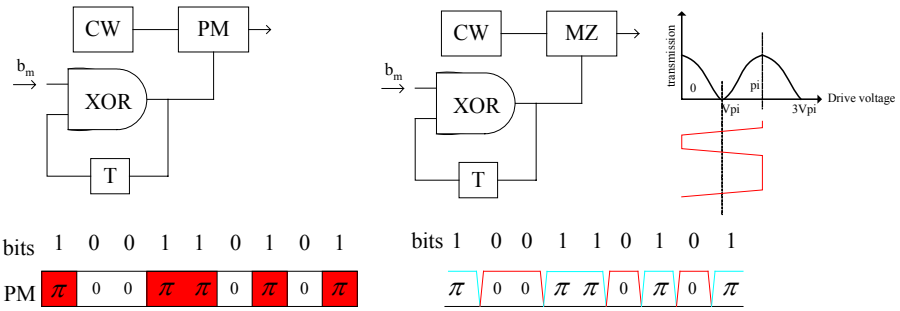

Figure 3.3 Principle of DPSK format generation by a) phase modulator and b) Mach Zenhder modulator

Decoding by Mach Zenhder Interferometer (MZI)

Being an interferometer as shown in Figure 3.4, the MZI consists of two 3 dB couplers and a specifically designed optical delay difference ΔL in one arm. The principle of operation relies on constructive or destructive interference of the two signals from the two arms after the second coupler output port.

It is known that a signal cross-coupled to the opposite arm in a coupler will experience a π/2 extra phase shift. In Figure 3.4 the input signal A_{in} is split into two parts by the first 3 dB coupler. The part of the signal that passes arm B and exits from the second coupler at port A_{out} has experienced an extra π phase shift. The part that passes arm A has an optical delay difference of $\beta \Delta L$. So the phase condition for constructive interference of the two parts of the signals at output port A_{out} is $\pi + \beta \Delta L = 2m\pi$ (m=1,2,3…). The delay length ΔL can be determined corresponding to a specific wavelength. At the output port B_{out}, the two parts of the signal have a phase difference of $\beta \Delta L$.

Comparing the two output ports we can see that the conditions for constructive or destructive interference can be satisfied at the two ports simultaneously when $\beta \Delta L = n\pi$ (n=1,2,3…). Since DPSK is obtained by π phase shifting of a lightwave, the fiber delay length is set to accommodate one bit time. The DPSK sequence will be demodulated at both output ports. The bit pattern modulation at the transmitter and the demodulated recovered bit pattern at the receiver are shown in Table 3.3.

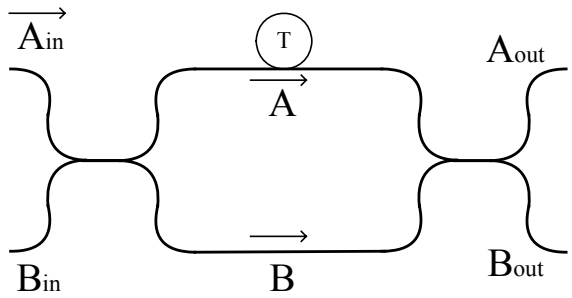

Figure 3.4 MZI set-up with one bit delay

Table 3.3 DPSK modulation and demodulation bit pattern

Tx	Bit	0	1	0	1	1	0	0	1	0
	DPSK	1	0	0	1	0	0	0	1	1
	Phase	π	0	0	π	0	0	0	π	π
Rx	PhaseA	π	π	0	0	π	0	0	0	π
A_{out}	PhaseB	0	π	π	0	π	π	π	0	0
	Bit	0	1	0	1	1	0	0	1	0
Rx	PhaseA	π+π/2	π+π/2	π/2	π/2	π+π/2	π/2	π/2	π/2	π+π/2
B_{out}	PhaseB	π+π/2	π/2	π/2	π+π/2	π/2	π/2	π/2	π+π/2	π+π/2
	Bit	1	0	1	0	0	1	1	0	1

3.2.2 Benefit from balanced receiver

From Table 3.3 we can see that after the MZI, there are two output ports with same signal power and same bit sequence. Figure 3.5 shows the set-up of single arm detection, balanced detection and comparison of eyes. The ideal balanced receiver consists of two photodiodes with

same characteristics mounted in a subtraction configuration, which can be realized by conversion in one branch to a negative electrical signal and then adding the two electrical signals. The balanced receiver is placed just after the MZI to receive signal from both branches. When the subtraction is executed, the DC term is eliminated. What's more; the intensity noise associated with the DC term is also eliminated at the same time. As a consequence the subtracted signal is judged at a threshold of zero, and has a doubled eye aperture. Therefore DPSK with balanced detection has an advantage of 3 dB higher receiver sensitivity compared to OOK theoretically.

In VPI simulations, however, we get a 2.3 dB sensitivity improvement. This is because we assume Gaussian noise density distribution, which is not perfect to characterize the DPSK noise density distribution, as will be discussed in next section.

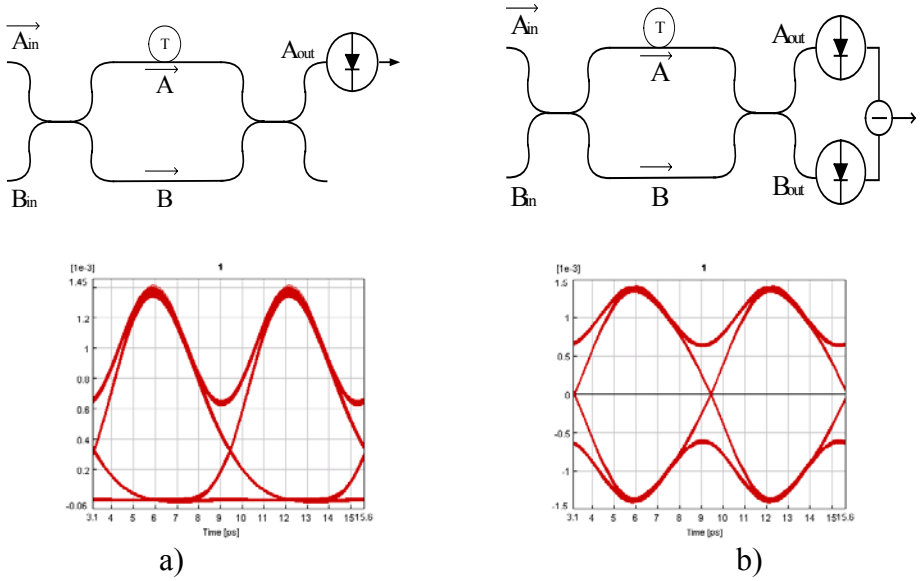

a) b)

Figure 3.5. MZI with a) single-end detection and eye. b) Balanced detection and eye.

The generation of RZ-DPSK and CSRZ-DPSK can simply be obtained by generating the DPSK format in a first stage and subsequently the RZ or CSRZ format in a second stage. However, when CSRZ-DPSK is generated, another π phase shift is added to the adjacent bit at CSRZ stage. Then the bit sequence after balanced detection can be reversed compared to the original bit sequence. This

problem can be solved by changing the order of subtraction of the two branches.

Compared with the spectrum of RZ, the DPSK spectrum has no impulse at carrier frequency and sub-carrier frequencies as shown in Figure 3.6. The derivation of the spectra of ASK and PSK are reviewed in Appendix B.

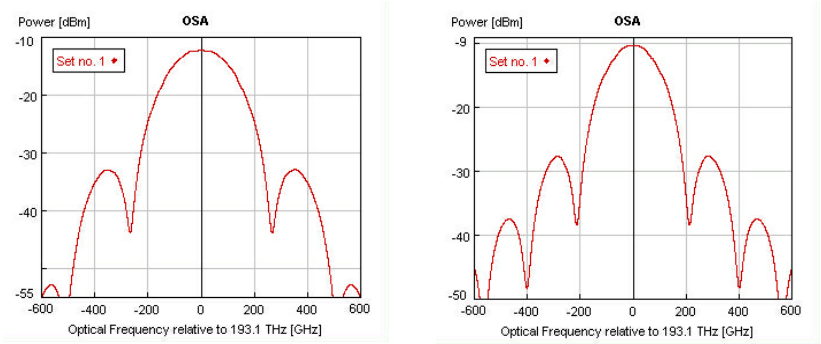

a) b)

Figure 3.6. Spectra of a) RZ-DPSK and b) CSRZ-DPSK.

3.2.3 Model for noise analysis of DPSK

Normally a Gaussian approximation is quite accurate and extensively used because the statistics of the received optical signal can be assumed to have a Gaussian distribution. However, ASE (Amplified Spontaneous Emission) noise from the optical amplifiers accumulates and is dominant along the system and must be considered. At the detector, beat noise is generated by ASE-ASE beating and signal-ASE beating; both of these processes give electrical noise at the baseband. In such a case it turns out the statistics of a received optical signal accompanied by noise is non-Gaussian [30], and the Gaussian approximation can not be trusted anymore.

Limitation on balanced DPSK detection

For instance, the probability density function (PDF) of DPSK after balanced detection is quite different from Gaussian PDF of ASK. In brief, to demodulate each bit, two bits from two arms will interfere constructively or destructively. Thus the combination of the two noise

distributions experience distortion during this process. The noise distribution becomes non-Gaussian and may be displaced from the center of the bit slot, and it may even not cover the whole bit slot as described in [12].

Up to now mathematical solutions leading to an accurate simulation model of a DPSK receiver are very cumbersome and still under investigation [30,31]. The much simpler Gaussian approximation is verified to be inaccurate when trying to approximate the PDF with non-Gaussian noise distribution encountered in balanced detection of DPSK. For instance in [32], the perfect balanced detection can accept 2 dB lower OSNR compared with Gaussian model assumption. The results show a significant Q value difference between numerical simulation and Gaussian assumption.

Approach with χ^2 model

Balanced detection of DPSK can be addressed by the χ^2 model discussed below; this model is much more accurate when the dominant noise processes are signal-spontaneous beat noise and spontaneous-spontaneous beat noise generated when an optical signal accompanied by optical spontaneous emission noise is received. It is assumed that all optical noise is accounted for in the form of random noise samples added to the optical signal waveform, but all post-detection electrical noise is excluded from the sampled band and instead accounted for by the BER estimator using deterministic methods [34].

Principle of χ^2 model

In brief, the variance of the detected optical beat noise, and the mean values of ‘one’ and ‘zero’ signals are determined from the statistics of the input signal. When BER is estimated by performing a χ^2 analysis, a two step process is needed. First, the parameters of the χ^2 fit are first estimated from the incoming samples. Then the overall non-Gaussian probability density functions are calculated, including the contribution from the Gaussian thermal noise and a Gaussian approximation of the shot noise. The non-central χ^2 distribution is estimated by performing a statistical analysis of the input signal samples by a separate analysis for ‘one’ and ‘zero’ bits in the received bit sequence. Secondly, the

probabilities of error for data 'one's and 'zero's are computed from the probability density functions [12]. The χ^2 distribution will be used in Chapter 6.

3.3 Principle and generation of DQPSK

DQPSK, being a four level phase modulation format, has the advantage of using half the bit rate, which implies half the signal spectral width. DQPSK experiments have been demonstrated in DWDM systems to achieve high spectral efficiency [25]. Several methods can be used to generate DQPSK format [35]. Here we introduce one approach.

3.3.1 DQPSK encoding

The DQPSK transmitter consists of two parallel MZM modulators with a $\pi/2$ phase shift in one of the two branches as shown in Figure 3.7.

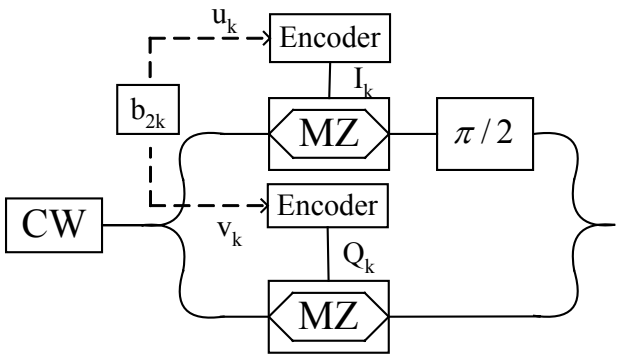

Figure 3.7. Schematic of DQPSK generation principle.

The initial launched bit sequence b_{2k} at the bit rate B is divided bit by bit alternately forming two bit sequences u_k, v_k each at the bit rate B/2. The u_k, v_k are encoded to form I_k and Q_k according to the mathematical formula given below [36]. Then the encoded bit sequences I_k and Q_k modulate two parallel MZMs individually. The lightwave in one branch is given an additional $\pi/2$ phase shift before

it is combined with the lightwave from the other branch; the output from the transmitter is the encoded DQPSK signal.

$$I_k = \overline{(u_k \oplus v_k)}(u_k \oplus I_{k-1}) + (u_k \oplus v_k)(v_k \oplus Q_{k-1})$$
$$Q_k = \overline{(u_k \oplus v_k)}(v_k \oplus Q_{k-1}) + (u_k \oplus v_k)(u_k \oplus I_{k-1})$$

The output field of the transmitter [9] can be written as

$$E(t) = E_0 \cos\left[\frac{(I_k - Q_k)\pi + \frac{\pi}{2}}{2}\right] e^{j}\left[\frac{(I_k + Q_k)\pi + \frac{\pi}{2}}{2}\right]$$

It is clear that there are four absolute phases $\frac{\pi}{4}$, $\frac{3\pi}{4}$, $\frac{5\pi}{4}$, $\frac{7\pi}{4}$ determined by the combination of bit value of I_k and Q_k, which is $\{0,1,2\}$. Therefore each symbol is coded with one of four possible combinations of the two bits I_k, Q_k, resulting in a four-level phase modulated signal.

3.3.2 DQPSK decoding

The DQPSK decoder is more complicated compared to a DPSK decoder since it needs two MZIs to demodulate two branches separately as shown in Figure 3.8.

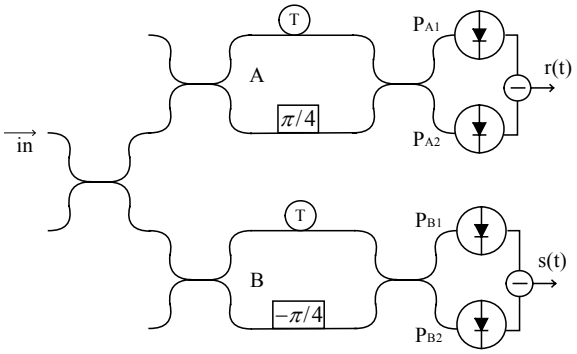

Figure 3.8. DQPSK demodulation by two MZIs with phase shift.

The launched signal is split into two arms by a 3 dB coupler and launched into two MZIs, separately. In each MZI, a relative phase shift of $\pm\pi/4$ is introduced between the two arms, at the same time the delay T is set to be 2/B.

To understand the principle of the DQPSK decoder, first the transfer function of a MZI is derived with reference to Figure 3.9.

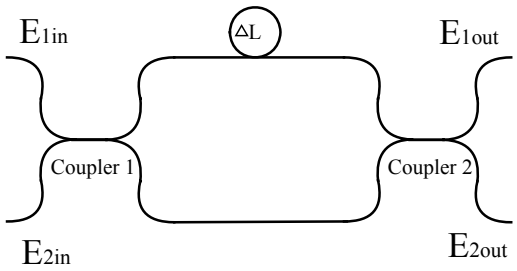

Figure 3.9. MZI schematic with two 3 dB couplers and a time delay.

The 3 dB coupler matrix can be written as [37]:

$$M_{coupler1} = M_{coupler2} = \begin{pmatrix} \cos(\pi/4) & i\sin(\pi/4) \\ i\sin(\pi/4) & \cos(\pi/4) \end{pmatrix}$$

As ΔL is the fiber delay length, the matrix for the phase shift between the two couplers is:

$$M_{phaseshift} = \begin{pmatrix} \exp(ik\Delta L) & o \\ 0 & 1 \end{pmatrix}$$

Then the propagation matrix for the MZI is as follows:

$$M_{MZI} = M_{coupler1} \cdot M_{phaseshift} \cdot M_{coupler2}$$

Then the signal power transmission of the MZI is layout as

$$\begin{pmatrix} E_{1out} \\ E_{2out} \end{pmatrix} = M_{MZI} \begin{pmatrix} E_{1in} \\ E_{2in} \end{pmatrix}$$

By combination of above, the output signal is represented as follows [38]

$$P_{1out} = \sin^2(\kappa\Delta l/2)P_{in}$$

$$P_{2out} = \cos^2(\kappa\Delta l/2)P_{in}$$

According to the derivation given above, the DQPSK decoder as shown in Figure 3.8 also provides the phase shifts on the two MZIs, separately. They can be expressed as follows:

$$\Delta\phi_A = \phi(t) - \phi(t-\tau) + \pi/4$$

$$\Delta\phi_B = \phi(t) - \phi(t-\tau) - \pi/4$$

According to the MZI formula derived above, the two outputs from MZI-A can be written as:

$$P_{A1}(t) = P_{in}\sin^2\left[\frac{\phi(t) - \phi(t-\tau) + \frac{\pi}{4}}{2}\right]$$

$$P_{A2}(t) = P_{in}\cos^2\left[\frac{\phi(t) - \phi(t-\tau) + \frac{\pi}{4}}{2}\right]$$

where we set

$$\Delta\phi(t) = \phi(t) - \phi(t-\tau)$$

So the final output after subtraction is:

$$r(t) = P_{A1} - P_{A2} = P_{in}\frac{\sqrt{2}}{2}\left[\sin\Delta\phi(t) - \cos\Delta\phi(t)\right]$$

According to the same principle, the two outputs from MZI-B can be written as:

$$P_{B1}(t) = P_{in}\sin^2\left[\frac{\phi(t) - \phi(t-\tau) - \frac{\pi}{4}}{2}\right]$$

$$P_{B2}(t) = P_{in}\cos^2\left[\frac{\phi(t) - \phi(t-\tau) - \frac{\pi}{4}}{2}\right]$$

So the final output after subtraction is:

$$s(t) = P_{B1} - P_{B2} = -P_{in}\frac{\sqrt{2}}{2}\left[\sin\Delta\phi(t) + \cos\Delta\phi(t)\right]$$

Since $\Delta\phi(t)$ can be $(-\pi/2,\ 0,\ \pi/2,\ \pi)$, then each bit of the original two sequences corresponds to one value above. Table 3.4 illustrates encoding and decoding bit pattern from transmitter to receiver. The original bit sequence is recovered after demodulation by the two branches.

Table 3.4 Encoding and decoding for DQPSK

b_{2k}	01	10	10	00	11	10	11	10	01	01
u_k	0	1	1	0	1	1	1	1	0	0
v_k	1	0	0	0	1	0	1	0	1	1
I_k	1	0	0	0	1	0	1	1	1	0
Q_k	0	0	1	1	0	0	1	0	1	1
Φ_k	7π/4	π/4	3π/4	3π/4	7π/4	π/4	5π/4	7π/4	5π/4	3π/4
Δ_k		π/2	π/2	0	π	π/2	π	π/2	-π/2	-π/2
r_k		1	1	0	1	1	1	1	0	0
s_k		0	0	0	1	0	1	0	1	1

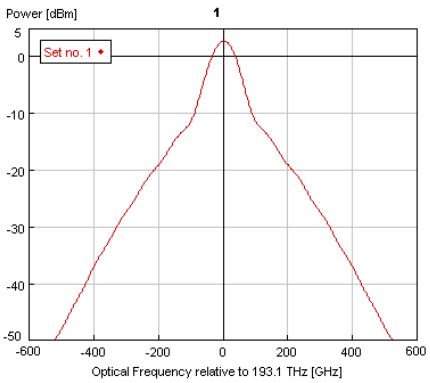

Figure 3.10. Spectra of DQPSK format.

Figure 3.10 shows that the spectrum of the DQPSK format has half the bandwidth than that of DPSK for the same bit rate. Furthermore, its generation method is more feasible for practical 160 Gb/s systems as it only requires components capable of 80 Gb/s operation, and it is more suitable for spectrally efficient WDM systems than the other formats.

3.4 Summary

We have given an overview of generation methods for modulation formats such as RZ, CSRZ, DPSK and DQPSK. Half the spectrum width from the CSRZ makes it a better candidate for spectral efficient design; more over the DPSK own the benefit of higher receiver sensitivity from balanced detection. Derivations have been presented pertaining to especially DPSK and DQPSK demodulation principle. The spectrum and power density characteristics of DPSK have also been discussed in a mathematical approach offering understanding in simple terms. The discussions indicate that DQPSK has the advantage of half modulation bandwidth, which is promising for ultra-high speed system application.

Chapter 4

Single channel 160 Gbit/s systems simulation

Numerous experiments on 40 Gbit/s WDM systems have been demonstrated. A distance of 10000 km has been achieved for a 40-channel 40 Gbit/s WDM system with bi-directional Raman amplification on SLA (super-large-core-area) and IDF (inversed dispersion fiber) spans [23]. However, even higher channel rates will be advantageous for lower cost and this will accelerate the effort to improve the capacity of a single channel [39-41]; consequently 160 Gbit/s systems as the next scenario are attracting increased research attention. Since the nonlinearity effects occurring for a few picoseconds pulse width in 160 Gbit/s systems are more complicated than for 40 Gbit/s systems, it is very important to investigate single channel systems before WDM systems are addressed.

Results for experiments on 160 Gbit/s single channel systems are listed in Table 4.1. RZ-DPSK modulation format was employed in Ludwig's experiment to achieve 410 km transmission with SLA+IDF span [44]. In another experiment, 480 km of system reach was achieved with short pulses of 2.8ps and NDSF [43]. Up to now the longest transmission distance of 550 km was demonstrated with SSMF [42]. The SLA+IDF span is demonstrated to outperform SSMF+DCF [4]. Experimental comparison of RZ-DPSK and RZ modulation format was investigated [69]. Since with EDFA, the maximum distance is limited to about 600-700 km, Raman amplification is very promising to greatly increase the system reach as it demonstrated in 40 Gbit/s systems. However, up to now, the simulation work on 160 Gbit/s mainly focuses on comparison of different modulation formats [45-48]. We notice that for 160 Gbit/s single channel systems, not much simulation work [46] has been published on newly developed SLA+IDF spans, Raman amplification, DPSK and DQPSK formats and new dispersion maps.

Table 4.1 Experiments demonstrated for 160 Gbit/s single channel systems

Authors	Fiber	Modulation format	Distance	Amplifier
J-L. Auge [43]	NDSF	2.8 ps short pulse	480 km	EDFA
G. Lehmann [42]	SSMF	2 ps RZ	550 km	EDFA
R. Ludwig [44]	SLA+IDF+ SSMF+DCF	RZ-DPSK	410 km	EDFA

The purpose of this chapter is to present a numerical simulation of 160 Gbit/s single channel systems in order to predict the longest transmission distance for different system configurations. New aspects of the research to be reported include SLA+IDF spans, discrete and distributed Raman amplification along with DPSK and DQPSK modulation formats. In particular, the goals of the research are to identify the optimum Raman pumping schemes to mitigate amplifier noise in the transmission, to identify the most favorable modulation formats that have largest tolerance towards dispersion and nonlinearities and to significantly increase the transmission system reach.

This chapter is organised as follows. The first section describes discrete Raman amplification consisting of four kinds of pumping schemes and it also provides an analysis of pulse width and fiber parameters. Following this discussion, a comparison of discrete and distributed Raman amplification is given. Section 2 deals with a comparison of distributed Raman amplification using three different pumping schemes and it gives the longest transmission distance, the optimal signal power distribution and the optimal span length margin. In the following Section 3, we present dispersion tolerance and nonlinearity margin of RZ, CSRZ, RZ-DPSK, CSRZ-DPSK and DQPSK formats for such systems. The different modulation formats versus single channel systems reach and SSMF and DCF span configurations are discussed. Such topics will be discussed for WDM systems in Chapter 6.

4.1 Discrete Raman amplification in transmission systems

Raman amplification is very attractive because of its various merits such as wideband flat gain profile and higher OSNR along the fiber compared to using conventional EDFA. However, up to now few papers exist that present numerical comparisons between different pumping schemes [47]. In this section, we compare different pumping configurations for discrete Raman amplification using SLA and IDF spans. For such spans different Raman pumping schemes are numerically simulated for 160 Gbit/s single channel transmission for the first time. We find that the optimal scheme is to pump the span in the middle where the IDF is located. A transmission distance of 1800 km is predicted and short pulses are preferred in these systems. We also compare the advantage of discrete Raman amplification and distributed Raman amplification.

4.1.1 Raman Model and pumping scheme setup

Raman model

In the Raman model, spontaneous Raman scattering distributed across the whole Raman gain bandwidth is taken into account. For simplicity, pump depletion is neglected and Rayleigh backscattering acts as the main Raman noise source. Because stimulated Raman scattering strongly depend on the polarization of the pump and launched signal, in order to get a realistic polarization-independent gain, we use half of the maximum gain coefficient under the condition of aligned polarizations between signal and pump. Thus all the terms containing gain coefficient are multiplied by a factor of 0.5. The simulated gain coefficient is introduced in Appendix C. Simplified signal, pump and noise power coupled equations for co-propagating pumping are as follows:

$$\frac{dP_s}{dz} = 0.5 \times g_R P_p P_s + \eta P_R - \alpha_s P_s$$
$$\frac{dP_p}{dz} = -\alpha_p P_p$$
$$\frac{dP_n}{dz} = -\alpha P_n + \eta P_n + 0.5 \times g_R P_p P_n + g_R N P_p$$
$$\frac{dP_R}{dz} = -\eta P_s + \alpha_s P_R$$

Here P_S is signal power, P_P pump power, P_n noise power, P_R Rayleigh backscattering power, g_R gain coefficient and η Rayleigh backscattering coefficient. Fiber loss coefficients α_P and α_S at pump and signal wavelength, respectively, are assumed to have the same value. The factor N represents spontaneous Raman scattering factor independent of polarization.

Setup and assumptions

Considering trade off between calculation time and BER calculation accuracy, a 512-bit PRBS sequence is adopted with transform-limited Gaussian signal pulse at a wavelength of 1552 nm. In order to provide the maximum gain, pump wavelength is upshifted 100 nm with respect to signal wavelength at a wavelength of 1450 nm. Figure 4.1 shows different Raman pumping schemes. The isolator is inserted in the span in order to block the backward pump power. For all the cases with backward pumping, we assume that Raman amplification effects only

take place at the fiber that just connected with pump laser. However, for the forward pumping set-ups, we assume the Raman amplification will affect all the fibers cascaded in front of it.

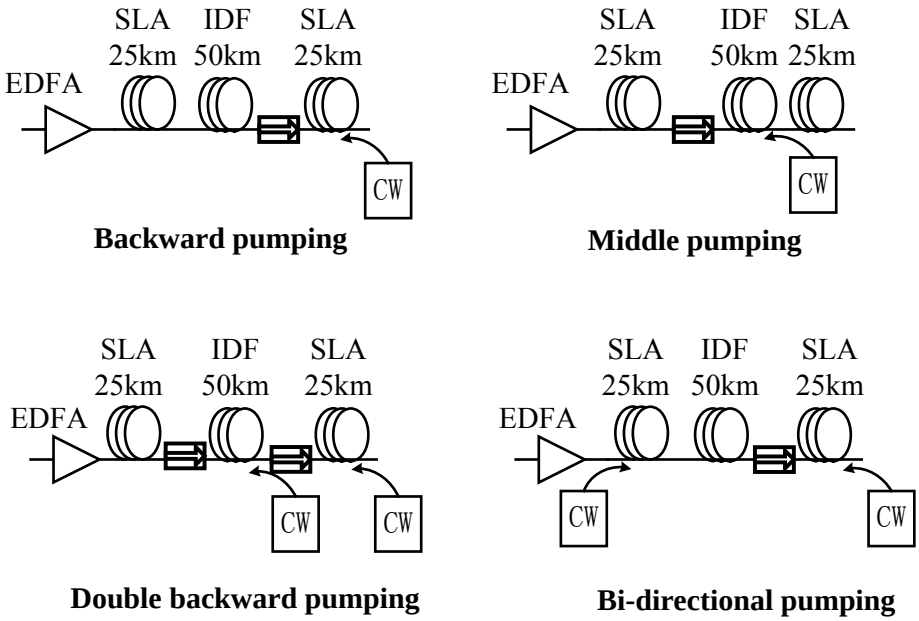

Figure 4.1. Four kinds of discrete Raman pumping schemes. Spans contain one or two isolators. CW: continuous pump power.

Symmetrical dispersion map is used and the span length is 100 km. The SLA has the following parameters: dispersion 20 $ps/km/nm$, dispersion slope 0.06 $ps/km/nm^2$, loss 0.2 dB/km, A_{eff} 105 μm^2, g_R 0.5 $(W \cdot km)^{-1}$. For the IDF we use dispersion –20 $ps/km/nm$, dispersion slope -0.06 $ps/km/nm^2$, loss 0.25 dB/km, A_{eff} 30 μm^2, g_R 1.5 $(W \cdot km)^{-1}$. Here the SLA and IDF are assumed to have the same values for η at 5.8×10^{-8} m^{-1} and for refractive index n_2 at 2.6×10^{-20}.

An optical filter with a bandwidth of 480 GHz is used before the receiver. For all the cases, an EDFA is set in front of the span to control the launched signal power level for power optimization.

4.1.2 Optimum signal power evolution and pump condition

After power calculation along fibers, the non-linear Schrödinger equation (NLSE) including dispersion, dispersion slope and nonlinearity is solved numerically by split-step algorithm [12]. Figure 4.2 shows a contour plot of the longest transmission distance at a BER of 1.0E-9, measured in number of 100 km spans.

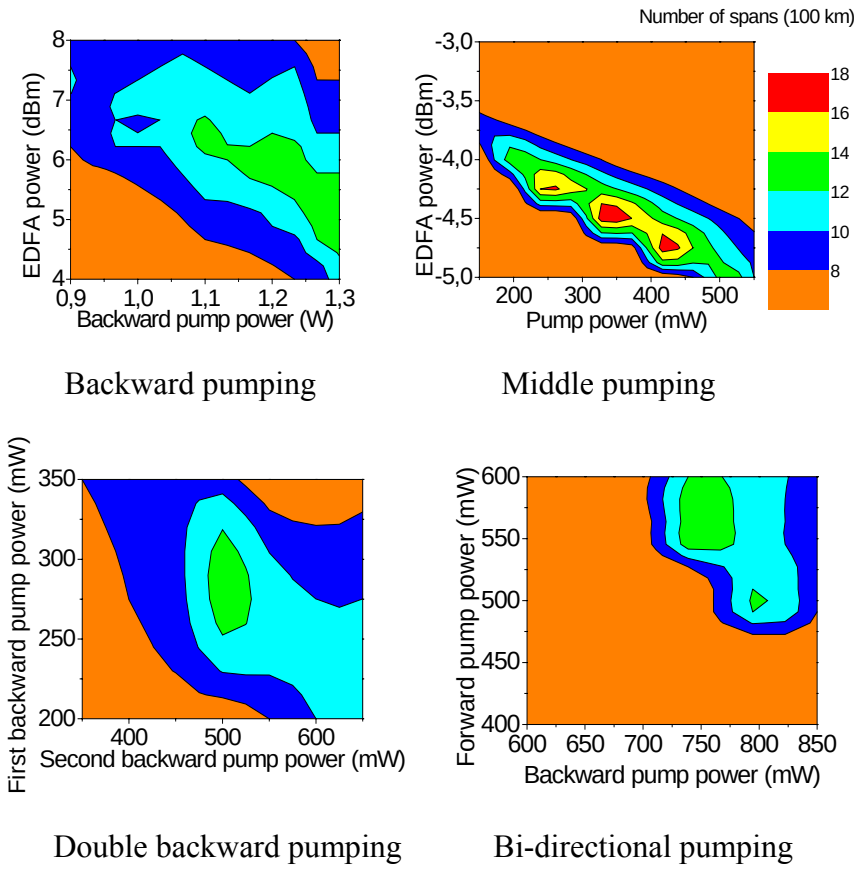

Figure 4.2. Contour plot of optimal longest transmission distance vs. combinations of EDFA and pump power for backward or middle pumping and vs. combinations of pump powers for double backward or bi-directional pumping.

The optimal combination of EDFA power and pump power are presented for backward and middle pumping schemes. For double backward pumping the figure shows optimal combination of first and second backward pump power, and for bi-directional pumping optimal combination of forward and backward pump power. Also in the latter two cases the EDFA input power was optimised for each combination of pump powers. However, it is kept in mind that with double backward pumping, pump power range is not fully investigated.

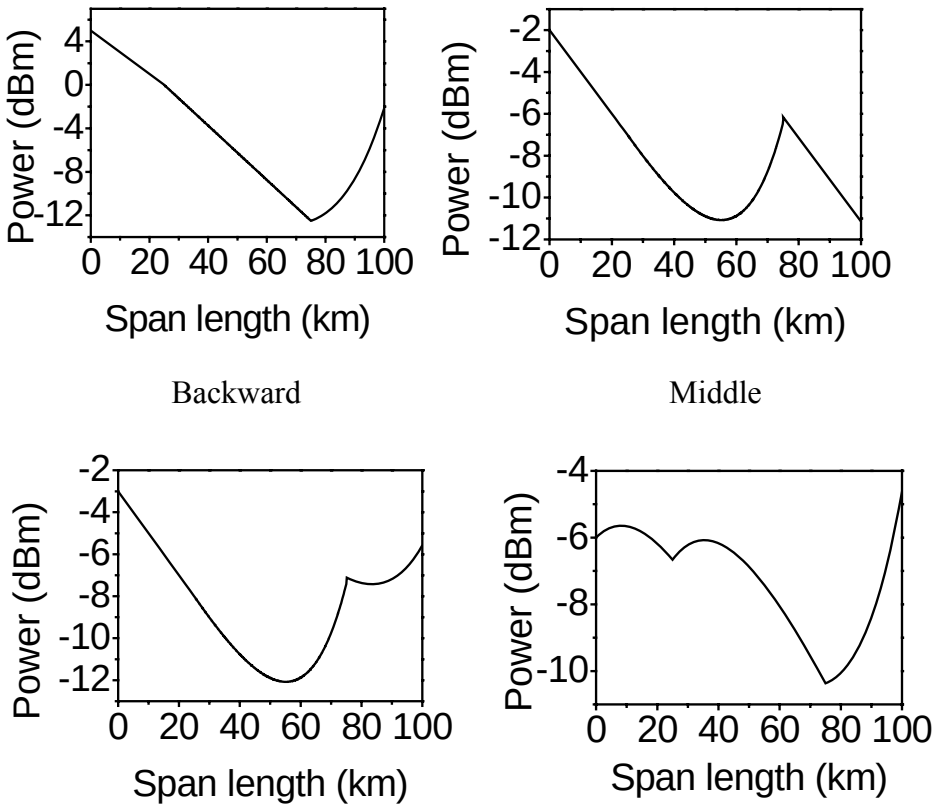

Figure 4.3. Signal power evolution inside the span based on longest transmission distance with respect to each pumping schemes.

The results were obtained with Gaussian pulse width 1 ps. A longest transmission distance of 1800 km can be reached by pumping IDF in the middle of the span. It is clear from Figure 4.2 that backward

pumping scheme requires largest pump power around 1.3 W, while middle pumping has the lowest pump power around 300 mW.

These can be explained by optimal power evolution inside spans as shown in Figure 4.3. It can be seen that for all cases, the signal power has a minimum value to keep enough OSNR. In the meantime, the middle pumping on IDF has the smallest average power level, which causes least nonlinearity effect compared to other schemes; consequently it gives the best performance. It is also noticed that although backward pumping scheme requires above 6 dB larger launched signal power than the other pumping schemes and much larger pump power is needed, the longest system reach is equal to the double backward and bi-directional pumping, thus it shows that less Raman pump source is preferred.

4.1.3 Transmission distance with pulse width and fiber parameters

Available longest transmission distance as a function of pulse width for different Raman pump schemes is investigated and the results are shown in Figure 4.4.

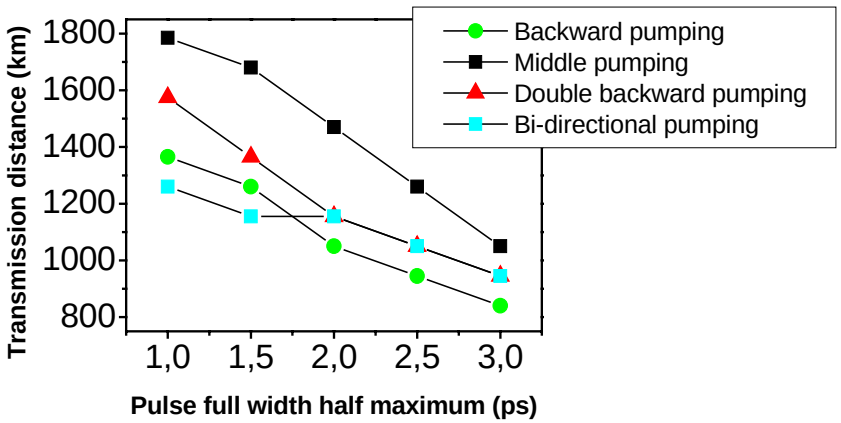

Figure 4.4 Transmission distance vs. pulse width for four different pumping schemes.

For all schemes, narrower pulse width is preferred for longer transmission distance due to quicker pulse broadening and thus less nonlinearity. It is also found that although the optimal pump level changes significantly for different pumping configurations, the optimal signal power distribution profile for the same pumping configuration stays constant regardless of pulse width variation.

Effective core area (A_{eff}) and dispersion of SLA in the span

In order to investigate the effect of dispersion and A_{eff} of fibers in the span, we change the dispersion of the SLA and IDF proportionally in the span. Figure 4.5 shows such a proportional variation of the SLA and IDF dispersion in case of a symmetrical dispersion map. We employ the middle pumping scheme mentioned earlier.

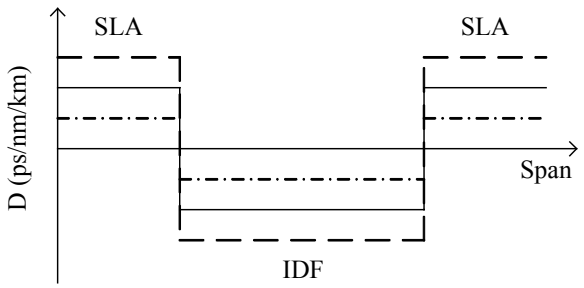

Figure 4.5. Proportional dispersion variation of SLA and IDF in symmetrical dispersion map with 100 km span length.

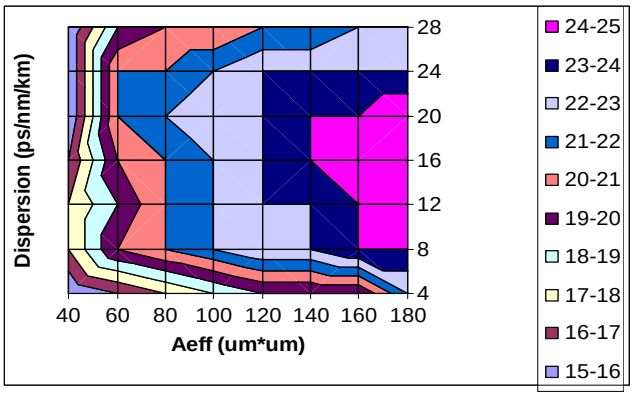

Figure 4.6. Contour plot of transmission distance in terms of number of 100 km spans with respect to the Aeff and dispersion of SLA.

The contour plot in Figure 4.6 shows the system maximum reach in terms of number of 100 km spans with respect to A_{eff} and dispersion of

the SLA. The results show that the optimum dispersion range is centered around 16 $ps/km/nm$, the same value as for a SSMF. The larger the effective core area of the SLA, the better the system performance. A transmission distance of 2400 km is predicted for A_{eff} above 160 μm^2.

Besides changing the A_{eff} of SLA, we now also change the core area of the IDF proportionally to remain at one third of SLA core area. The optimal dispersion range and A_{eff} of SLA is calculated again. Figure 4.7 shows that the larger the core area of the SLA and IDF, the better the system performance. A longer system distance of 2900 km can be reached with a core area of the SLA above 180 μm^2, consequently an IDF core area above 60 μm^2 is preferred. The optimum dispersion of the SLA is around 20 $ps/km/nm$, which means a large dispersion value outperforms a small dispersion. These results match with [48].

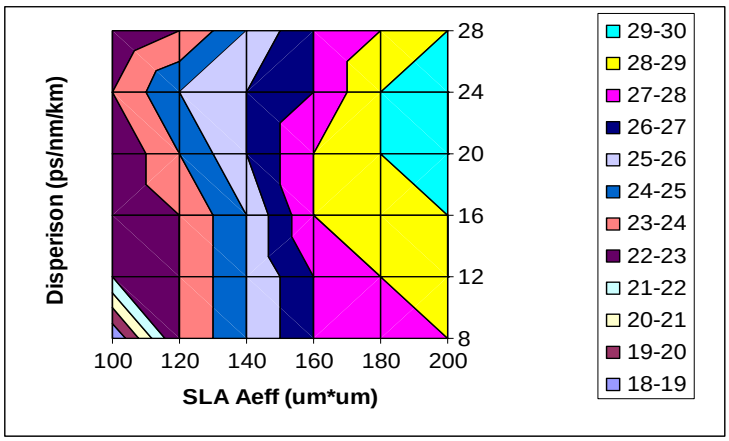

Figure 4.7 Contour plot of transmission distance vs. core area and dispersion of SLA; the IDF core area is changed proportionally to remain at 1/3 of SLA value.

4.1.4 Impact of OSNR and nonlinearity

To determine which impairment is dominant among OSNR degradation, nonlinearity, and multi-path interference (MPI), we compare discrete and distributed Raman amplification to investigate the impact of OSNR, nonlinearity and MPI. Figure 4.8 shows the

discrete and distributed Raman amplification set-ups. Unlike the discrete set-up a) with an isolator to block the pump propagation along the consecutive fiber sections, the Raman pump power in b) passes all the fiber sections and amplifies the signal with the remaining pump power.

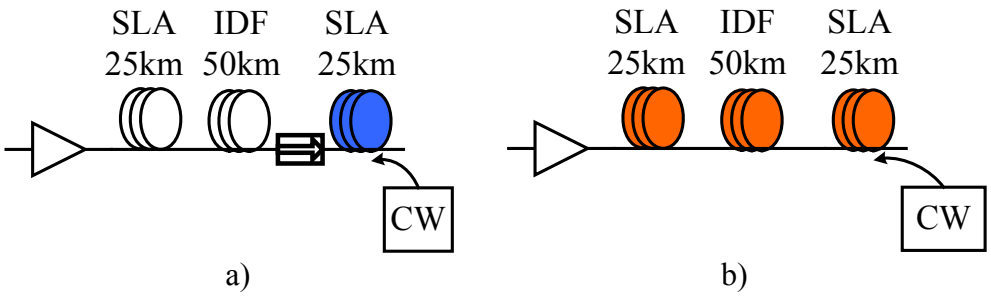

Figure 4.8. Backward Raman pumping a) discrete and, b) distributed.

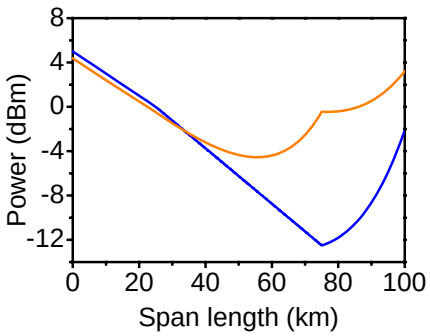

Figure 4.9. Optimal power evolution for discrete (blue) and distributed (orange) Raman amplification for longest transmission, respectively.

We optimize the launched signal power and pump power based on longest transmission distance available for each set-up. The pulse width is 1 ps. We find that the system performance of distributed Raman amplification is much better than that of discrete amplification with nearly doubled transmission distance.

Figure 4.9 gives the optimal power evolution based on Figure 4.8 for the two set-ups. It shows nearly the same launched signal power of 5 dBm. The average signal power by distributed Raman amplification

is higher because the IDF and SLA both provide Raman gain, thus the OSNR presents a slower decrease with respect to a longer distance.

However, the higher signal power also gives higher nonlinear phase shift described as $\phi_{NL} = \int_0^L \gamma P_s(z)dz$ ($\phi_{NL} = \sum_{i=1..n} \gamma P_i \Delta l$, $L = \Delta l \cdot n$ in numerical formulation) and MPI. Here L is the fiber length. P_i is the particular power in fiber piece number *i*. Table 4.2 gives the calculated ϕ_{NL}, OSNR and MPI are measured by the VPI simulator. From Table 4.2 we see that although the nonlinear phase shift and MPI of distributed Raman amplification are larger than for discrete Raman amplification, the OSNR is also larger. This indicates that the OSNR is the dominant limiting factor in system performance.

Table 4.2 Comparison of two pumping schemes

	With Isolator	Without Isolator
OSNR	39.3 dB	42.6 dB
Normalized nonlinear Phase shift ϕ_{NL}	0.75	1
MPI	-51.5 dBm	-43.8 dBm

Figure 4.10 shows the optimal power combination for longest transmission distance in the two cases. With distributed Raman amplification, the pump power can be reduced by 400 mW compared to discrete amplification. Furthermore, compared to 1400 km system reach for discrete backward amplification about 2600 km system reach, i.e. nearly twice as much, can be obtained by distributed amplification.

In brief, discrete pump schemes have been compared for 160 Gbit/s single channel systems. The optimal pumping scheme is found to be IDF pumping in the middle of the span. Transmission distance of 1800 km can be obtained with a span length of 100 km using symmetrical SLA and IDF dispersion map. Optimal pump power range is stable against pulse width variation. In all the cases shorter pulses give better performance. Optimization of signal and pump power is critical in reaching best balance between OSNR, nonlinearities and Raman noise. The dominant limiting factor is not nonlinearity and MPI, but OSNR. Consequently, fully distributed amplification offers much longer system reach with higher OSNR.

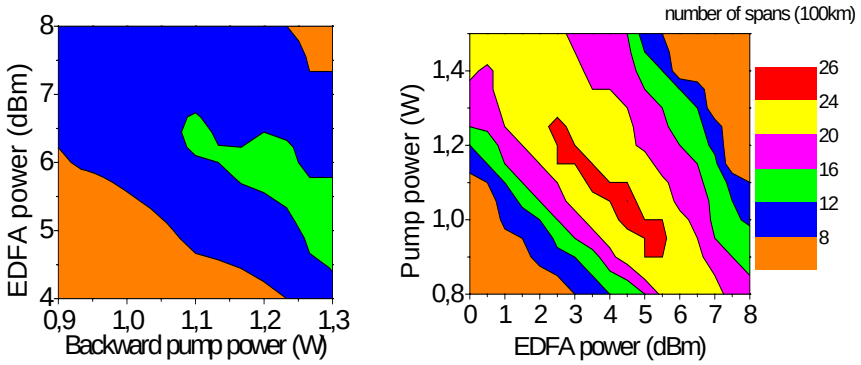

a) b)

Figure 4.10. Optimal combination of EDFA power and pump power for longest system transmission. a) Discrete backward pumping, b) distributed backward pumping.

4.2 Distributed Raman assisted system

Distributed Raman amplification has emerged as a most attractive amplification scheme in recent research on 40 Gbit/s WDM transmission with merits of uniform gain profile and up to 10 THz dynamic operation bandwidth [49]. Pure Raman or hybrid Raman/erbium amplifications have been suggested [50, 51] as a way to improve the in-line signal to noise ratio in 160 Gbit/s per-channel WDM systems compared to using lumped erbium doped fiber amplifiers. Recent simulations indicate that symmetrical dispersion maps are favourable in case of distributed amplification [52]. Management of effective area and the noise performance have also been investigated in dispersion managed fiber spans [53, 54].

In this section, we focus on 160 Gbit/s single channel systems and the use of distributed Raman amplification. With realistic super large effective area fiber and symmetrical dispersion map, we investigate three Raman pumping configurations, backward pumping, bi-directional pumping and second-order pumping. In order to obtain a proper balance between nonlinearity and OSNR, the signal evolution inside a span is adjusted by changing signal and pump power toward

the maximum system reach. The pumping configuration characteristics and optimum span lengths for the systems are presented.

4.2.1 Principle of pumping schemes and model setup

Raman Model

In the model, we included the Raman noise sources mentioned above in the signal spectrum, which would be the case in reality, thus the balance between smaller power variation and generated Raman noise should be carefully designed. In principle, the coupled wave equations give a simple description of Raman effect in the fiber as mentioned in Chapter 2.1.2.

Because of the large spectral width of a 160 Gbit/s RZ signal, the coupled equations must include pump depletion, spontaneous Raman emission, Rayleigh backscattering, multiple Rayleigh backscattering and intra Raman effects within the signal spectrum. The Raman models we use consider all these effects as mentioned in Chapter 2.1.3. The power evolution of each frequency component is calculated in an iterative way by coupling itself with all other frequency components propagating in the forward and backward direction into account. With respect to signal evolution in the time domain, the nonlinear Schrödinger equation (NLSE) is solved numerically using the split step method at more recent VPI model. In addition to dispersion, dispersion slope and SPM, the NLSE also takes intra pulse Raman scattering and XPM effects into account, which are necessary for treating the short pulses used as the 160 Gbit/s signals.

Simulation Parameters and Span Configurations

Transform-limited Gaussian pulses at 1552 nm with a full-width-half-maximum of 1 ps are encoded with a PRBS length of 2^{10} –1 [47] and launched into the transmission span. Symmetrical dispersion management is used with 35 km super large effective area (SLA) fiber at both ends and 35 km inverse dispersion fiber (IDF) in the middle of the span. Table 4.3 gives the values of the fiber parameters for the SLA and IDF. Here D is the dispersion, S the dispersion slope, n_2 the nonlinear index, A_{eff} the effective area, g_R the Raman gain coefficient and η the Rayleigh backscattering coefficient. For simplicity we

assume that the nonlinear index, fiber loss and effective area are wavelength independent.

Table 4.3 Fiber parameters

	D	S	n_2	Loss	Aeff	g_R	η
	(ps/nm/km)	(ps/km/nm^2)	(m^2/W)	dB/km	μm^2	(1/W/km)	(1m)
SLA	20	0.06	2.23×10^{-20}	0.2	105	0.3	4×10^{-8}
IDF	-40	-0.12	2.37×10^{-20}	0.25	30	1.28	16.6×10^{-8}

A third order Gaussian optical filter with a 5 nm bandwidth and a 110 GHz bandwidth electrical Bessel filter are used at the receiver. An analytical fit to the Raman gain response of pure silica fiber [8] is used, with accurate experimental values for the gain peaks in the SLA and IDF.

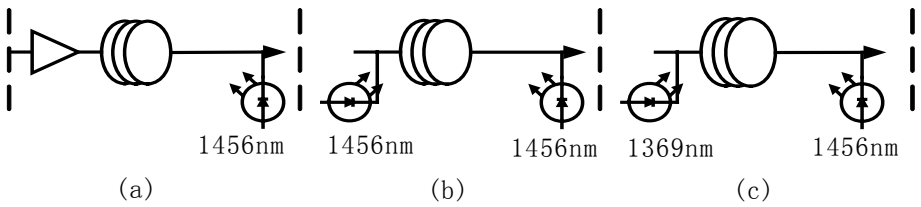

Figure 4.11. Pumping configurations: (a) backward pumping, (b) bi-directional pumping, (c) second order bi-directional pumping.

The three Raman pump configurations are illustrated in Figure 4.11. For backward pumping a), the pump is placed at the end of the span, while an EDFA with 5 dB noise figure is used at the input. The bi-directional pumping scheme b) uses two pumps at 1456 nm wavelength, whereas in the second order pumping configuration c), a backward pump at 1456 nm and a forward pump at 1369 nm are used. The pump at 1369 nm has the maximum gain at 1456 nm. Thus the 1456 nm pump power can be amplified by pump power at 1369 nm during propagation along fiber and consequently will not decrease quickly due to fiber loss and has more remain power to amplify the signal.

4.2.2 Optimization of Signal power evolution and pump power

For all the results presented below, a BER of 10^{-9} is taken as the criterion for defining the maximum system reach.

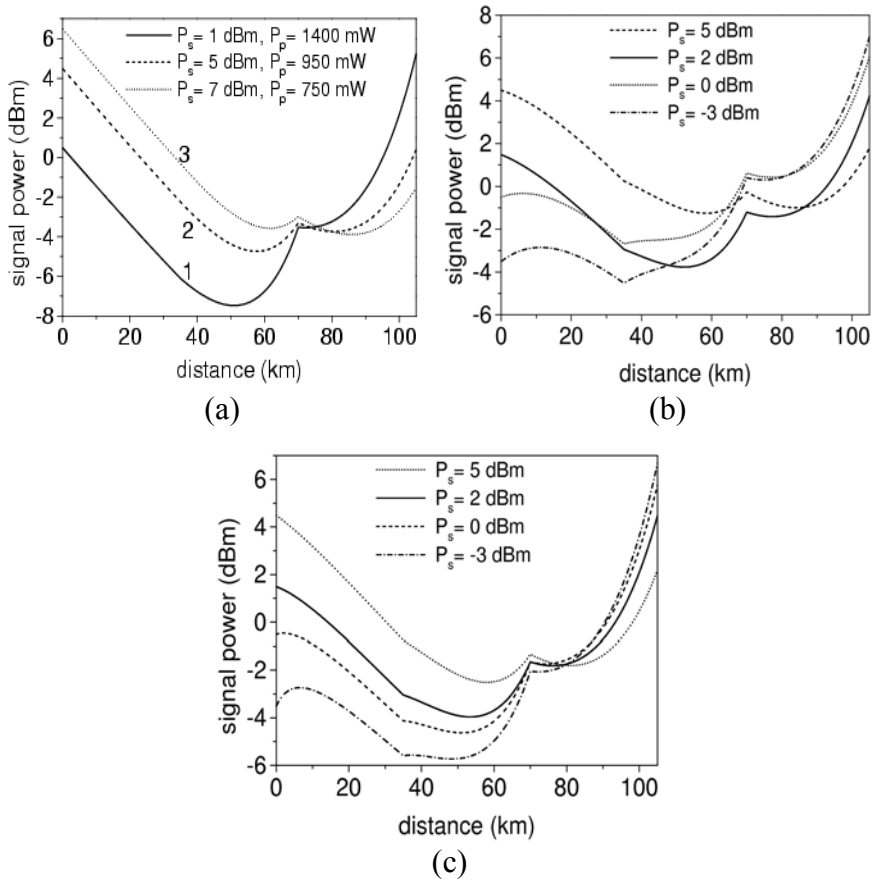

Figure 4.12. Signal power evolution in a 105 km span for (a) backward pumping, (b) bi-directional pumping, (c) second order bi-directional pumping. The pump powers in (a), (b) and (c) have been set to maximize the transmission distance for –3, 0, 2 and 5 dBm span input signal power, respectively.

Figure 4.12 shows the optimal signal power evolution resulting in

the longest system reach for all three pumping configurations, while Figure 4.13 shows the systems reach contours as a function of signal and pump power for each pump configuration.

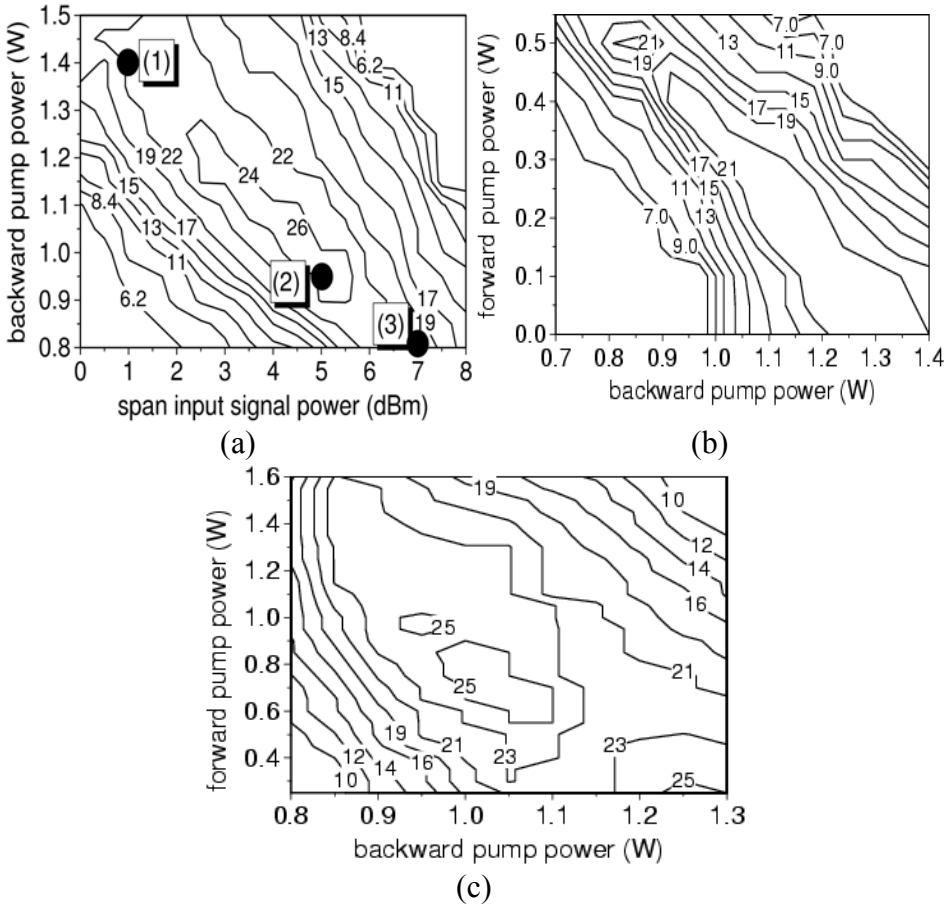

Figure 4.13. Number of transmitted 105 km spans as a function of (a) span input signal power and pump power for backward pumping, (b) backward and forward pump power for bi-directional pumping; (c) backward and forward pump power for second order bi-directional pumping.

In Figure 4.12 a) curves 1, 2 and 3 correspond to the three sets of span input signal power and backward pump power indicated with points in Figure 4.13 a). Curve 2 presents the signal power distribution

along the fiber span for longest system reach. Curve 1 and 3 present signal power distributions in case of 15% degradation of the system reach. Curve 1 is expected to result in less nonlinearity accumulation compared to curve 2, but the system reach is degraded due to reduction in OSNR stemming from more Raman induced noise. This suggests the existence of a minimum signal power limit in the power distribution. Curve 3 corresponds to less Raman induced noise because of lower pump power, but nonlinearity accumulation is higher than for curve 2 and becomes the limiting factor.

Hence, there is also an upper limit for the signal power distribution set by nonlinearities. The optimized signal power evolutions for longest reach are also shown in Figure 4.12 b) and c) for bi-directional and second order pumping at different input signal power, respectively.

For all investigated pumping configurations and signal input power levels, it can be seen that the signal power has to remain above –6 dBm within the span to get optimal results. In all optimal system reach cases, although large signal power variations can be tolerated in both SLAs, the lowest signal power in the span is reached within the IDF. Therefore there is a trade-off between OSNR and nonlinearity, which means the IDF constitutes a nonlinearity bottleneck in the system.

For all the pumping configurations, about the same optimal longest distance of 2500 km is reached. From Figure 4.13, we define the optimal power operation range for the three pumping configurations to be within 15% shorter reach compared to the maximum transmitted distance of 2500 km, i.e. in the 2200 - 2500 km range. In the backward pumping case the optimum pumping power range is 200 mW. However, for bi-directional pumping both pump power levels are much more critical, the tolerance of the optimum range for both pump powers decreases from 200 to 100 mW. In the second order pumping case the pump power tolerance is the largest, namely more than 200 mW for the backward pump power and more than 600 mW for the forward pump power.

4.2.3 Pump schemes comparison and span length

For both bi-directional and second order pumping, extensive calculations have been performed of longest transmission distance for different span input signal power levels. The results are shown in

Figure 4.14. It is clear from Figure 4.14 that backward pumping is most sensitive to decreasing incident signal power due to OSNR limitations, while second order pumping offers large tolerance to decreasing signal power. Above 2200 km system reach, second order pumping can accept around 9 dB span input signal power variation, while for bi-directional and backward pumping it is limited to 5 and 3 dB. The results from Figure 4.13 and Figure 4.14 indicate that for a single channel system, backward pumping has acceptable pump power margin; it is also the simplest and most practical pumping scheme. Second order pumping offers the largest pump and span input signal power tolerance. Furthermore, it has good potential for being used in WDM transmission at 160 Gbit/s because it allows lower incident signal power, which mitigates nonlinear degradation between channels. On the other hand, it is also a more costly pumping scheme.

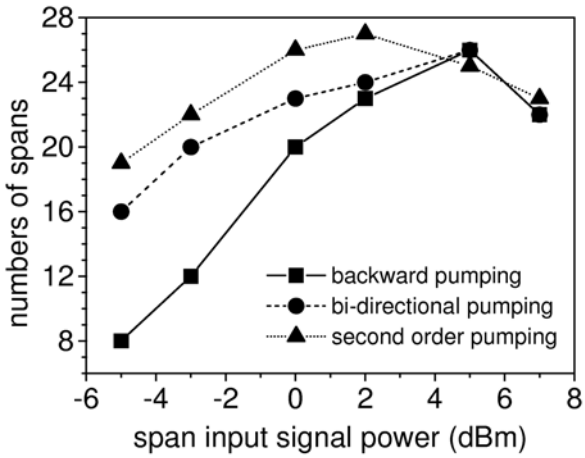

Figure 4.14. Maximum transmitted spans as a function of span input signal power. Span length is 105 km.

Since backward pumping has good performance and is the simplest and most cost effective pumping scheme, we focus on backward pumping in the following.

We now investigate the influence of span length on the system reach by scaling the fiber length linearly without changing any other fiber parameters. From Figure 4.15 it is clear that the longest transmission distances have large span length tolerance. The span length can be increased from 45 to 120 km while maintaining a system

reach above 2500 km. The large span loss tolerance is very beneficial for practical designs.

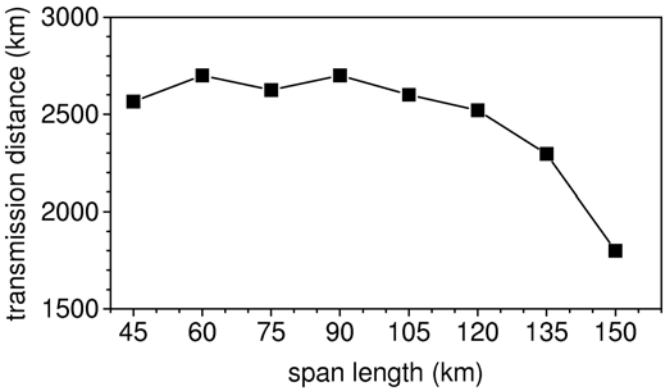

Figure 4.15. Longest transmission distance versus span length for backward pumping.

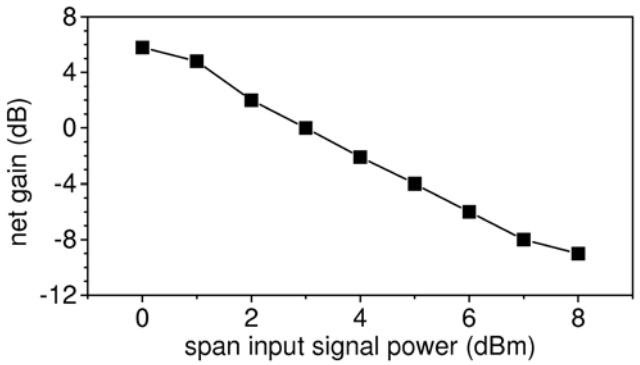

Figure 4.16. Net-gain versus span input signal power for backward pumping with 105 km span length.

The signal net gain, defined as the ratio between output and input signal power was also investigated. For each incident signal power in case of optimum system reach, the net gain as a function of span input signal power is shown in Figure 4.16. The data are collected from the power contour in Figure 4.12 a). More than 6 dB positive net gain can be realized while still maintaining good performance, which means

that placing an EDFA before the span is not necessary, instead the positive net gain can be used to compensate insertion loss between the spans.

In conclusion, 160 Gbit/s single channel transmission using a scheme consisting of two SLA fibers separated by one IDF fiber and Raman amplification has been investigated numerically. Backward pumping, bi-directional pumping and second order pumping were investigated. For the three schemes about the same systems reach of 2500 km was obtained. For the single channel system considered, backward pumping is not only the simplest configuration, but it also offers good pump power margin. Second order pumping shows the largest pump power and input signal power tolerance. All three configurations offer a span length tolerance of 45 to 135 km and positive net gain can be obtained. Second order pumping could be more attractive for WDM applications because it allows lower input power levels that would mitigate the influence of nonlinearities.

4.3 Modulation format comparison on system performance

New modulation formats that offer large dispersion and nonlinear tolerance pave the way to greatly increased system capacity and transmission distance [55]. Recent research on high bit rate systems above 40 Gbit/s emphasize employing modulation formats such as DPSK and DQPSK [56,25].

At 160 Gbit/s, modulation formats are also investigated both in simulations and experiments [57]. However high speed electronic components have not yet been developed for 160 Gb/s. For instance the method to generate phase-modulated format at 160 Gbit/s is under investigation. Recently, RZ-DPSK format was used in a single channel 160 Gbit/s transmission system based on polarization multiplexing and an integrated chip as transmitter [44]. However, the 160 Gbit/s RZ-DPSK signal is aggregated by optical time-division multiplexing of 4 channels of 40 Gb/s RZ-DPSK signals, thus the generated 160 Gbit/s signal is not strictly phase related between adjacent bits. Recently, Bell Labs put forward new proposals on generating the real CSRZ and RZ-

DPSK modulation formats at 160 Gbit/s by controlling the polarization state evolution in a fiber [58,59]. However, DQPSK is not investigated in 160 Gbit/s systems up to now.

In this section, we investigate dispersion and nonlinearity tolerance of modulation formats for 160 Gbit/s systems based on SSMF&DCF spans. The RZ-DQPSK modulation format is compared with RZ, CSRZ, RZ-DPSK and CSRZ-DPSK in 160 Gbit/s single channel systems for the first time. We find that RZ-DQPSK offers nearly three times better dispersion tolerance than CSRZ-DPSK. We compare RZ, RZ-DPSK and CSRZ-DPSK modulation formats for Raman amplified single channel systems. It is found that the RZ-DPSK format gives the longest system reach compared to other formats. The dispersion map is also investigated for different modulation formats based on SSMF&DCF spans.

4.3.1 Dispersion and nonlinearity tolerance for different modulation formats

The system set-ups for different modulation formats are illustrated in Figure 4.17. The generation methods for the various modulation formats are described as follows.

To obtain the RZ format with duty cycle of 50% and the CSRZ format, the CW light is modulated by a Mach-Zenhder modulator by using proper bias and voltage swing.

The DPSK signal is generated by a phase modulator; subsequently it can be carved to RZ or CSRZ pulse shape. The DPSK data generated by the DPSK pre-coder is then applied a phase modulator (PM), which then transfers the data to the CW light. The generated optical DPSK signal is then launched into a MZ modulator to carve RZ or CSRZ pulse shapes. As a result RZ-DPSK or CSRZ-DPSK signals are generated. A DQPSK signal needs two 80 Gb/s DPSK encoders with uncorrelated data sequences accompanied by $\pi/2$ phase shift between them [60].

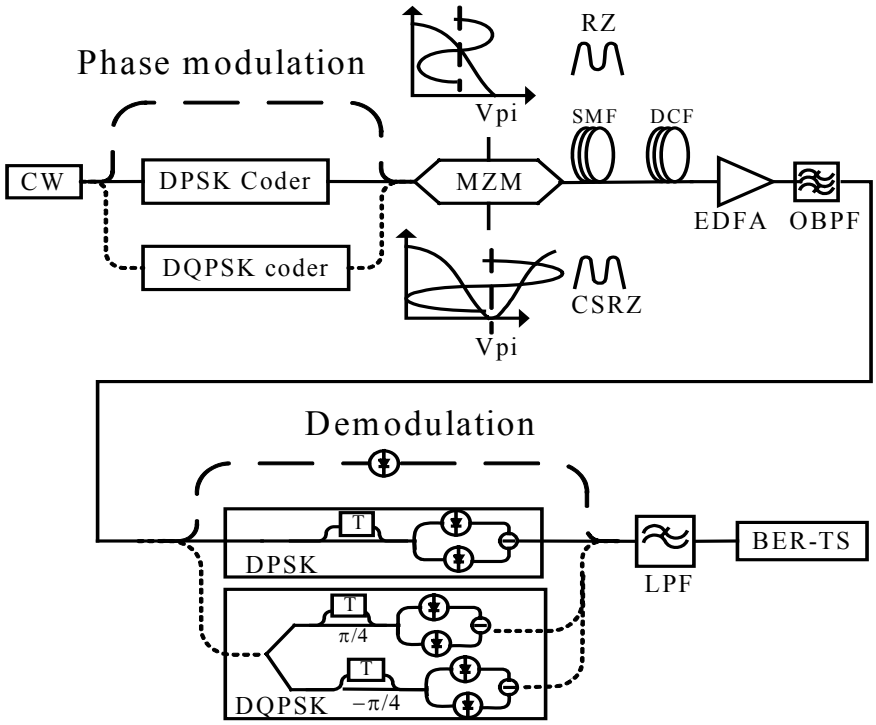

Figure 4.17. Setup for generation, transmission and demodulation of the different modulation formats.

OBPF: optical bandpass filter, LPF: electrical low pass filter

In the receiver, following an EDFA as preamplifier with 4 dB noise figure, a one-bit delay MZI is needed to demodulate the family of DPSK signals. For DQPSK, two interferometers are needed to decode the two tributary data sequences. Balanced detection is used for the family of DPSK signals.

The transmission span is composed of 80 km SSMF and 12 km DCF with complete dispersion and slope compensation. The dispersion parameter of the SSMF is 15 ps/nm/km, for the DCF -100 ps/nm/km.

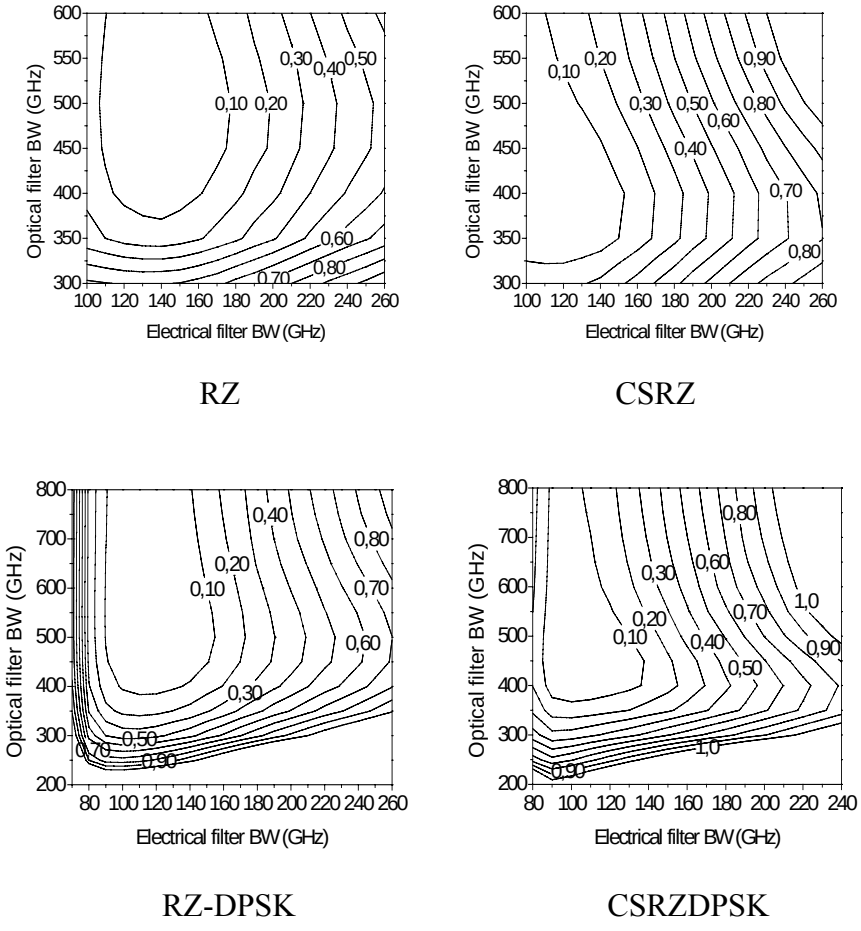

Figure 4.18. Optical and electrical filter bandwidth optimization of penalty in dB from highest receiver sensitivity for different modulation formats.

For each modulation format, we use third-order Gaussian optical filter and third-order Bessel electrical filter. By optimizing the bandwidths of the filters in terms of maximum receiver sensitivity for the corresponding modulation formats separately, we get the optimal filter bandwidth. Figure 4.18 shows contour plots of penalty in dB from highest receiver sensitivity versus optical and electrical filter bandwidth for each modulation format. It can be seen that the optimal DPSK receiver requires a narrower electrical filter bandwidth

compared to OOK. The electrical filter bandwidth of RZ, CSRZ, RZ-DPSK and CSRZ-DPSK is then 100, 90, 90 and 85 GHz, respectively. The optical filter bandwidth is 500, 400, 550 and 400 GHz, respectively.

However, the Gaussian assumption of noise probability density distribution for PSK signals is not accurate; we get a sensitivity enhancement of 2.3 dB for NRZ-DPSK compared with NRZ, while only 1.7 dB for RZ-DPSK compared with RZ. We use eye-opening penalty (EOP) 1dB as criterion to describe the signal degradation in systems. The eye-opening at the receiver is normalized to the back-to-back eye-opening according to EOP=$10\log_{10}$(eye-opening at reciever/B2B eye-opening).

One span results

Figure 4.19 shows the normalised eye-opening as a function of residual dispersion obtained by varying the DCF length, for a span average input power of 0 dBm. The dispersion tolerance of 1 dB eye opening penalty is equal to 1.4, 2.4, 1.5 and 2.2 ps/nm for RZ, CSRZ, RZ-DPSK and CSRZ-DPSK. However, the most significant improvement is offered by RZ-DQPSK, where dispersion tolerance exceeds 6.2 ps/nm.

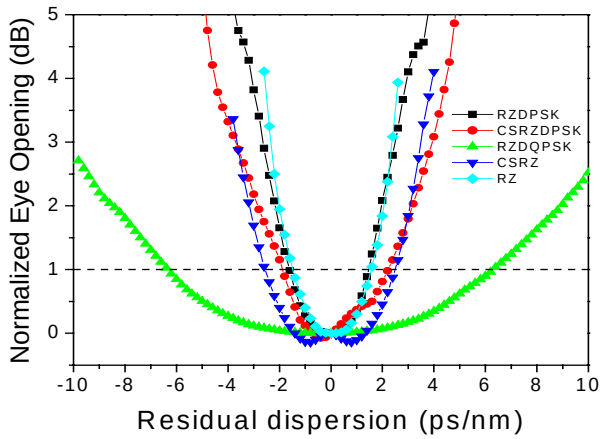

Figure 4.19. Normalized eye opening vs. span residual dispersion for the five modulation formats.

Figure 4.20 shows the tolerance to launched power for the five modulation formats. It can be seen that RZ-DQPSK not only offers improved dispersion tolerance, but also results in resilience to self-phase modulation similar to that of CSRZ and CSRZ-DPSK.

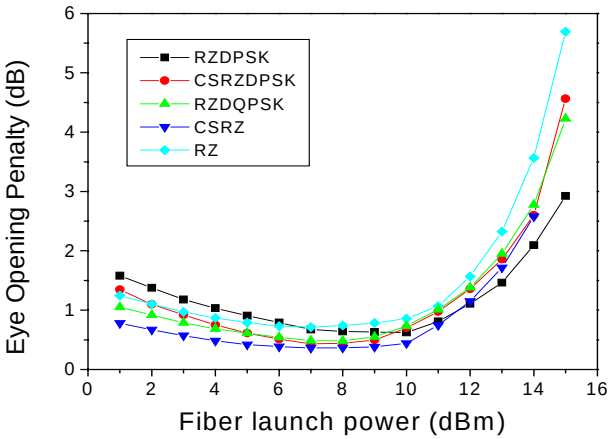

Figure 4.20. Eye-opening penalty vs. span launch power for the five modulation formats.

From the discussion, we find that for single channel systems, the RZ-DQPSK format has much larger dispersion tolerance than the other modulation formats, and similar sensitivity to fiber nonlinearity compared to other DPSK related formats.

Three span results

We investigate RZ, CSRZ, RZ-DPSK and CSRZ-DPSK in the same system set-up as shown in Figure 4.17 but with 3 spans. The margins for both dispersion and nonlinearity are calculated for an eye-opening penalty of 1 dB. The residual dispersion is obtained by changing DCF length.

Figure 4.21 shows contour plots of receiver penalty in dB after three spans each using post DCF compensation. It can be seen that the carrier-suppressed formats as CSRZ and CSRZ-DPSK outperform RZ and RZ-DPSK in terms of dispersion tolerance. Furthermore, RZ-DPSK and CSRZ-DPSK are more robust to ASE noise with lower OSNR, which shows the advantage of balanced detection. CSRZ-DPSK has the largest dispersion margin of 2 ps/nm and is most robust

to accumulated ASE noise. RZ has narrowest dispersion tolerance of 0.6 ps/nm. However, the nonlinear upper limit in the simulation of the different modulation formats is identical as 7dBm.

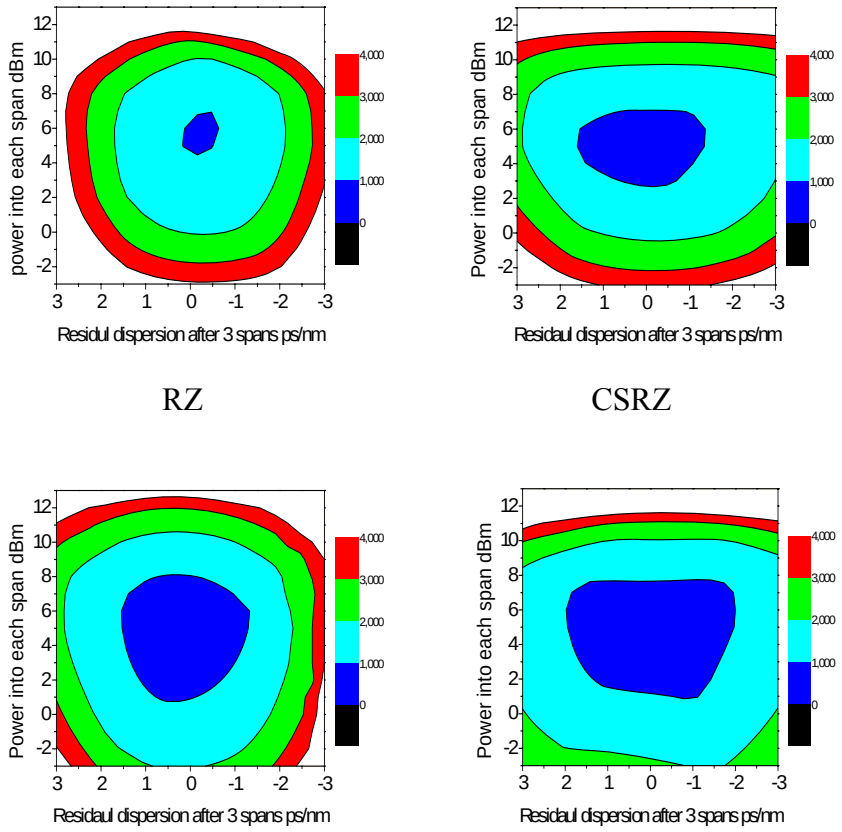

Figure 4.21. Contour plot of receiver penalty vs. residual dispersion and span input power for four modulation formats after three spans with post DCF compensation (Penalty range 0-4 dB).

4.3.2 Dispersion management for different modulation formats based on SSMF+DCF span

Dispersion map is one of the key techniques to obtain an optimized balance between dispersion and nonlinearity. The approach is to choose the different fiber sections in the link in an optimal way to give a better dispersion design. The aim is to provide the system with higher tolerance to dispersion and nonlinearity induced effects such as SPM and XPM. Another approach is to use new kinds of fiber to reduce the nonlinearity and allow a higher input signal power. Some research on 160 Gbit/s systems have been published as the EDFA and DCF positions in the span are studied, and then the proper input power to each section of fiber is determined [61,62]. In this section, various modulation formats are adopted to investigate the effect on the decision of optimized dispersion map.

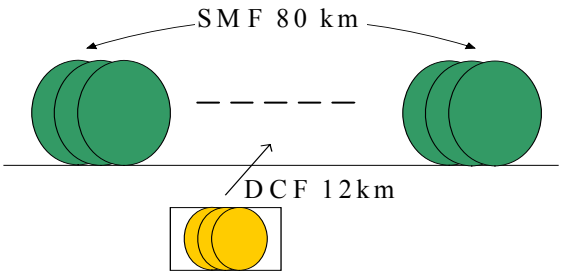

Figure 4.22. Dispersion map of SSMF+DCF span.

The length of the SSMF and DCF is 80 and 12 km, respectively. The dispersion of the SSMF and DCF is 15 and -100 ps/nm/km, respectively. The dispersion maps are investigated by changing the DCF position in the 80 km of SSMF as shown in Figure 4.22. We investigate the modulation format effect on the dispersion map design. The results are shown in Figure 4.23 for an EOP of 1 dB. The RZ-DPSK accepts largest power margin of 7 dB, while it is 6 dB, 3 dB and 2 dB for CSRZ-DPSK, CSRZ and RZ, respectively. Pre-compensation is better for RZ and RZ-DPSK format. This can be understood that the narrower pulse compared to CSRZ and CSRZ-DPSK broadens quicker, then it is better to recover it early before it is dispersive and get deteriorated too much. Therefore in the design of dispersion map, RZ and RZ-DPSK format prefer a dispersion compensation taken place close to the beginning of the span.

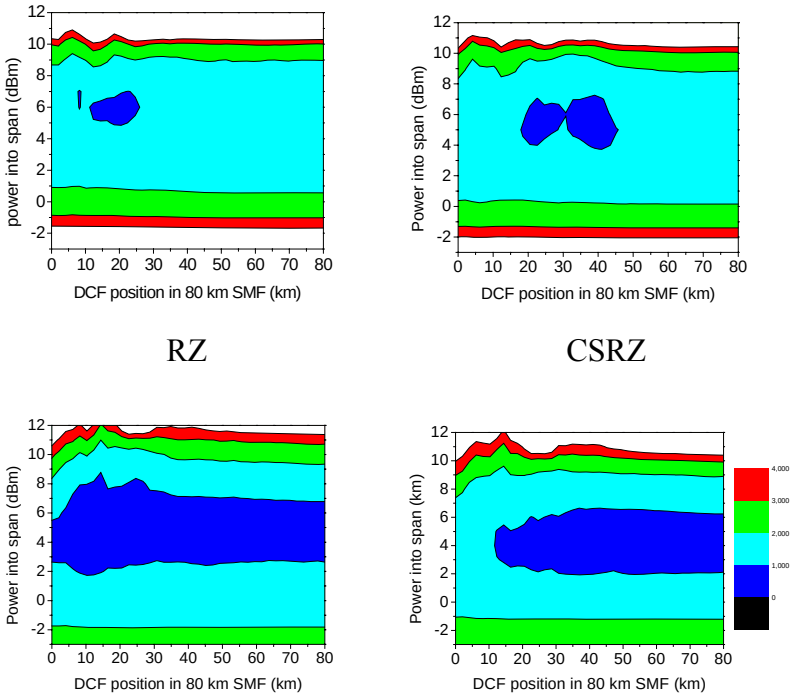

Figure 4.23. Contour plots of EOP in dB vs. DCF position and span input power for the four modulation formats after four spans.

Recently a new proposal pertaining to WDM systems has appeared. The dispersion management of the whole link can be designed by optimal choice of three main parameters, namely the pre-compensation, in-line-compensation and post–compensation along the link. This topic is treated in Chapter 6.

4.3.3 Transmission based on Raman amplification and various modulation formats

Based on the investigation above, it is possible to evaluate the longest system distance reach under a combination of Raman amplification

and modulation format. Figure 4.24 illustrates the system set-up. The continuous wave is carved by a MZM, so the generated pulse width is much broader than 1 ps we used in section 4.1 and section 4.2. In this case we use a duty cycle of 50% for RZ and RZ-DPSK pulses.

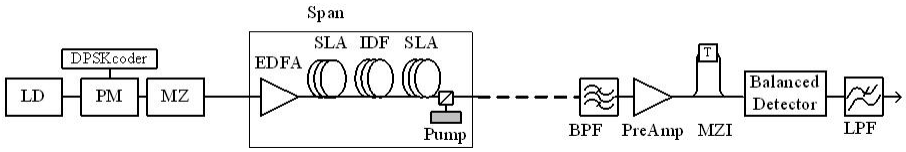

Figure 4.24. Single channel system set-up using Raman amplification.

We still use symmetrical span configuration with a span length of 105 km. Instead we adopt IDF-typeII with two times larger dispersion and dispersion slope than IDF-typeI to expect less nonlinearity from the shorter IDF length in the span. The fiber parameters are listed in Table 4.4.

Table 4.4 Fiber parameters

	Length(km)	D(ps/nm/km)	D. slope (ps/nm/nm/km)	Loss (dB/km)	Max gain coefficient (1/W/km)
SLA	35	20	0.06	0.2	0.3
IDF	35	-40	-0.12	0.25	0.9

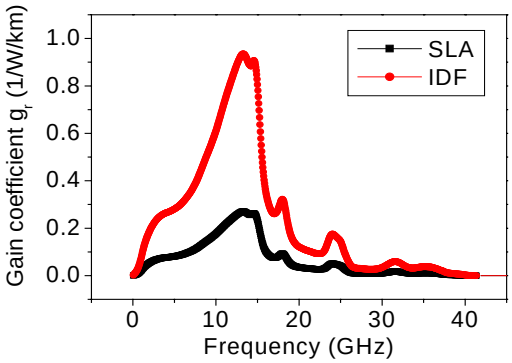

Figure 4.25. Realistic gain profile of SLA and IDF used in simulation.

Since through simulation in section 4.2, we found nearly the same

performance for the different pumping schemes, we use backward pumping at 1450 nm for simplification in the following discussion. Here we carry out the simulation with the measured real gain profile of SLA and IDF-typeII as shown in Figure 4.25. The receiver adopted a 3rd order Gaussian optical filter and a 3rd order Bessel electrical filter. The optimized filter bandwidths corresponding to different modulation formats are used in the simulation. A MZI and a balanced detector are used to demodulate RZ-DPSK format.

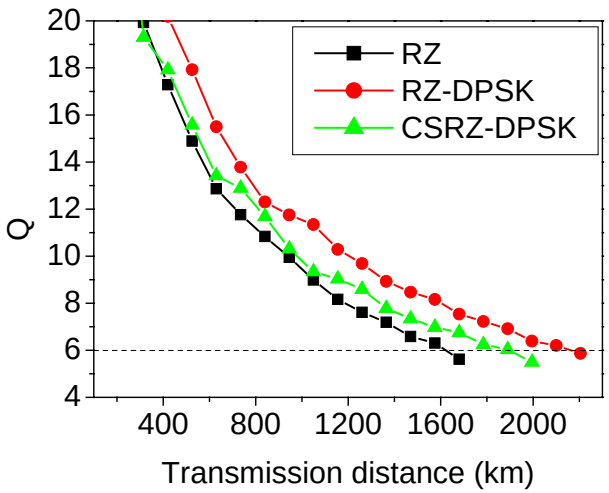

Figure 4.26. Longest transmission distance for RZ, RZ-DPSK and CSRZ-DPSK by optimizing signal and pump power.

We optimized both pump and signal powers to get longest transmission distance at Q=6. Figure 4.26 gives the longest transmission distance for single channel systems for RZ, RZ-DPSK and CSRZ-DPSK formats. The 3 dB receiver sensitivity improvement from DPSK and balanced detection is advantageous; the transmission distance can be increased significantly above 2000 km. RZ-DPSK gives longest system reach of 2300 km due to narrower pulse width compared to CSRZ-DPSK pulse width the reason being that the pulses disperse quicker and therefore suffer less SPM. The investigation of this topic for WDM systems will be discussed in Chapter 6.

4.4 Summary

To obtain the longest system reach, 160 Gbit/s single channel transmission using a scheme consisting of two SLA fibers separated by one IDF fiber and Raman amplification has been investigated numerically. Optimization of signal and pump power is critical in reaching best balance between OSNR, nonlinearities and Raman noise.

Two kinds of Raman amplification are concerned. Discrete pump schemes have been compared and the optimal pumping scheme is found to be IDF pumping in the middle of the span. Transmission distance of 1800 km can be obtained with a span length of 100 km using symmetrical SLA and IDF dispersion map. Three different distributed Raman amplification schemes: backward pumping, bi-directional pumping and second-order pumping are evaluated numerically. For the three schemes about the same systems reach of 2500 km was obtained with a 105 km span. Backward pumping is not only the simplest configuration, but it also offers good pump power margin. Second order pumping shows largest pump power and input signal power tolerance.

In addition, various modulation formats such as RZ, CSRZ, RZ-DPSK, CSRZ-DPSK and RZ-DQPSK are compared for 160 Gb/s single channel systems. The RZ-DQPSK format is found to outperform other formats in dispersion tolerance. Subsequently, CSRZ-DPSK shows better dispersion and nonlinearity margin. RZ and RZ-DPSK prefer the early dispersion compensation in the span. However, RZ-DPSK can reach longest transmission distance of 2300 km.

In a brief summary, based on the simulations above, we find the following. 1) Distributed Raman amplification is better than discreet Raman amplification in regard to providing longer transmission systems. 2) By adopting distributed Raman amplification and new kind of fiber SLA+IDF, 2500 km transmission distance can be achieved for 160 Gbit/s single channel systems. 3) Based on the results above, if shorter pulse source for example 1 ps had been used, the generated DPSK would expect to achieve a much longer system reach. 4) The employment of DPSK gives significant improvement on system reach, dispersion margin and ASE tolerance. 5) The DQPSK is potentially advantageous due to its much larger dispersion tolerance if the

transceiver could be integrated in a well-designed condition. 6) The larger effective core area and suitable dispersion could be the next fiber scenario for ultra-high speed systems.

Chapter 5

160 Gbit/s single channel system experiments

Recently, some experiments have been published on 160 Gbit/s single channel systems [63-69]. Field experiment has been demonstrated on 116 km installed SSMF fiber [65]. 300 km of system reach was achieved with EA modulator based OTDM module [66]. Up to now the longest transmission distance of 550 km was demonstrated with SSMF [42]. However, to the best of our knowledge, all the published experiments in [42-44] and [63-69] use EDFA as the in-line amplifier.

In this chapter, as a new feature in our research, we will investigate distributed Raman amplification in single channel 160 Gbit/s systems. The purpose of this chapter is to present investigations on 160 Gbit/s single channel systems to achieve the longest possible transmission distance using different system configurations, and to suggest

improved dispersion map for Raman application. We experimentally characterize distributed Raman amplification in a SSMF based 160 Gbit/s transmission system. The aim of the experiment is to find the optimum Raman pumping scheme to maintain the OSNR in the transmission link, thus potentially increasing the system reach. As a result 174 km error free transmission is obtained, and optimum operation conditions are investigated.

In the second experiment to be reported, we experimentally characterize dispersion maps in 160 Gb/s transmission systems. We investigate two dispersion compensation maps, namely symmetrical and post dispersion map based on Raman amplification in a SSMF transmission span. We find that a post compensation map offers better power tolerance.

5.1 Raman-assisted transmission system based on span of SSMF and DCF

A number of state-of-the-art transmission experiments on 160 Gbit/s single channel systems have been demonstrated. Some experiments use conventional fibre spans based on SSMF and DCF along with EDFAs as in-line amplifiers [64-66]. Recent experiments tend to adopt new types of fibre and various Raman amplification schemes to amplify the signal in the span [50]. However, SSMF is found to offer better dispersion tolerance than some new types of fiber in 160 Gbit/s transmission systems [62].

In this section, we report on our experiment with a 160 Gbit/s single channel system with distributed Raman amplification taking place in both the SSMF and the DCF. The work was performed in cooperation with Leif Oxenløwe and Andrei Siahlo. To the best of our knowledge, this is the first time distributed Raman amplification is employed in a 160 Gbit/s system in the whole span of SSMF and DCF. We achieve a 174 km transmission distance over standard single mode fibre.

5.1.1 Experimental set-up

The experimental set-up is shown schematically in Figure 5.1 in the case of the full 174 km transmission link. The 10 GHz optical pulses at the wavelength of 1557 nm, with full-width-half-maxima width of 2.1 ps, are generated in a mode-locked fibre ring laser. The pulse train is modulated with a 2^7-1 PRBS sequence using a Mach-Zender modulator. Subsequently the optical signal is multiplexed to 160 Gbit/s (MUX). In the MUX the polarisations are adjusted to give the same amplitude on all channels after the polarisation beam splitter (PBS). An optical clock signal is generated simultaneously by intensity modulating a continuous lightwave at 1551 nm with a 10 GHz sinusoidal electrical clock. The 10 GHz sinusoidal electrical clock is the same as the one used to drive the mode-locked fibre ring laser in order to get clock synchronization. The optical data signals and the clock are transmitted together through the fibre spans in order to get the same temporal phase characteristics.

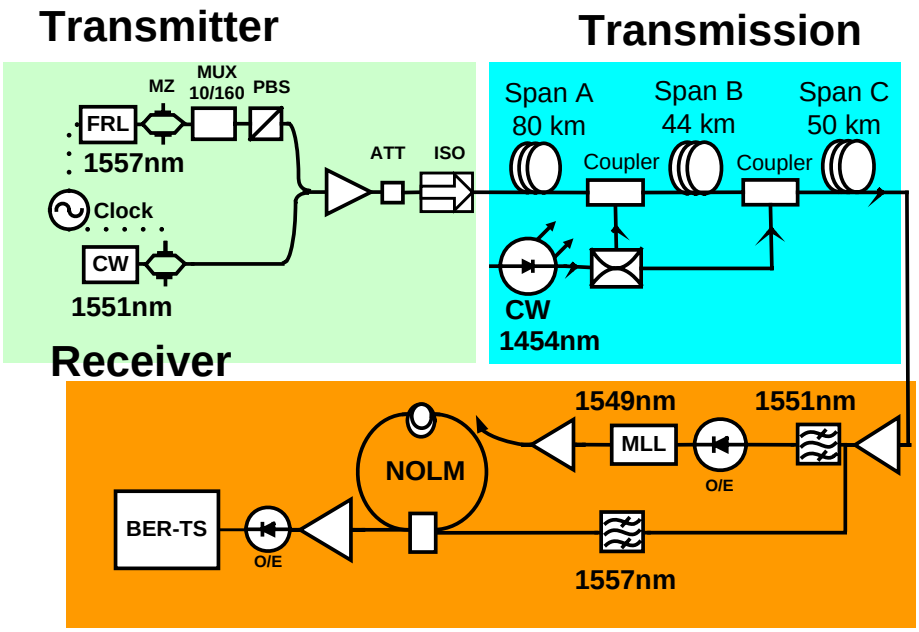

Figure 5.1. Setup for experimental demonstrations of single channel 160 Gbit/s Raman amplified system using three kinds of fiber length and Raman pumping scheme. The transmission link in one case is shown here, all three cases in Figure 5.2.

A high power Raman pump (up to 28 dBm) at the wavelength of 1454 nm is employed in the transmission span instead of in-line EDFAs.

After transmission, the 10 GHz optical clock is filtered out and converted to an electrical clock to drive another mode-locked laser (MLL) which generates 2 ps optical clock pulses with low timing jitter (~200 fs). It is used as the control pulse source to demultiplex the 160 Gbit/s signal to a 10 Gbit/s signal in a non-linear optical loop mirror (NOLM) with 500 m of HNLF (high-nonlinear-fiber). The 10 Gbit/s signal is detected in a pre-amplified receiver and the bit error rate (BER) is measured in a BER test set (BER-TS).

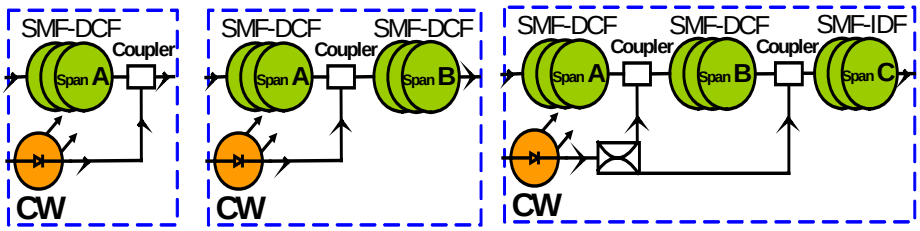

1) 2) 3)

Figure 5.2. Transmission fiber links 1) 80km, 2) 124km and 3) 174km.

The total transmission distance is composed of up to three different spans as shown in Figure 5.2. Span A consists of 80 km SSMF followed by 11.9 km DCF for post dispersion compensation. Span B consists of 44 km SSMF followed by 6 km DCF for post compensation. Span C consists of 26 km SSMF followed by 24 km IDF (inverse dispersion fibre). The losses of spans A, B and C are 25, 12 and 15 dB, respectively. The dispersion at the data wavelength (1557 nm) of span A, B and C is 0.05, 0.05 and -2 ps/nm, respectively. The polarisation mode dispersion (PMD) of the SSMF and the DCF fibres is 0.034 and 0.117 $ps/\sqrt{km}$, respectively.

For all the links, backward pumping is used at the end of the DCF since it has a much larger Raman gain coefficient than the SSMF. The residual pump power also amplifies the signal in the SSMF. In link 1), Raman pumping is used at the end of span A. In link 2), Raman pumping is still used at the end of span A. In link 3), the pump power is split in a 3 dB coupler to obtain backward pumping on both span A and B.

Figure 5.3 a) shows the optimum 160 Gbit/s eye pattern of the signal obtained from an oscilloscope before the signal was injected into the fiber span. The MUX was polarization controlled to give all channels same polarisation and amplitude. The data trace before and after transmission is shown in Figure 5.3 b). The unchanged pulse width indicates good dispersion compensation along the fiber link.

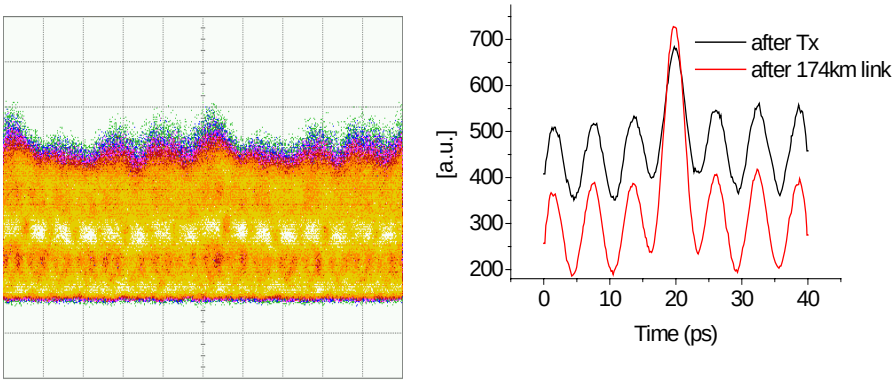

a) b)

Figure 5.3. a) Eye pattern of multiplexed 160 Gbit/s signal after polarisation controlled MUX. b) Autocorrelation trace of data pulse before and after 174km fiber link.

Figure 5.4 shows the pump power characteristic at a pump wavelength of 1454 nm. We found that a high pump power of 800 mW can be obtained, and this can provide a Raman on-off gain of up to 28 dB for 12 km of DCF.

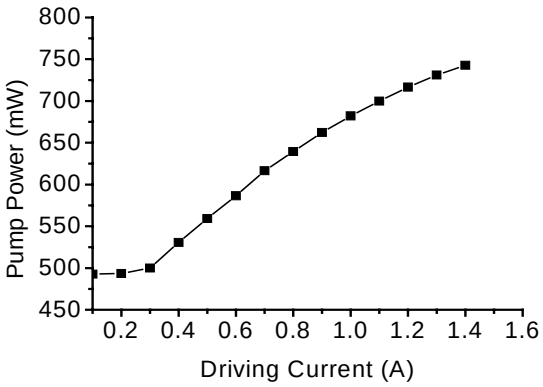

Figure 5.4. Pump power vs. driving current for Raman pump at 1454 nm.

5.1.2 Power characterisation on system performance

Figure 5.5 shows the receiver power penalty versus the total pump power for all three links. It is clearly seen that the optimum system performance is strongly dependent on the pump power. With longer transmission fibre length, the pump power range for minimum penalty becomes narrower and hence more critical. The launched optimum signal power used for the different transmission links is also shown in Figure 5.5 and Figure 5.6.

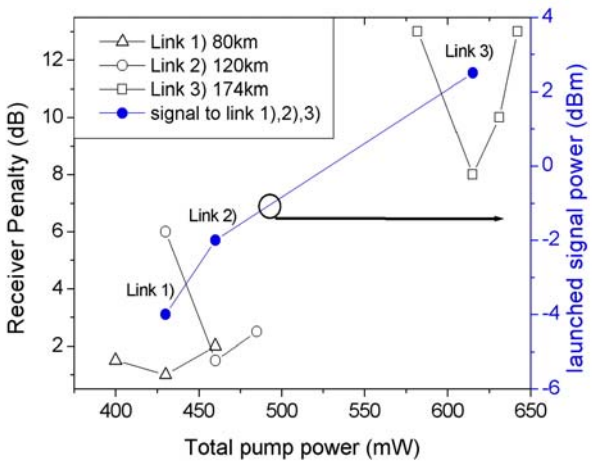

Figure 5.5. Receiver power penalty vs. total pump power for the three transmission links along with corresponding launched signal power.

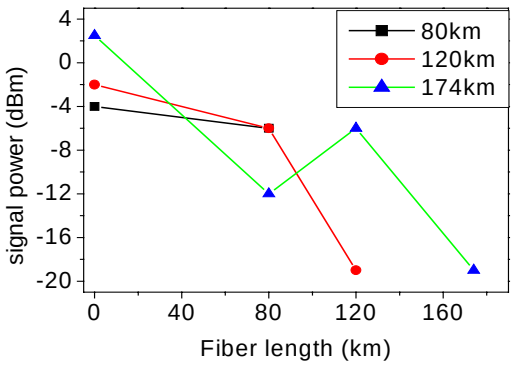

Figure 5.6. Optimal signal power after each span for maximum capability of pump power.

Figure 5.7 shows the BER vs. received power for link 1) with the same pump power but for two different launched signal power levels. Sub-optimum signal power can cause 10 dB more power penalty at a BER of 10^{-9} due to the high span loss induced OSNR degradation.

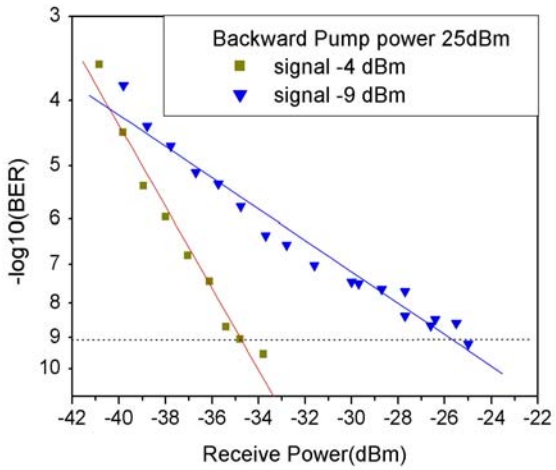

Figure 5.7. Receiver sensitivity vs. input signal power for link 1).

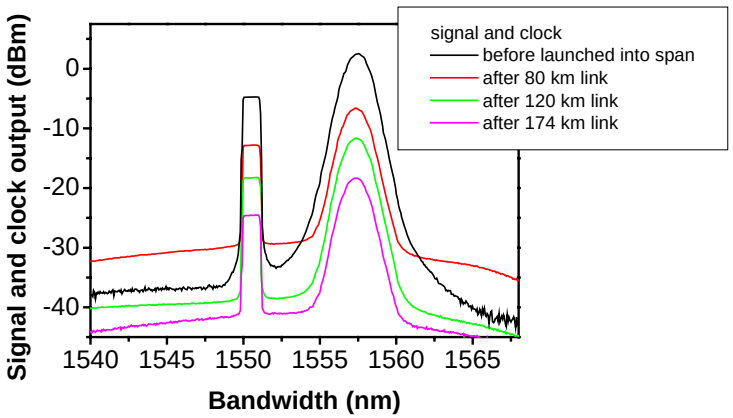

Figure 5.8. Signal and clock spectra before launched into span and after 3 different links, respectively.

Figure 5.8 shows the signal and clock spectrum before being launched into the span and after having passed through three different

fiber links of 80, 120 and 174 km length, respectively. The OSNR of the signal decreased from an initial value of 35 dB to the minimum value of 20 dB after 174 km.

5.1.3 System transmission performance

Figure 5.9 shows the BER performance for different transmission lengths. Raman amplification can give excellent performance for 80 and 124 km spans. The power penalties are only 1 and 2 dB, respectively. For 174 km span length power penalty is 8 dB. One reason is that the dispersion of span C is not fully compensated. Another reason is that, after splitting in the 3 dB coupler, the pump power does not provide sufficient Raman gain for the 174 km link as shown in Figure 5.8. The corresponding Raman on-off gain drops from optimum 23 to 18 dB. A higher launched signal power is needed as shown in Figure 5.8, which in turn results in signal degradation due to fibre non-linearity. Figure 5.10 a) and b) present the 10 G back-back and 160 G/10 G back-back electrical eye diagrams. Figure 5.10 c) and d) present the 160 G/10 G DEMUX optical and electrical eye diagrams after 174 km fiber link.

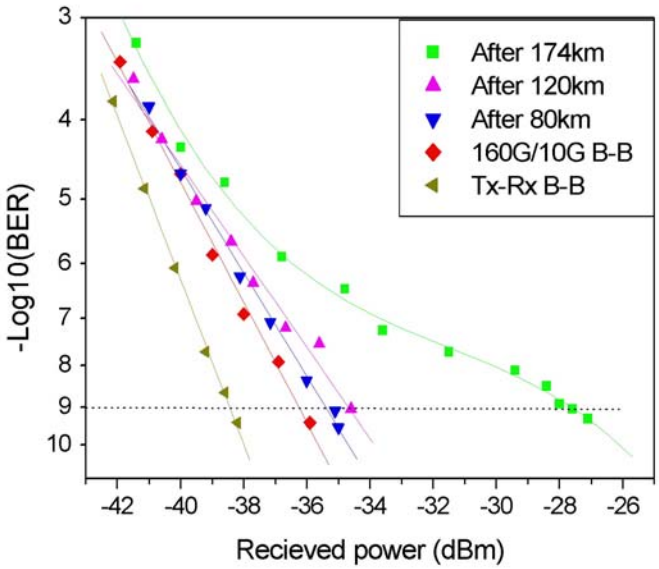

Figure 5.9. BER performance for different transmission links.

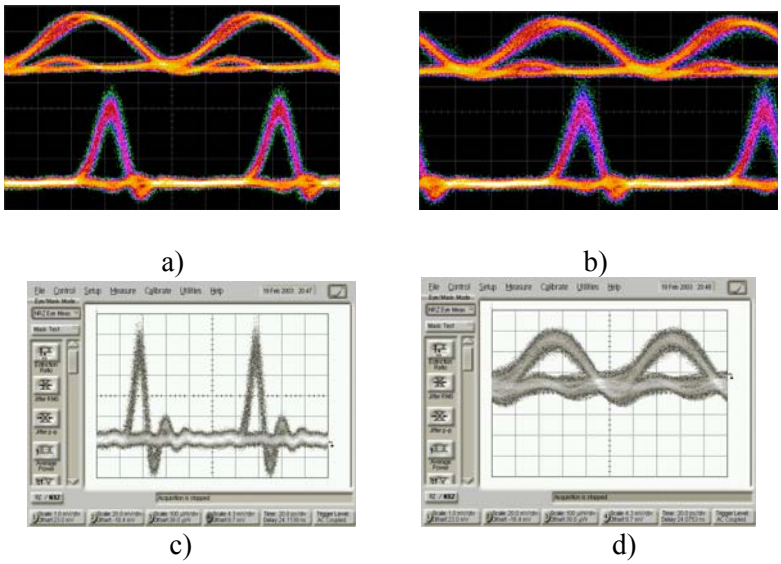

Figure 5.10. Eye diagrams. a) Tx-Rx 10G B-B, b) 160 G/ 10 G B-B, c) demux to 10Gbit/s after 174km measured with 50G bandwidth, d) demux to 10Gbit/s after 174km measured with 10G bandwidth.

We have demonstrated, for the first time, 160 Gbit/s single channel transmission using distributed Raman amplification in both the SSMF and DCF. A transmission distance of 174 km was achieved by optimizing both pump power and launched signal power. This suggests a potential for easy upgrading of existing installed fiber systems to 160 Gbit/s Raman amplified systems – ignoring safety problems associated with the use of very high pump powers in practical installations.

5.2 Dispersion map optimization with Raman amplification

Dispersion maps have been investigated for single channel EDFA-based transmission systems experimentally [4]. The results show that for 160 Gbit/s systems larger effective core area is preferable. However with Raman amplification, an investigation of the combination of dispersion management and Raman amplification is

interesting and meaningful. In this experiment, we investigate the combined effects of dispersion compensation and Raman amplification in a SSMF-based 160 Gbit/s single channel system. The optimum dispersion map is proposed.

5.2.1 Schematic of experimental set-up

A schematic of the experimental set-up is shown in Figure 5.11. A 10 GHz pulse train is generated by a mode-locked fiber ring laser (ML-FRL) at 1558 nm, which is encoded with a 2^7-1 PRBS sequence by a Mach-Zehnder modulator. The modulated signal is launched into a 2^7-1 PRBS maintaining multiplexer (MUX) to generate a 160 Gbit/s OTDM data signal. A second pulse train from the MLL is launched into a 400 m HNLF-based NOLM that generates the wavelength converted optical clock signal at 1540 nm. The clock and data signals are combined and launched into the fiber span, which is composed of two 40 km SSMFs and one 13 km DCF with complete dispersion compensation at 1558 nm.

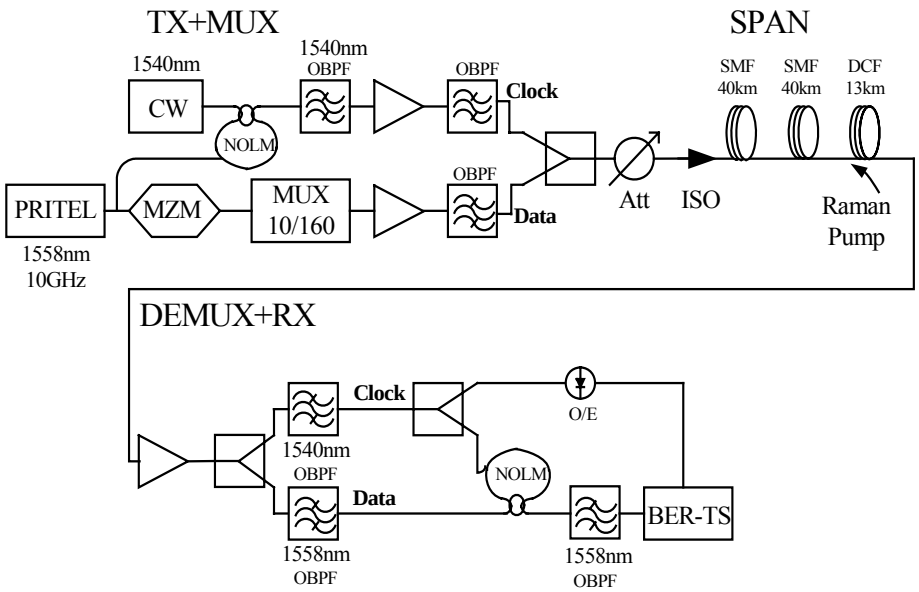

Figure 5.11. Experimental set-up for backward Raman amplification in different dispersion maps.

At the output of the span, a 3 dB coupler is used to split the optical power, and two filters are used to select the clock and data signals separately. The optical data and clock signals are injected into the second NOLM with 500 m of HNLF for demultiplexing. The clock is also used to drive the BERTS. Contrary to the first experiment, the clock signal is generated simultaneously with the data signal and transmitted along the whole link together with the data signal.

Figure 5.12 a) shows the autocorrelation trace of the initial data pulse from the mode-locked fiber ring laser having a pulse width 2.2ps. After MUX, the autocorrelation data trace in Figure 5.12 b) shows that the pulse width is maintained. The clock pulse width after wavelength conversion is 2.5 ps, which is sufficient for demutiplexing.

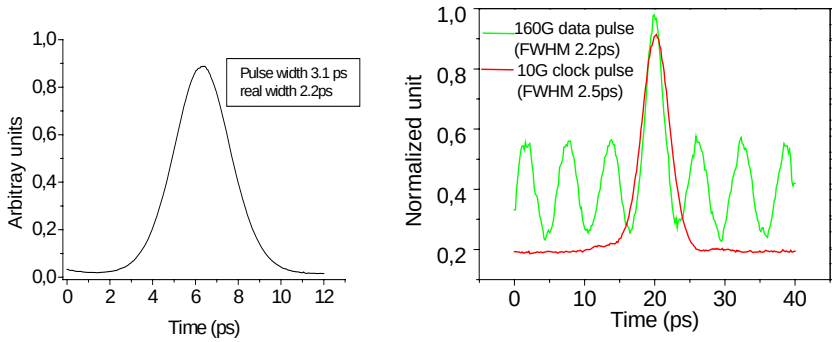

a) b)

Figure 5.12. Autocorrelation trace a) data pulse from mode-locked fiber ring laser, b) 160 Gbit/s data pulse and 10 GHz clock pulse before launched into span.

5.2.2 Experimental results

First we investigate the span and characterize it with and without Raman amplification by optimizing the signal power in the two cases. The optimal input optical power is 16 dBm with EDFA and 4.5 dBm with Raman amplifier.

The two inset figures in Figure 5.13 show the clock and data spectrum at the input and output of the span with EDFA or Raman, respectively. The wavelength spacing between signal and clock is sufficient to overcome spectrum overlap problems. We can see that the

clock and data power decrease by same amount with EDFA, while with Raman amplifier the data power stays high. The system performance in Figure 5.13 shows that Raman amplification can improve the receiver sensitivity by 2 dB compared with the EDFA case.

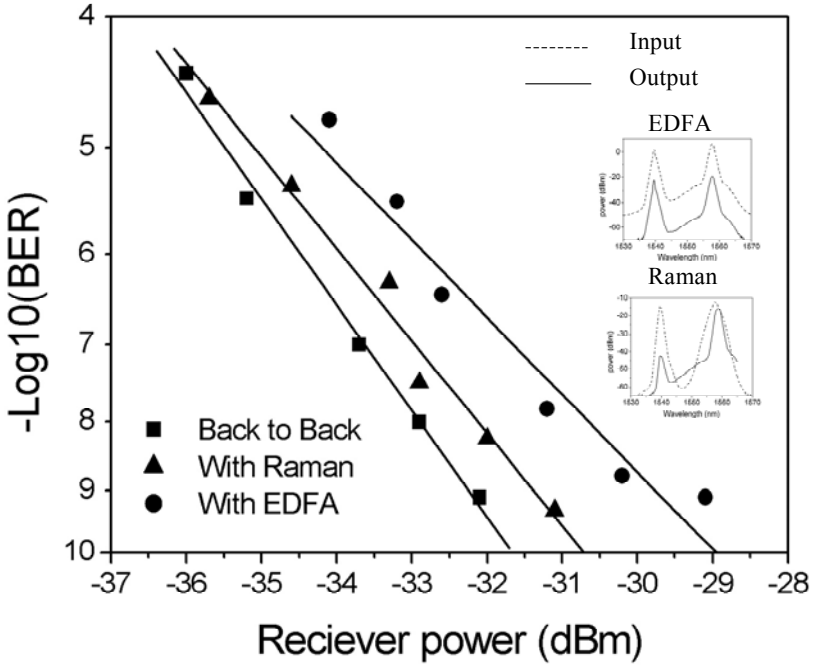

Figure 5.13. BER curves for back-to-back, transmission with EDFA and transmission with Raman.

The combined effect of dispersion map and Raman amplification is analyzed in Figure 5.14. We apply the same Raman gain at the end of the span for both maps in order to compensate the fiber loss of 23 dB. The post compensation dispersion map with DCF at the end of the span offers larger tolerance with respect to the launched signal power and less receiver penalty than the symmetrical dispersion map, where the DCF is placed in the middle of the span. The explanation is that for the same Raman gain, post compensation needs less pump power and consequently reduces Raman noise.

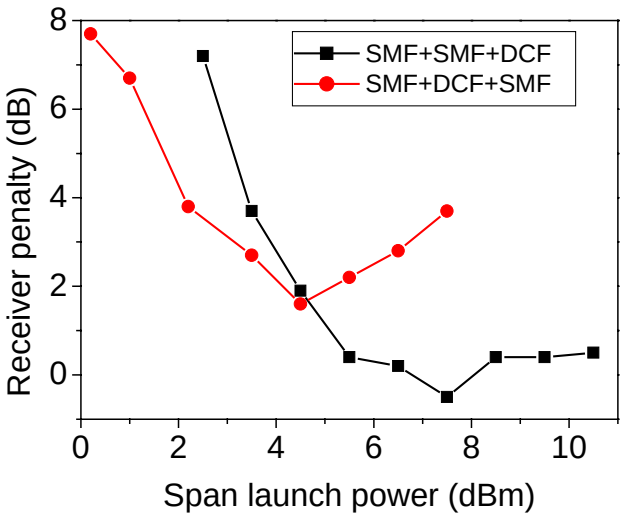

Figure 5.14. Receiver penalty of symmetrical and post dispersion compensation with same Raman on-off gain.

In summary, a transmission span for use in a 160 Gb/s system was investigated with respect to dispersion map and Raman amplification. Raman amplification reduced the transmission penalty by 2 dB compared to the EDFA case. The post compensation dispersion map is more tolerant to launch power.

5.3 Summary

Distributed Raman amplification in SSMF+DCF links is demonstrated for 160 Gb/s OTDM transmission. Raman amplification can significantly improve the system reach compared to the EDFA case and has considerable potential for applications in high-speed systems. The dispersion map is also important for achieving an optimal Raman induced signal power evolution that provides a proper balance between signal nonlinearity and amplification, which in turn will give the best system performance.

Chapter 6

160 Gbit/s WDM system

WDM experiments with 160 Gbit/s per channel systems have recently been demonstrated and the record achievements are listed in Table 6.1 [70-75]. A 2000 km transmission distance in a 6-channel WDM system with a channel bit rate of 170 Gbit/s was achieved by employing RZ-DPSK modulation format [72]. With RZ format, the distance obtained is 400 km [71]. By using SSMF, an 8-channel system was demonstrated with 430 km transmission distance [73]. Computer simulations of 160 Gbit/s WDM systems have also been performed [76,77]. However, few simulation works deal with DPSK format, Raman amplification and new fiber such as SLA+IDF in 160 Gbit/s WDM systems.

In this chapter, we numerically investigate DPSK modulation formats in 160 Gbit/s per-channel systems. Raman amplification is employed to greatly increase the system reach. We predict longest Raman-amplified transmission reach, nonlinear effects as well as dispersion and power margins for RZ-DPSK and CSRZ-DPSK. Furthermore, we evaluate the potential of these two modulation

formats for high spectral efficiency. In the following section, we numerically investigate 160 Gbit/s single channel and WDM systems with regard to optimizing dispersion map along the link. By adjusting pre, post and in-line dispersion, the optimum dispersion map that gives the best balance between dispersion and nonlinearities can be found. RZ-DPSK offers a larger pre- and in-line dispersion tolerance than RZ. The optimal in-line dispersion is reduced for WDM systems.

Table 6.1 Experiments demonstrated on 160 Gbit/s WDM systems

Authors	Capacity (Gb/s)	Distance	Fiber	Format	Spectral Efficiency
A. H. Gnauck [72]	6*170.6	2000 km	TW-RS	RZ-DPSK	0.53 bit/s/Hz
M. Schmidt[73]	8*170	430 km	SSMF	CSRZ	0.53 bit/s/Hz
M. Daikoku[74]	4*160	225 km	NZ-DSF	CSRZ	0.53 bit/s/Hz
B. Mikkelsen[71]	6*160	400 km	Truewave fiber	RZ	0.53 bit/s/Hz
R. Leppla[75]	8*170	430 km	SSMF	3 ps	0.53 bit/s/Hz
S. Kawanishi[70]	19*160	430 km	DSF		0.33 bit/s/Hz

6.1 System employing Raman and advanced modulation format

Advanced modulation formats have been extensively employed in 40 Gbit/s WDM systems to achieve high spectral efficiency and to greatly upgrade the system capacity. For instance, ultra high spectral efficiency of 1.6 bit/s/Hz over 320 km NDSF (nonzero-dispersion-shifted-fiber) using CSRZ-DQPSK (carrier suppressed return to zero–differential quadrature phase shift keying) has been reported [78]. And a distance-capacity product of 20 Pbit·km/s has been achieved by CSRZ-DPSK across the C and L band [79,80]. RZ on-off keying and RZ-DPSK have been compared numerically for single channel 40 Gbit/s systems with Raman amplification [81,82]. Furthermore, RZ-DPSK and CSRZ-DPSK have been compared numerically in DWDM 40 Gbit/s systems without Raman amplification [79]. However, the increased complexity and cost of WDM systems with many channels and high spectral efficiency drive the channel bit rate from 40 to 160 Gbit/s. As a consequence, the signal spectrum of a single channel

is broadened which leads to significant nonlinear distortions such as intra and inter Raman crosstalk, IXPM, IFWM in addition to XPM and FWM. The advantages of DPSK with its higher sensitivity in balanced detection attract interest although the transceiver setup becomes more complicated. In 160 Gbit/s per-channel experiments, many new components and techniques are employed to investigate RZ-DPSK [83]. A record reach of 2000 km was demonstrated in a 6-channel WDM system using RZ-DPSK and FEC technique [57]. However, to the best of our knowledge, for 160 Gbit/s per-channel systems, few numerical investigations of DPSK modulation formats have been reported [84,85].

6.1.1 System configuration

The transmitter consists of 5 laser sources and the channel wavelengths are allocated with equal channel spacing with center channel at 1552 nm. Each channel is carrying an uncorrelated PRBS and is RZ-DPSK or CSRZ-DPSK modulated onto a lightwave by a phase and a Mach-Zehnder modulator [79]. Each laser source has a random initial optical phase to take into account realistic XPM and FWM interactions between channels. The polarization state for all channels is identical and PMD effects are ignored. The system configuration is shown in Figure 6.1.

A symmetrical dispersion map, a so-called 'ABA' map, is used with a 105 km span length. The span dispersion and dispersion slope are fully compensated by using two 35 km SLAs (super large effective area fibers) and a 35 km IDF (inverse dispersion fiber) [82]. The dispersion, dispersion slope, nonlinear coefficient and attenuation of the SLA equal 20 ps/nm/km, 0.06 ps/nm^2/km, 2.23×10^{-20} m^2W and 0.2 dB/km, respectively, while the values for the IDF are -40 ps/nm/km, -0.12 ps/nm^2/km, 2.37×10^{-20} m^2W and 0.25 dB/km, respectively.

Before each span there is an EDFA, which is used to optimize the signal input power into the span. The noise figure of the EDFA is 5 dB. A Raman amplifier is backward pumped at a wavelength of 1450 nm, and we assume the Raman gain is the same for all channels since the total bandwidth of all channels is much smaller than the Raman gain bandwidth. The simulated Raman gain profile is fitted to the realistic characteristics of the SLA and IDF as shown in Figure 4.25. The

maximum Raman gain coefficient equals 0.3 $W^{-1}km^{-1}$ and 0.9 $W^{-1}km^{-1}$ for the SLA and IDF, respectively.

The receiver contains an optical preamplifier with a noise figure of 4 dB. In the receiver, a 6th-order optical Gaussian filter and a 5th-order electrical Bessel filter are used. We employ a one bit delay Mach-Zehnder interferometer (MZI) and balanced detection for demodulation of the RZ-DPSK and CSRZ-DPSK formats. The nonlinear Schrödinger equation is solved by the split step method incorporated in the simulation tool *VPItransmissionMakerV5.5* to take into account linear and nonlinear items including not only dispersion, XPM, FWM and SPM effects but also IXPM, IFWM and intra-inter Raman effects. A pseudorandom bit sequence of length 2^{10}–1 is used in the simulations as a reasonable compromise between accuracy and simplicity. We use a χ^2 statistics model for the noise density distributions in the DPSK receiver [86].

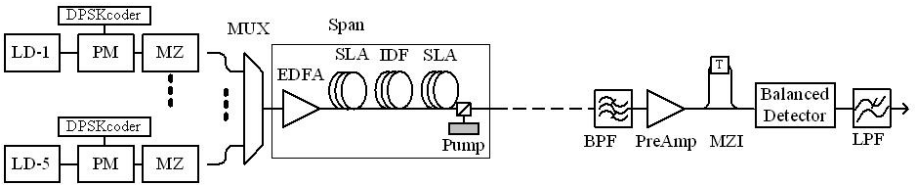

Figure 6.1. 5-channel Raman-amplified 160 Gbit/s transmission system configuration. PreAmp: pre-amplifier, BPF: band-pass filter, LPF: low-pass filter. T: one bit delay.

6.1.2 WDM systems

We investigate the system performance at 160 Gbit/s per-channel with 5 channels placed on a 400 or 300 GHz spacing frequency grid, equivalent to a spectral efficiency of 0.4 and 0.53 bit/s/Hz, respectively. We evaluate the performance of the center channel at 1552 nm, which experiences the strongest nonlinear effects from adjacent channels. The transmission performance is optimized for longest system reach by adjusting the per-channel input span signal power and Raman pump power. Then the Q-values are extracted after each span.

The results are shown in Figure 6.2 in terms of Q-value as a function of transmission distance for the two spectral efficiencies. For

the rather large channel spacing of 400 GHz, corresponding to the spectral efficiency of 0.4 bit/s/Hz, the RZ-DPSK format gives best performance of 2300 km for Q=6 (BER=10^{-9}). The reason is that SPM is the limiting mechanism in this system, so the narrower pulse width of RZ-DPSK, compared to CSRZ-DPSK, induces quicker pulse broadening and hence less SPM. However, when the channel spacing is reduced to 300 GHz, corresponding to an increased spectral efficiency of 0.53 bit/s/Hz, the system reach of RZ-DPSK is reduced from 2300 to 1600 km. In contrast, the performance of the CSRZ-DPSK format is almost unchanged with 1900 km system reach, which shows its larger tolerance to nonlinear and linear noise.

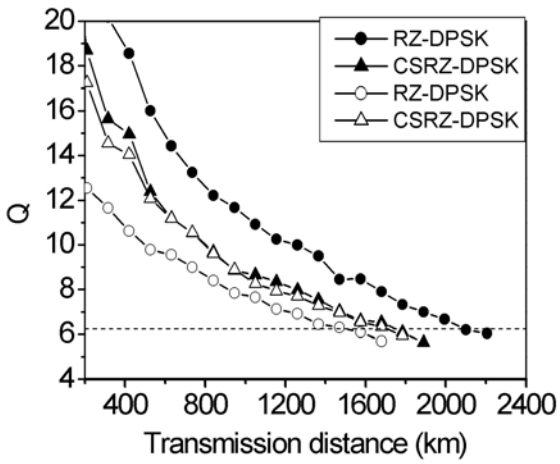

Figure 6.2. Longest five-channel WDM system reach. At 0.4 bit/s/Hz (filled symbols), optimized Raman pump powers for RZ-DPSK and CSRZ-DPSK are 1.05 W and 1.05 W, respectively; at 0.53 bit/s/Hz (open symbols), these values are 0.9 W and 0.8 W, respectively. The optimized span per-channel input power for each Q=6 case is shown in Figure 6.3.

Figure 6.3 shows transmission distance as a function of span input power per-channel for Q=6. The Raman pump power is optimized for longest transmission distance for each span input power. The curves in Figure 6.3 show that for small input power the systems perform better when the input power is increased due to better OSNR; however when the power exceeds the optimum value, the nonlinear impairments

become noticeable and degrade the system performance. At the spectral efficiency of 0.4 bit/s/Hz, RZ-DPSK offers longer transmission distance than CSRZ-DPSK due to quicker pulse broadening and less SPM. However, this is reversed when the spectral efficiency is increased to 0.53 bit/s/Hz. It can be explained as the wider spectrum of RZ-DPSK, compared to CSRZ-DPSK, causes larger interplay between signal spectrum and linear noise, thus inducing lower OSNR which dramatically reduces the transmission distance. Therefore a higher input power is needed for RZ-DPSK; for instance at 0.53 bit/s/Hz, RZ-DPSK has 2 dB lower power margin than CSRZ-DPSK, at a transmission distance of 1260 km.

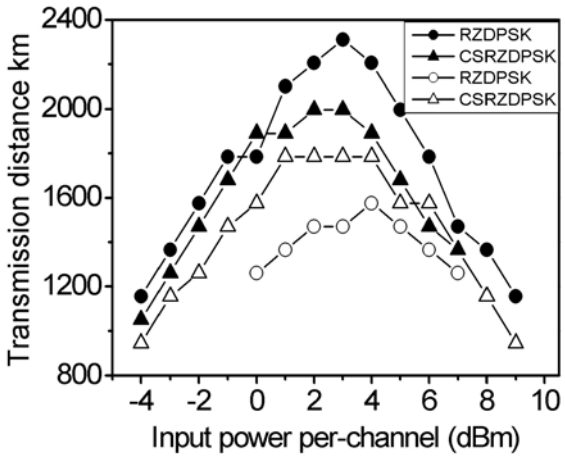

Figure 6.3. Transmission distance vs. span input power per channel at spectral efficiencies of 0.4 bit/s/Hz (filled symbols) and 0.53 bit/s/Hz (open symbols).

In dense WDM systems, the mutual interactions between signals and also between signals and ASE noise cause inevitable linear and nonlinear cross-talk impairments. Therefore, to give an accurate comparison between various modulation formats, optimization of optical and electrical filters in the receiver for each channel spacing is important [86]. We evaluate the filter performance on the basis of highest receiver sensitivity after 4 spans. In Figure 6.4 we plot the optimum optical and electrical filter bandwidth in the case where the channel spacing is still larger than the signal bandwidth. The optimal results show that for smaller channel spacing larger electrical

bandwidth is needed. This demonstrates that in narrow channel spacing WDM systems the impairment from pulse amplitude degradation is more important than ISI and ASE noise. This impairment can be reduced by using wider electrical filter bandwidth.

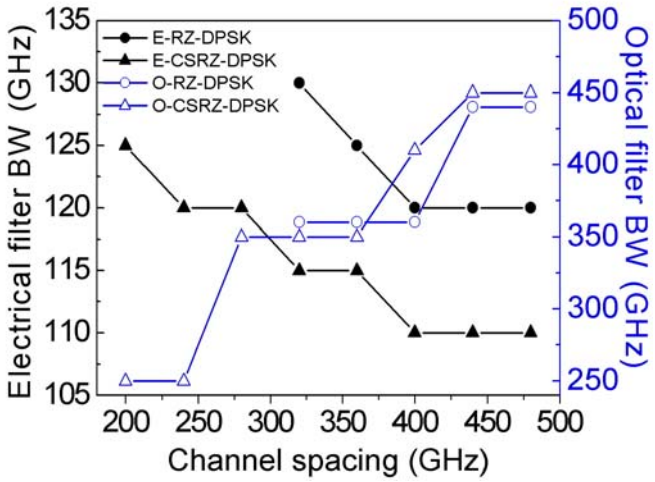

Figure 6.4. Optimization of optical and electrical filter bandwidths vs. channel spacing. E indicates electrical, O optical bandwidth.

The results in Figure 6.5 are obtained after two spans of transmission without Raman amplification. We use eye-opening penalty (EOP) as performance criterion. The penalty was found by comparing eye-opening at the output of the receiver with and without transmission. In Figure 6.5 (a) and (b) we present contour plots for EOP as a function of residual dispersion and input power per channel; the curves apply for EOP=1dB and spectral efficiencies of 0.4 and 0.53 bit/s/Hz, respectively. When the spectral efficiency is increased the dispersion margin for CSRZ-DPSK remains at 2 ps/nm, while the margin for RZ-DPSK drops from 1.7 ps/nm to 1 ps/nm. The induced nonlinear effects interact with dispersion resulting in an offset from the zero dispersion point in agreement with [87]. The input power tolerance of CSRZ-DPSK slightly exceeds that of RZ-DPSK, while the power tilt stems from the numerical step size of power.

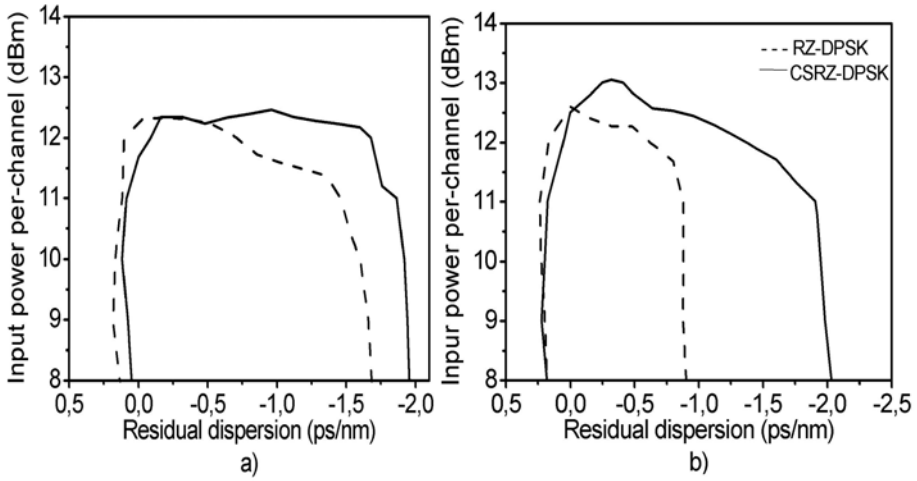

Figure 6.5. Margin of residual dispersion and input power per-channel for EOP=1 dB at a) 0.4 bit/s/Hz and b) 0.53 bit/s/Hz.

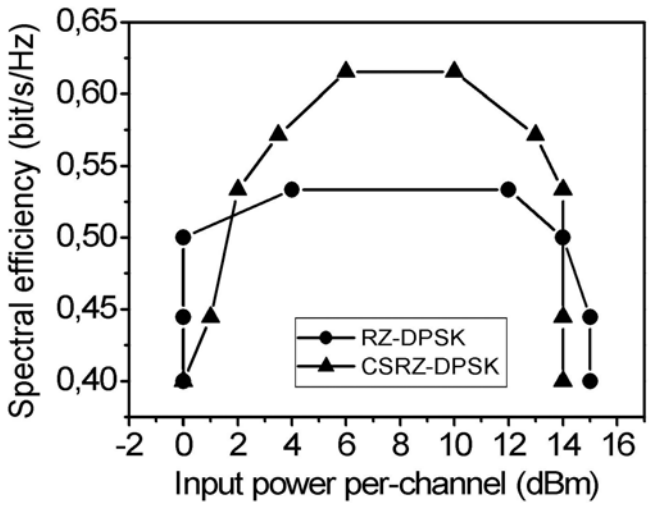

Figure 6.6. Spectral efficiencies vs. per-channel input power for Q=6.

Figure 6.6 shows the maximum allowable spectral efficiency as a function of per-channel input power after two spans for Q=6. In the low power linear regime where ASE is dominant, the allowable spectral efficiencies increase with increasing input power until an optimum is reached. However, for high input power the allowable spectral efficiencies drop due to nonlinear effects. Because of its

narrower spectrum the CSRZ-DPSK format allows a larger spectral efficiency than RZ-DPSK for same input power – like for 40 Gbit/s systems for instance.

We have presented numerical simulations for DPSK modulation formats in 160 Gbit/s 5-channel WDM systems using an ABA dispersion map and Raman amplification. Compared to RZ-DPSK, CSRZ-DPSK is more robust against XPM and FWM due to its narrower spectrum; at narrow channel spacing it provides double dispersion tolerance and nearly stable 1900 km transmission distance with slightly larger power margin. Furthermore, CSRZ-DPSK allows higher spectral efficiency. The receiver was optimized with respect to optical and electrical filter bandwidth, which is essential for evaluation of ultra high speed WDM system performance.

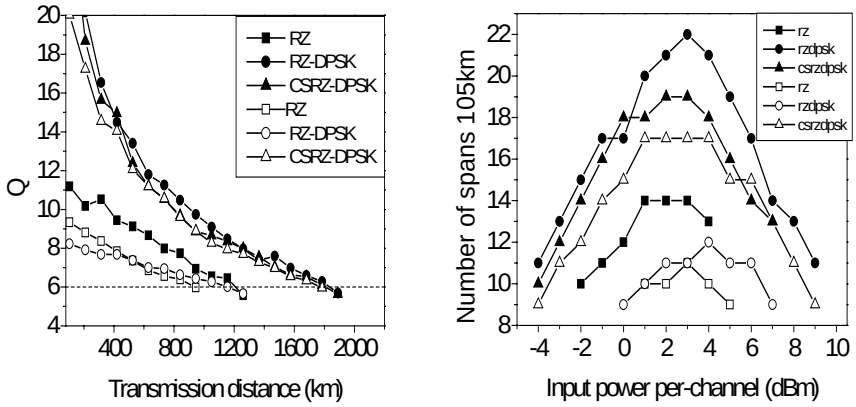

a) b)

Figure 6.7. Transmission distance at 0.4 bit/s/Hz (filled symbols) and 0.53 bit/s/Hz (open symbols) under optimization of Raman amplification, individually. a) Longest five-channel WDM system reach. b) Transmission distance vs. per channel input power.

In addition, the RZ format is employed in order to compare results with RZ-DPSK and CSRZ-DPSK. From Figure 6.7, it is clear that RZ gives much shorter transmission distance and smaller per-channel input power margin than the other two formats. The DPSK format provides significant improvements in WDM system performance.

6.2 Dispersion management optimization in RZ and RZ-DPSK systems

Dispersion management, as an approach to control the signal pulse width evolution along the fiber link, plays an important role to mitigate dispersive and nonlinear impairments in high-speed long-haul transmission systems. Up to now dispersion maps have evolved from simply concatenating hundreds of same fiber span in the transmission line to a dynamic optimization design of dispersion map along the whole transmission link by varying the dispersion map profile. In principle, the dispersion management along the whole transmission link is characterized by three parameters, namely pre-compensation at the beginning of the link, in-line compensation at each span and post-compensation at the receiver. By adjusting these three parameters the optimum balance between dispersion and nonlinearities can be achieved.

The merit of the above-mentioned dispersion maps can be explained as follows. For high-speed systems above 40 Gbit/s, short pulse width leads to large dispersive pulse broadening and results in increased intra-channel nonlinear distortion such as IXPM and IFWM [90]. IXPM stems from the overlapping of neighboring pulses and result in pulse timing jitter. IFWM comes from overlapping of pulse spectra due to dispersion and the generated FWM component causes a shadow pulse within 0-bit timeslots. However, all the above-mentioned considerations call for considerable simulation work. Yann et al have presented an extensive simulation of SSMF based systems considering the three phenomena mentioned above. Recent research has proposed some empirical rules for a quick optimal dispersion management design [87-89] for 40 Gbit/s transmission systems. The modulation formats have also been investigated with a view to dispersion tolerance of 40 Gbit/s systems [91-98].

For 160 Gbit/s systems, some N×160 Gbit/s experiments have been demonstrated with different span configurations and various types of fibers. Some dispersion optimization work has been presented in [90]. However that work did not take Raman amplification into account, hence the Q-value was rather low already after 3 spans (span length 100 km). Another drawback was that the dispersion slope was

neglected. Furthermore, the application of RZ-DPSK format was not investigated.

In contrast to published work, we employ Raman amplification to provide a large improvement in Q-value. We also take dispersion slope into account, as this is important when evaluating a realistic dispersion profile in 160 Gbit/s systems. In comparing RZ and RZ-DPSK, we present dispersion map features for 160 Gbit/s single channel and WDM systems.

6.2.1 Schematic of dispersion map configuration

The system configuration is shown in Figure 6.8. The RZ or RZ-DPSK format is employed at 160 Gbit/s at a wavelength of 1552 nm with a PRBS bit pattern length of 1024. The backward Raman pump is used in each span to greatly increase the OSNR. In front of each span, an EDFA with a noise figure of 4 dB is used to provide a constant input signal power. At the end of the link, the receiver incorporates an optical preamplifier with a noise figure of 4 dB. The Mach-Zehnder interferometer (MZI) and balanced detector are used for demodulation of the RZ-DPSK format.

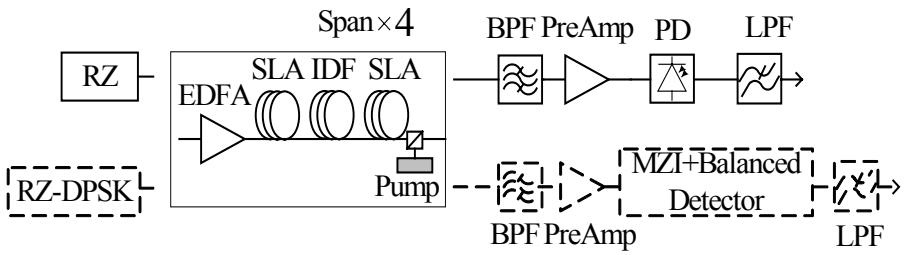

Figure 6.8. System configuration for optimization of four spans of dispersion map using the two modulation formats RZ and RZ-DPSK.

The link represented in Figure 6.9 consists of four spans with span length of 100 km and extra fibers inserted at both sides of the transmission link providing pre- and post-dispersion compensation. The span dispersion and dispersion slope are compensated by using two super large effective area (SLA) fibers of same length symmetrically placed on both sides of the span and one inverse

dispersion fiber (IDF) in the middle of the span. The dispersion, dispersion slope and effective core area of the SLA equal 20 ps/nm/km, 0.06 ps/nm^2/km and 105 μm^2, respectively, while for the IDF these values are -40 ps/nm/km, -0.12 ps/nm^2/km and 30 μm^2, respectively. The SLA is chosen to alleviate nonlinear effects, the IDF to reduce loss of the link.

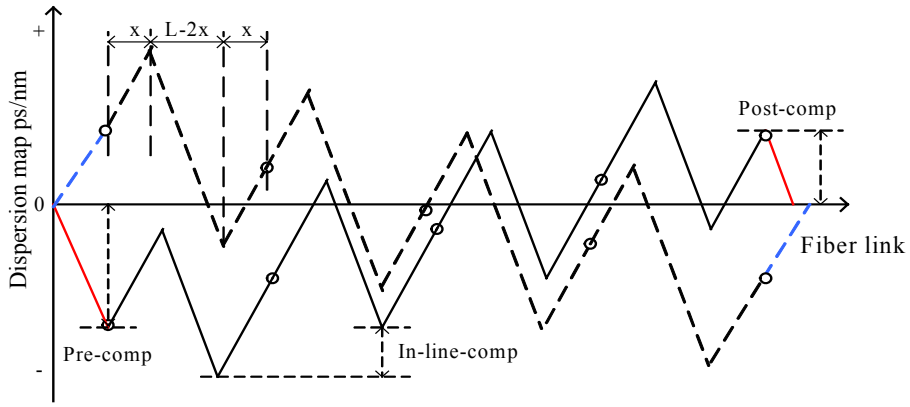

Figure 6.9. Dispersion map of transmission link consisting of four spans (100 km each) for two cases; the fibers used for pre- and post-compensation are of the same kind, namely either SLA (solid line) or IDF (dotted line). Each span is separated by open circle.

The pre-dispersion compensation is obtained by either IDF or SLA right after the transmitter. The total residual dispersion at the receiver end, namely the post dispersion, is fully compensated to zero by SLA or IDF according to the residual dispersion after the link. The in-line compensation is obtained by varying the SLA and IDF lengths while keeping the total span length at 100 km. For simplicity, in Figure 6.9 we consider two cases where the pre- and post-dispersion compensation in the same link are provided by sole SLA or IDF, thus having the same dispersion sign, while we neglect the use of opposite dispersion sign by IDF (pre) + SLA (post) or SLA (pre) + IDF (post).

The SLA length x as shown in Figure 6.9 can be calculated as follows. D_{SLA}, D_{IDF} and D_{inline} denote the dispersion of SLA, IDF and the in-line dispersion value, respectively. The span length L is 100 km.

$$D_{SLA} \cdot x + D_{IDF}\left(\frac{L}{2} - x\right) = \frac{D_{inline}}{2}$$

Therefore x is given by:

$$x = \frac{D_{inline} - L \cdot D_{IDF}}{2(D_{SLA} - D_{IDF})}$$

6.2.2 Single channel systems

In the single channel case, the input signal power is 6 dBm. Pump power of 750 mW provides about 19 dB Raman gain that compensates most of the span loss. A 3rd order Gaussian optical filter with bandwidth 600 GHz and a 3rd order Bessel electrical filter with bandwidth 120 GHz are used in the receiver. We define the system Q penalty as $10\log_{10}(Q_{max}/Q)$ from the maximum Q value that could be obtained.

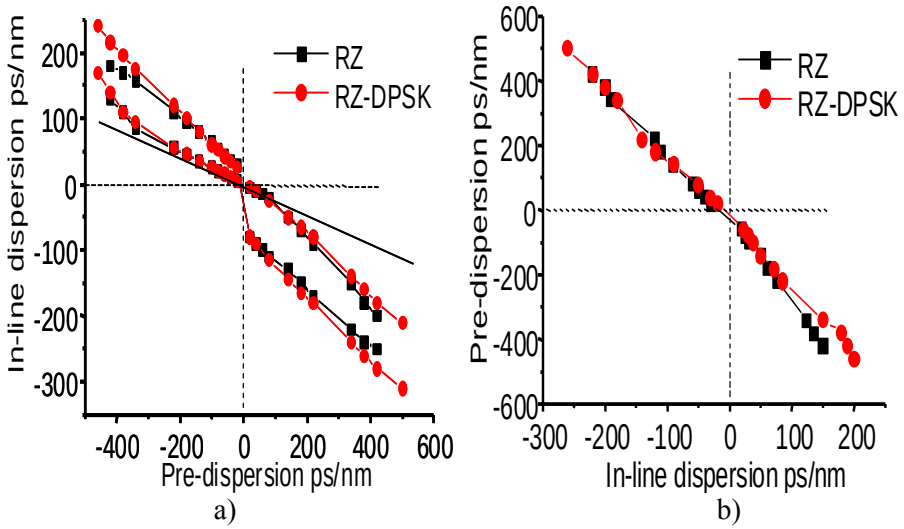

Figure 6.10. a) Contour plots of Q for 1 dB Q penalty for RZ and RZ-DPSK, respectively. b) The optimal combination of pre- and in-line dispersion compensation for maximum Q value.

Figure 6.10 a) is a contour plot of Q as a function of pre- and in-line compensation; curves are shown for the combination of pre- and in-line compensation for 1dB Q penalty in case of the two modulation formats RZ and RZ-DPSK, respectively. The solid line shows the allowable dispersion adjustment limit that fits with the two link cases shown in Figure 6.9. (Otherwise, the pre and post compensation fiber will not be the same type of fiber). We can see the RZ-DPSK format has larger pre-dispersion tolerance and slightly larger in-line dispersion

tolerance than RZ. Figure 6.10 b) gives the in-line dispersion D_{inline} that maximizes the Q value for a given pre-dispersion D_{pre}. The results fit with a linear analytical rule in [89] D_{pre}=-N*D_{inline}/2 where N is the span number.

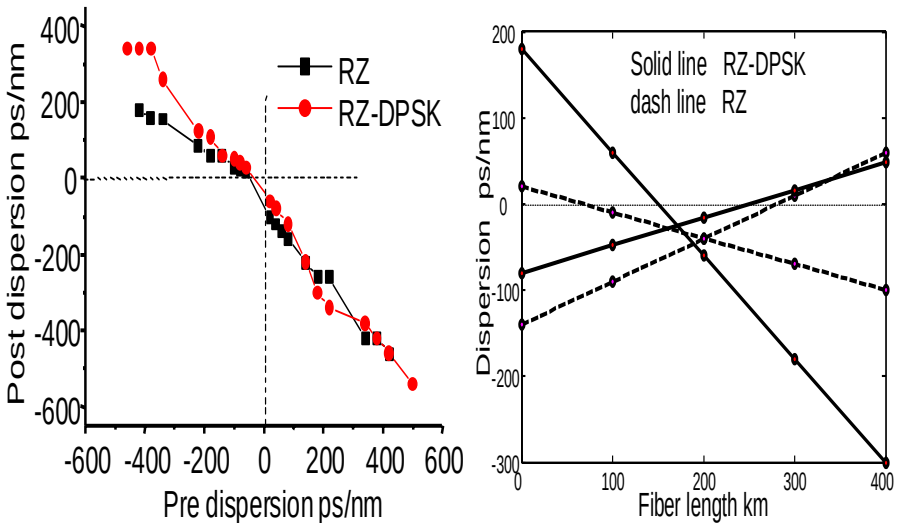

Figure 6.11. a) The optimal combination of pre- and post- dispersion for 1dB Q penalty from maximum Q value. b) Dispersion maps giving highest Q value for RZ or RZ-DPSK individually; local dispersion excursions are not shown for simplicity.

Figure 6.11 a) shows the optimal combination of pre- and post-dispersion compensation corresponding to Figure 6.10 b) for the two formats. It is shown that for RZ-DPSK a higher post-dispersion is preferred. Figure 6.11 b) presents the optimal dispersion maps giving highest Q value for the two formats individually at both positive and negative pre-dispersion; local dispersion excursions and pre, post dispersion fiber are not shown for simplicity. It can be seen that for RZ a negative dispersion profile along most of the link is preferable. The best RZ-DPSK performance is achieved when the zero dispersion point is near the middle of the link, giving an almost symmetrical map.

6.2.3 5-channel WDM systems

In the WDM systems studied, the transmitter consists of 5 laser sources and the channel wavelengths are allocated with equal channel spacing

of 400 GHz with center channel at 1552 nm. Each channel is carrying an uncorrelated 1024 bit long PRBS sequence. The polarization states of all channels are identical and PMD is ignored. Each laser source has a random initial optical phase to take into account realistic XPM and FWM interactions between different channels. We evaluate the performance of the center channel at 1552 nm because it experiences the strongest nonlinear effects from adjacent channels. For a relevant comparison between WDM and single channel systems, the Raman pump power and per-channel input power are still 750 mW and 6 dBm respectively as in the single channel system. A 6th order Gaussian optical filter with 400 GHz bandwidth and a 5th order Bessel electrical filter with 120 GHz bandwidth are used.

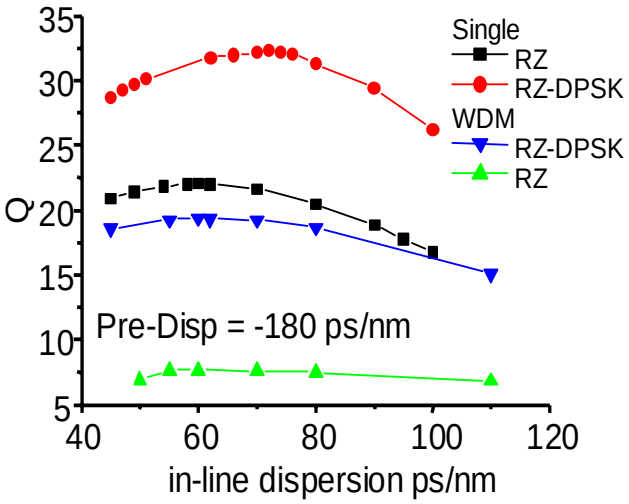

Figure 6.12. Q vs. in-line dispersion at pre-dispersion of -180 ps/nm for single channel and WDM systems.

With pre-dispersion equal to -180 ps/nm for both formats, it is found in Figure 6.12 that the in-line dispersion margin within 1dB Q penalty is nearly the same for the single channel and WDM systems. It is also found that in the WDM system the optimal design for pre- and in-line dispersion still fits the linear rule shown in Figure 6.10 b), but with a slightly steeper slope because the in-line dispersion that maximizes Q is reduced. This can be explained because with smaller in-line dispersion, less pulse overlapping occurs and then less IFWM power [89] per channel is generated which means this nonlinear impairment on the signal is reduced.

6.3 Summary

Five-channel 160 Gbit/s WDM systems using ABA dispersion map and Raman amplification have been investigated numerically. Transmission distance and system margin are evaluated for RZ-DPSK and CSRZ-DPSK formats. The results show that RZ-DPSK can offer 2300 km system reach at large WDM channel spacing, while CSRZ-DPSK is more robust against nonlinear effects in the fibers and offers a reach of 1900 km at a spectral efficiency of 0.53 bit/s/Hz. CSRZ-DPSK can also provide twice the dispersion tolerance of RZ-DPSK and larger spectral efficiency. We numerically investigate 160 Gbit/s single channel and WDM systems with regard to optimizing the dispersion map along the link. The numerical simulation confirms that the optimal in-line dispersion and pre-dispersion can be related by a linear design rule. RZ-DPSK has larger in-line dispersion tolerance and larger post-dispersion than RZ. For RZ a more negative dispersion map is preferable while an almost symmetrical map is better for RZ-DPSK. In WDM systems the smaller in-line dispersion is preferable than in single channel systems.

Chapter 7

Conclusion

As the market is recovering, WDM systems operating at 40 Gbit/s per channel will be employed in the near future. Research on 160 Gbit/s systems can support the long-term development and operation of WDM networks by exploring the possibilities for increasing the channel speed in future upgrading scenarios. This thesis presents simulation forecasts of the potential of 160 Gbit/s single channel and WDM systems with regard to transmission reach and systems tolerances.

Raman amplification

160 Gbit/s single channel transmission using a symmetrical fiber span consisting of two SLA fibers separated by one IDF was investigated numerically in two schemes, namely discrete and distributed Raman amplification. The purpose of the research was to achieve the longest transmission distance by optimal combination of signal and pump power in the two cases.

Discrete Raman amplification was investigated based on four different pumping schemes. The optimal pumping scheme was found to be pumping the IDF in the middle of the span. With 1 ps Gaussian pulse width, a transmission distance of 1800 km could be predicted with a span length of 100 km using symmetrical SLA and IDF-I. For all the four pumping schemes, it was found that a narrower pulse width can give a longer transmission distance because of quicker dispersive

pulse broadening and hence less SPM. The optimal pump power range was stable against pulse width variation.

The distributed Raman amplification was investigated for three different pumping schemes all with a symmetrical SLA, a new fiber type IDF-II and a span length of 105 km. For the three schemes backward pumping, bi-directional pumping and second-order pumping about the same systems reach of 2500 km was obtained based on optimal adjustment of launched signal power and pump power. All three configurations allowed a span length in the 45 to 135 km range with 2500 km systems reach. It was also found that second order pumping had largest pump power and input signal power tolerance.

In short, through the simulations the following was found. 1) Distributed Raman amplification is better than discrete Raman amplification for providing longer transmission systems. 2) By adopting distributed Raman amplification, 2500 km transmission distance was achieved in single channel 160 Gbit/s systems. 3) Second order pumping scheme is attractive in WDM systems because it allows lower input power level, which in turn will reduce the influence of nonlinearities. 4) Larger core area fiber is preferred to achieve longer system reach.

Two experiments on 160 Gbit/s OTDM systems were presented. We demonstrated, for the first time, distributed Raman amplification in both SSMF and DCF. A transmission distance of 174 km was achieved by optimizing both pump power and launched signal power. This shows the potential for easy upgrade of existing installed fiber systems to 160 Gbit/s Raman amplified systems.

In another experiment a transmission span with two SSMFs and one DCF in a 160 Gbit/s system was investigated with respect to dispersion map using backward pumped Raman amplification. It was demonstrated that Raman amplification can reduce the transmission penalty by 2 dB compared to the EDFA case. The post compensation dispersion map was more tolerant to launch power.

Modulation format

In 160 Gbit/s EDFA-based single channel systems, various modulation formats such as RZ, CSRZ, RZ-DPSK, CSRZ-DPSK and RZ-DQPSK were compared in terms of dispersion tolerance and nonlinear margin based on spans consisting of SSMF and DCF. It was found that the

RZ-DQPSK format has much higher dispersion tolerance than other formats due to its half symbol rate and consequently much narrower spectrum width. CSRZ-DPSK has better dispersion tolerance than RZ, CSRZ and RZ-DPSK formats.

In 160 Gbit/s Raman based systems, a symmetrical fiber span with realistic fiber Raman gain profile in the SLA and IDF-II was adopted. The three modulation formats RZ, RZ-DPSK, CSRZ-DPSK were investigated. In single channel systems, RZ-DPSK can provide a longer transmission distance of 2300 km than CSRZ-DPSK and RZ. In WDM systems, RZ-DPSK and CSRZ-DPSK offer significant advantages with regard to long transmission distance and per-channel input signal power margin compared to RZ. Compared to RZ-DPSK, CSRZ-DPSK allows higher spectral efficiency by being more robust against XPM and FWM due to its narrower spectrum, thus providing double dispersion tolerance and nearly stable 1900 km transmission distance.

Based on the simulations concerning Raman amplification and modulation format the following can be predicted. 1) If the generated DPSK signal adopts short pulse width such as 1 ps, a system reach longer than 2300 km can be obtained for single channel systems. 2) The DQPSK format offers much larger dispersion tolerance than other formats and therefore potentially longer transmission distance.

Dispersion map

The optimal dispersion map in high-speed transmission systems can control the signal pulse width evolution along the fiber link and consequently reduce the intra and inter nonlinear effects in the system. The simulations give a meaningful insight into the system dispersion tolerance in the terms of pre-dispersion, in-line dispersion and post-dispersion tolerance.

Raman amplification was included to provide a large improvement in Q-value and the dispersion slope was also taken into account. In comparing RZ and RZ-DPSK, the numerical investigations of dispersion map features of 160 Gbit/s single channel and WDM systems confirmed that the optimal in-line dispersion and pre-dispersion was related by a linear design rule. RZ-DPSK has larger in-line dispersion tolerance and larger post-dispersion than RZ. For RZ a more negative dispersion map is preferable while an almost

symmetrical map is better for RZ-DPSK. In WDM systems, a smaller in-line dispersion than in single channel systems is preferable.

In conclusion, the results show that Raman amplification is very effective for improving the system reach and the pumping scheme is very important for achieving best system performance. Advanced modulation formats such as DPSK and DQPSK are very promising for high-speed long-haul systems.

Suggestions for further work

Hopefully in the near future, a 160 Gbit/s transoceanic systems experiment can be realized by employing DPSK modulation format, Raman amplification and other techniques such as use of dispersion compensation modules and polarization OTDM multiplexers. Fibers with large effective core area are advantageous in such future long-haul transmission systems. Furthermore, advanced dispersion management can provide larger dispersion and nonlinear tolerance and lead to cost savings by allowing relaxed specifications of fibers and fewer WDM compensation devices.

To further increase the available transmission distance, the next simulation research on single channel systems could be an investigation of orthogonal polarized adjacent OTDM tributary channels that form a multiplexed 160 Gbit/s signal; such an approach is believed to reduce the intra-channel nonlinear effects. In WDM systems orthogonal polarized adjacent channels are extensively employed in experiments. However, this approach has not been investigated very much in simulations when it comes to transmission distance, especially for 160 Gbit/s systems. Another interesting topic could be combining multiple Raman pumps to get optimal gain shape within the required bandwidth. The proposal on dispersion management in terms of optimization of the three dispersion compensation parameters is also promising to further increase the system reach.

Appendix A

EDFA noise figure derivation

1. SNR_{in}

Before the EDFA, only shot noise exists in SNR_{in}

So the variance of the noise current is

$$\delta_s^2 = 2q(I_p + I_d)\cdot\Delta f \qquad 1)$$

P_{in} is the input signal power and R is the responsivity. The average current is

$$I_p = RP_{in} \qquad 2)$$

The dark current $I_d \approx 0$

Therefore the combination of above gives $\delta_s^2 = 2qRP_{in}\cdot\Delta f$ 3)

2. SNR_{out}

After the EDFA with gain G, the noise is composed of shot noise and spontaneous emission as

$$\delta^2 = 2qRGP_{in}\cdot\Delta f + (\Delta I)^2 \qquad 4)$$

The beating of spontaneous emission with signal produces noise current

$$\Delta I = 2R\sqrt{GP_{in}P_{sp}}\cdot\cos\theta$$

P_{sp} is the spontaneous noise power and θ as the phase between the two signals. S_{sp} is the noise power spectral density.

$P_{sp} = 2S_{sp}\cdot\Delta f$, $\cos^2\theta = 1/2$ (the average value is taken)

Therefore $(\Delta I)^2 = 4(RGP_{in})(RS_{sp})\Delta f$ 5)

So by introduction of 5) into 4),

$$\delta^2 = 2qRGP_{in}\Delta f + 4RGP_{in}RS_{sp}\Delta f \qquad 6)$$

3. Noise figure

Since the noise figure is defined as $F = \frac{SNR_{in}}{SNR_{out}}$, the combination of above gives

$$F = \frac{SNR_{in}}{SNR_{out}} = \frac{\frac{(I_p)^2}{\delta_s^2}}{\frac{(I_0)^2}{\delta^2}}$$

$$= \frac{\frac{(RP_{in})^2}{2qRP_{in}\Delta f}}{\frac{(GRP_{in})^2}{2qRGP_{in}\Delta f + 4RGP_{in} \cdot RS_{sp}\Delta f}}$$

$$= \frac{(RP_{in})^2}{2qRP_{in}\Delta f} \cdot \frac{2qRGP_{in}\Delta f + 2R^2GP_{in}P_{sp}}{(GRP_{in})^2}$$

$$= \frac{2q + 4RS_{sp}}{2qG}$$

$$= \frac{1}{G}\left(\frac{P_{sp}}{h\nu\Delta f} + 1\right)$$

Appendix B

Power spectral density of ASK and PSK

1. Power spectral density of ASK signal

The signal $Z(t)$ is obtained by modulating a cosine signal at angular frequency ω_c with an NRZ bit sequence $D(t)$ [33].

$$Z(t) = D(t)(A\cos(\omega_c t)) \tag{1}$$

The autocorrelation function of $Z(t)$ is expressed as

$$R_{ZZ}(t, t+\tau) = E\{Z(t), Z(t+\tau)\} \tag{2}$$

So the power spectral density $G_z(f)$ of $Z(t)$ is

$$G_Z(f) = F\{R_{ZZ}(\tau)\} = \frac{A^2}{2} F\{R_{ZZ}(\tau)\cos(w_c\tau)\}$$

$$= \frac{A^2}{4}\{G_D(f - f_c) + G_D(f + f_c)\} \tag{3}$$

$G_D(f)$ is the power spectral density of $D(t)$. $D(t)$ is expressed as follows. We assume $d(t)$ is an NRZ bit sequence, with T_b as the bit slot.

$$\left\{ \begin{array}{c} d(t) = \sum_{k=-\infty}^{\infty} b_k g[t-(k-1)T_b], b_k = 0 or 1 \\ g(t) = \left\{ \begin{array}{c} 1, for 0 \le t \le T_b \\ 0, else \end{array} \right\} \\ D(t) = d(t - T_b) \end{array} \right\} \tag{4}$$

Then the autocorrelation function of $D(t)$ is

$$R_{DD} = \begin{cases} \frac{1}{4} + \frac{T_b - |\tau|}{4T_b}, for |\tau| \le T_b \\ 0, for |\tau| \succ T_b \end{cases} \tag{5}$$

Then the power spectral density $G_D(f)$ is

$$G_D(f) = \frac{1}{4}(\delta(f) + \frac{\sin^2(\pi f T_b)}{(\pi f T_b)^2}) \tag{6}$$

By combination of 3) and 6), so the power spectral density of $Z(t)$ is

$$G_z(f) = \frac{A^2}{16}(\delta(f - f_c) + \delta(f + f_c) + \frac{\sin^2(\pi(f - f_c)T_b)}{(\pi(f - f_c)T_b)^2} + \frac{\sin^2(\pi(f + f_c)T_b)}{(\pi(f + f_c)T_b)^2}) \tag{7}$$

2. Power spectral density of PSK signal

The PSK waveform $Z(t)$ can be described as

$$Z(t) = D(t)(A\cos(\omega_c t)) \tag{8}$$

The difference from ASK is that $D(t)$ is a random binary sequence with period T_b and value (1, -1) not (1, 0). The autocorrelation of $D(t)$ is

$$R_{DD} = \begin{cases} 1 - |\tau| / T_b & |\tau| < T_b \\ 0 & |\tau| > T_b \end{cases} \tag{9}$$

So the power spectral density of $D(t)$ is

$$G_D(f) = F(R_{DD}) = T_b \frac{\sin^2(\pi f T_b)}{(\pi f T_b)^2}) \tag{10}$$

Therefore the power spectral density of $Z(t)$ derived from (3) is

$$G_z(f) = \frac{A^2}{16}(\frac{\sin^2(\pi(f - f_c)T_b)}{(\pi(f - f_c)^2 T_b} + \frac{\sin^2(\pi(f + f_c)T_b)}{(\pi(f + f_c)^2 T_b}) \tag{11}$$

Comparing equations (7) and (11), it is clear that there are two impulses $\delta(f - f_c)$, $\delta(f + f_c)$ at the carrier frequency in the ASK power spectrum, while they disappear in the PSK spectrum. It is one of the advantages of PSK that it has a smooth spectrum profile. However, when the rise time of the applied electrical voltage to the modulator is not zero, the two impulses will appear to some extent.

Appendix C

Simple Raman Mathematical model

Raman phenomena are sub-picosecond nonlinear effects determined by fiber characteristics. In order to establish an accurate numerical model, an approximate analytical formula, namely a Raman response function, is accepted to describe the phenomena [8]. Here the time constants τ_1 and τ_2 are adjusted to fit the actual Raman gain profile.

$$h(t) = \frac{\tau_1^2 + \tau_2^2}{\tau_1 \tau_2^2} \exp(-\frac{t}{\tau_2}) \sin(\frac{t}{\tau_1})$$

The gain coefficient is given by

$$g(f_k, f_i) = 2\rho\gamma(f_k, f_i)\,\mathrm{Im}\left[\tilde{h}(\Delta\omega)\right]$$

f_k, f_i defines two wavelengths. ρ defines fractional Raman contribution to nonlinear response. $\mathrm{Im}[\tilde{h}(\Delta\omega)]$ is the imaginary part of the normalized Raman response function [12].

$$\mathrm{Im}\left[\tilde{h}(\Delta\omega)\right] = \frac{\tau_1^2 + \tau_2^2}{\tau_1^2 \tau_2^2} \frac{4\pi\Delta f / \tau_2}{\left[\frac{1}{\tau_1^2} + \frac{1}{\tau_2^2} - 4\pi^2 \Delta f^2\right]^2 + \left[\frac{4\pi\Delta f}{\tau_2}\right]^2}$$

The gain maximum is also strongly determined by germanium concentration and effective area A_{eff} through γ ($\gamma = \frac{n_2 \omega_0}{c A_{eff}}$) in silica fiber. c is vacuum light speed, A_{eff} as fiber effective core area, n_2 is refractive index, ω_0 as light carrier angular frequency. The simulated gain profile can be close to the measured gain profile.

Parameters τ_1 , τ_2 and ρ can be adjusted to provide a good fit to the measured Raman spectrum and the fractional contribution of Kerr and Raman nonlinearities. The commonly used values are ρ = 0.17, τ_1=12.2 fs, τ_2=32 fs giving an offset of 13 THz and a width of 10 THz. Figure A shows the comparison of the approximated Raman gain according to (1) and (2) and a realistic spectrum which has been measured in silica fibers [12].

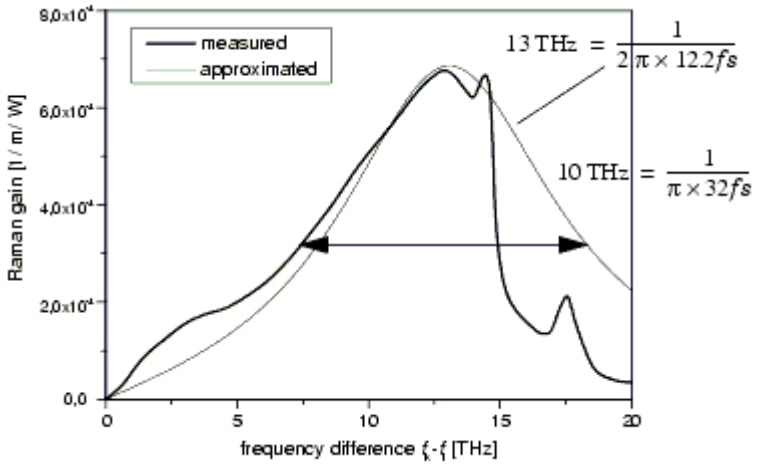

Figure. A. Comparison of measured and approximated Raman gain shape.

Appendix D

Simulation parameters

All the simulations were carried out using the simulation software "*VPI Transmission Maker*" version 5.5. In Table below we present the detailed list of parameters used in our computer simulations.

Table Simulation parameters

Global Simulation parameters	Value
PRBS length	1024 bits
Sample Rate	5120 GHz
Laser frequency	193.1 THz
Laser linewidth	10 MHz
Raman laser emission	193.1+13 THz
Raman linewidth	10 MHz

Fiber parameters	Value
Frequency resolution	100 GHz
Noise bandwidth	6 THz
Noise center frequency	(192+195 THz)/2
Noise polarization	Unpolarized
Max step width	1 km
Minimum step size	5 m

Photodiode parameters	Value
Photodiode dark current	0 A
Photodiode responsivity	1 A/W
Photodiode thermal noise	10 pA/$\sqrt{Hz}$

Reference

[1] T. Tsuritani, K. Ishida, A.Agata, K. Shimomura, I. Morita, T. Tokura, H. Taga "70GHz spaced 40×42.7Gbit/s transmission over 8700km using CS-RZ DPSK signal, all-Raman repeaters and symmetrical dispersion-managed fiber span", OFC 2003, paper PD-23.

[2] Frignac, Yann, "Transmission of 256 wavelength-division and polarization-division-multiplexed channels at 42.7 Gb/s (10.2 Tb/s capacity) over 3$MUL@100 km of TeraLight fiber", OFC 2002, paper FC51-FC53.

[3] R. Ludwig, S. Ferber, C. Boerner, C. Schubert, C. Schmidt Lang-horst E. Hilliger, M. Kroh, V. Marembert and H. G. Weber, "160 Gbits DPSK-transmission –Technologies and System Impact," ECOC 2004, Paper Tu1.1.3.

[4] J. Berger, Q. le, A. Wietfeld, S Ferber, L. Nielsen, B. Schmauss, H.G. Weber, "160 Gbit/s transmission over dispersion managed fibre set", ECOC 2003, Paper Mo3.6.6.

[5] B. J. Eggleton, B. Mikkelsen, G.Raybon, A. Ahuja, J.A. Rogers, P.S. Westbrook, T. N. Nielsen, "Tunable dispersion compensation in a 160-Gb/s TDM system by a voltage controlled chirped fiber bragg grating ", IEEE Photonics Technology Letters, vol.12, No.8, August 2000, pp. 1022-1024.

[6] C. Rasmussen, T. Fjelde, J. Bennike, F. Liu, B. Mikkelsen, et al, "DWDM 40 G transmission over trans-Pacific distance using CSRZ-DPSK, enhanced FEC and all-Raman amplified 100km UltraWave fiber spans", OFC 2003, paper PD-18.

[7] Y. Frignac, et al. “Numerical optimasation of pre and in-line dispersion compensaton in dispersion –managed system at 40 Gbit/”, OFC 2004, paper ThFF5.

[8] Govind P. Agrawal, Nonlinear fiber optics, third version, Academic Press, 2001

[9] Ivan Kaminow/Tingye Li, Optical fiber telecommunications IVA components and IVB Systems, Academic Press, 2002

[10] K. Rottwitt, J. Bromage, J. Du, A. Stentz, “Design of distributed Raman amplifiers”, ECOC 2000, paper 4.4.1

[11] Jake Bromage, “Raman amplification for fiber communications systems”, OFC 2003, Tutorial, TuC1-1.

[12] VPItransmissionMaker, VPIsystems.

[13] L. G. Nilsen, Y. Qian, B- Palsdottir, P. Gaarde, S. Dyrbøl, T. Veng, “Module for simultaneously C+L-band dispersion compensation and Raman amplification” OFC 2002, paper TuJ6.2.

[14] T. Miyamoto, T. Tsuzaki, T. Okuno, M. Kakui, et al, “Raman amplification over 100 nm-bandwidth with dispersion and dispersion slope compensation for conventional single mode fiber” OFC 2002, paper TuJ7.

[15] A. Kung, A. Agarwal, S. Banerjee, D. F. Grosz, D. N. Maywar, M. Movassaghi, T. H. Wood, “10 Gb/s and 40Gb/s ultra-long haul transmission on a common all- Raman single-wide-band platform” ECOC 2002, paper 1.1.1.

[16] V. E. Perlin, H. Winful, “Optimal design of flat-gain wide-band fiber Raman amplifiers” Journal of Lightwave Technology, Vol.20, No.2, Feb. 2002, pp 250-251.

[17] C. R. S. Fludger, V. Handerek, “Ultra-wide bandwidth Raman amplifiers” OFC 2002, paper TuJ3.

[18] S. Kado, Y. Emori, S. Namiki, "Gain and noise tilt control in multi-wavelength bi-directionally pumped Raman amplifier" OFC 2002, paper TuJ4.

[19] Frignac, Yann, "Transmission of 256 wavelength-division and polarization-division-multiplexed channels at 42.7 Gb/s (10.2 Tb/s capacity) over 3$MUL@100 km of TeraLight fiber" , OFC 2002, p. FC51-FC53

[20] G. Charlet, E. Corbel, J.Lazaro, A. Klekamp, R. Dischler, P, Tran, W. Idler, H. Mardoyan, A. Konczykowska, F. Jorge, S. Bigo, "WDM Transmission at 6 Tbit/s capapcity over transatlantic distance, using 42.7 Gb/s disfferential phase-shift keying without pulse carver," OFC 2004, Paper PDP36.

[21] B. Zhu, L. E. Nelson, S. Stulz, A.H. Gauck, et al, "6.4-Tb/s (160×42.7 Gb/s) transmisison with 0.8 bit/s/Hz spectral efficiency over 32×100 km of fiber using CSRZ-DPSK format," OFC, 2003, paper PD19-1.

[22] I. Morita, N. Edagawa, "50 GHz spaced 64*42.7 Gbit/s transmission over 8200km using Raman repeaters with large 65 km spacing," ECOC 2003, paper Th4.3.1.

[23] C. Rasmussen, T. Fjelde, J. Bennike, F.Liu, S. Dey, B. Mikkelsen, P. Mammyshev, P. Serbe, P. Wagt, Y. Akasaka, D. Harris, D. Gapontsev, V. Ivshin, P. Hall, "DDWDM 40 G transmission over trans-pacific distance (10000km) using CSRZ-DPSK, enhanced FEC and all-Ramn amplified 100km UltraWave fiber spans," Journal of Lightwave Technology, vol.22, No.1, January, 2004, pp. 203-207.

[24] A. Agarwal, S. Banerjee, D.F. Grosz, a. P. Kung, D.N. Maywar, A. Gurevich, T. H. Wood, "Ultra-high-capacity long-haul 40 Gb/s WDM transmission with 0.8 b/s/Hz spectral efficiency by means of strong optical filtering" IEEE Photonics Technology Letters, vol.15, No.3, March 2003, pp. 470-472.

[25] N. Yoshikane, I. Morita, "1.14 b/s/Hz spectrally efficient 50*85.4 Gb/s transmission over 300 km using copolarized CS-RZ DQPSK signals", OFC 2004, paper PDP38.

[26] Y. Zhu, K. Cordina, R.Feced, H. Kee, R. Rickard and A. Hadjifotiou,"1.6 bit/s/Hz orthogonally polarized CSRZ-DQPSK transmission of 8×40 Gbit/s over 320 km NZDSF," OFC 2004,paper TuF1.

[27] N. Yoshikane, I. Morita, "160% spectrally-efficient 5.12 Tb/s (64*85.4 Gb/s RZ-DQPSK) transmission without polarization demultiplexing," ECOC 2004, paper Th4.4.3.

[28] A. H. Gnauck, P. J. Winzer, S. Chandrasekhar, C. Dorrer, "Spectrally efficienct (0.8b/s/Hz) 1-Tb/s (25*42.7Gb/s) RZ-DQPSK transmission over 28 100km SSMF spans with 7 optical add/drops," ECOC 2004, Paper Th4.4.1.

[29] Govind P. Agrawal, Optical fiber communication systems, third version, Academic Press, 2001

[30] G. Bosco, P. Poggiolini, "On the Q Factor Inaccuracy in the Performance Analysis of Optical Direct-Detection DPSK Systems," IEEE Photonics Technology Letters, vol. 16, February 2004, pp. 665-667.

[31] R. Freund, L. Molle, N. Hanik, A. Richter, "Design issues of 40 Gbit/s WDM-system for metro and core network application", ECOC 2004 ,Paper Tu3.5.1

[32] Peter Winzer, S. Chandrasekar, Hoon kim, "Impact of filtering on RZ-DPSK reception", IEEE Photonics Technology Letters, Vol.15, No.6, June, 2003, pp. 840-842.

[33] K. Sam Shanmugam, Digital and analog communication systems, John Wiley & Sons, 1979

[34] P. J. Winzer, R. J. Essiambre, "Optical Receiver Design Trade-Offs," OFC 2003, Paper ThG1.

[35] M. Serbay, C. Wree and W. Rosenkranz, "Comparison of six different RZ-DQPSK transmitter set-ups regarding their tolerance towards fiber impairments in 8×40 Gb/s WDM systems", in LEOS 2004 Workshop on Advanced Modulation Format, CA, paper ThB3.

[36] R.A. Griffin, A. C. Carter, "Optical differential Quadrature phase-shift key for high capacity optical transmission", OFC 2002, paper WX6.

[37] G. P. Agrawal, Applications of Nonlinear fiber optics, Academic Press

[38] B. H. Berbeek, et al, "Integrated four channel Mach Zehnder multi demultiplexer fabricated with phosphorous doped SiO2 waveguide in Si", Journal of Lightwave Technology, 1988, Vol 6, No. 6 pp1011-1015.

[39] V. Marembert, C. Schubert, S. Ferber, K. Schulze, C. Schmidt, C. Boerner, M. Kroh, S. Watanabe, F. Futami, R. Okabe and H. G. Weber, "Single/channel 640 Gbits DPSK Transmission over 160 km fiber link," ECOC 2004, Paper Th4.4.2

[40] A. Suzuki, X. Wang, Y. Ogawa and S. Nakamura, "10x320Gb/s (3.2Tb/s) WDM/OTDM transmission in C-band by semiconductor-based devices," ECOC Paper Th4.1.7.

[41] B. Mikkelsen, G. Raybon, R. J. Essambre, A. J. Stentz, T. N. Nielsen, D.W. Pechham, L. Hsu, L. Gruner-Nielsen, K. Dreyer, J. E. Johnson, "320 Gb/s single channel pseudolinear transmission over 200 km of Nonzero-dispersion fiber," IEEE Photonics Technology Letters, Vol.12, No.10, October, 2000, pp. 1400-1402.

[42] G. Lehmann, W. Schairer, H. Rohde, E. Sikora, Y. R. Zhou, A. lord, D. Payne, J. P. Turkiewicz, E. Tangdiongga, G. D. Khoe, and H.de Waardt, "160 Gb/s OTDM Transmission field trial over 550 km of legacy SSMF", ECOC 2003, Paper We1.5.2.

[43] J. L. Auge, M. Cavallari, M. Jones, P. Kean, D. Watley and A. Hadjifotiou, "Single channel 160 Gbs OTDM propagation over 480 km of standard fiber using a 40 GHz semiconductor mode-locked laser pulse source," OFC 2002, Paper TuA3.

[44] R. Ludwig, S. Ferber, C. Boerner, C. Schubert, C. Schmidt, J. Berger, M. Kroh, E. Hilliger V. Marembert and H. G. Weber,

"160 Gbits DPSK Transmission System with High Long-Term Stability," OECC 2004, Paper 14C4-2.

[45] Sebastian Randel, Beate konrad, Anes Hodzic and klaus Petermann, "Comparison of Modulation Format for DWDM Transmission of 160 Gbut/s OTDM-Channel with Spectral Efficiency of 0.8 bit/s/Hz," ECOC 2003, paper Mo4.2.6.

[46] D. Dahan, G. Eisenstein, "Numerical Comparison Between Distributed and Discrete Amplification in a Point-to-Point 40-Gb/s 40-WDM-Based Transmission System With Three Different Modulation Formats," Journal of Lightwave Technology, vol. 20, march, 2002, pp. 379-388.

[47] R. Hainberger, T. Hoshida, T. Terahara, H. Onaka, "Comparison of Span Configurations of Raman-Amplified Dispersion-Managed Fibers", IEEE Photon. Technol. Lett., vol. 14, pp. 471-473, April 2002.

[48] A. Hodzic, B. Konrad, K. Petermann, "Alternative Modulation Formats in N×40 Gb/s WDm Standard Fiber RZ-Transmission Systems," Journal of Lightwave Technology, vol. 20, April, 2002, pp.598-607.

[49] B. Zhu, L. Nelson, L. Leng, S. Stulz, M. Pedersen and D. Peckham, "Transmission of 1.6 Tb/s (40×42.7Gb/s) Over Transoceanic Distance with Terrestrial 100-km Amplifier Spans", in Tech. Dig. Opt. Fiber Commun. Conf., OFC'03, paper FN2, 2003.

[50] B. Mikkelsen, G. Raybon, B. Zhu, R.J. Essiambre, P.G. Bernasconi, K. Dreyer, L. W. Stulz and S.N. Knudsen, "High spectral efficiency (0.53 bit/s/Hz) WDM transmission of 160 Gb/s per wavelength over 400 km of fiber", in Tech. Dig. Opt. Fiber Commun. Conf., OFC'01, paper ThF2, 2001.

[51] B. Cuenot, "Comparison of Engineering Scenarios for N×160 Gb/s WDM Transmission Systems", IEEE Photon. Technol. Lett., vol 15, pp. 864-866, June 2002.

[52] M. Vasilyev,"Raman-Assisted Transmission: Toward Ideal Distributed Amplification", in Tech. Dig. Opt. Fiber Commun. Conf., OFC'03, paper WB1, 2003.

[53] A. Kobyakov, M.Vasilyev and A. Evans, "Performance Analysis of Raman Amplifiers Based on Dispersion-Managed Fibers", in Tech. Dig. Opt. Fiber Commun. Conf., OFC'03, paper WB2, 2003.

[54] H. Kidorf, K. Rottwitt, M. Nissov, M. Ma, E. Rabarijaona, "Pump interaction in a 100-nm bandwidth Raman amplifier", IEEE Photon. Technol. Lett., vol. 11, pp. 530-532.

[55] A. Gnauck, et al, "40-Gb/s RZ-Differential phase shift keyed transmission", OFC 2003, paper ThE1.

[56] B. Zhu, et al, "6.4-Tb/s(160×42.7 Gb/s) transmission with 0.8 bit/s/Hz spectral efficiency over 32×100 km of fiber using CSRZ-DPSK format", OFC 2003, paper PD19-1.

[57] A. H. Gnauck, et al, "1-Tb/s(6×170.6 Gb/s) transmission over 2000 km NZDF using OTDM and RZ-DPSK format", IEEE Photonics Technology Letters. 15, 1618-1620 (2003).

[58] Lothar Moller, Yikai Su, Chongjin Xie, Ronald Ryf, Christopher R. Doerr, Xiang Liu and Larry L. Buhl, "Generation of a 160 Gbs RZ-DPSK signal and its detection with a one-bit mach-Zehnder interferometer," ECOC 2004, Paper Th4.4.6.

[59] L. Moller, Y. Su, X. Liu, J. Leuthold, C. Xie, "Generation of 160 Gb/s Carrier-Suppressed Return-to-Zero Signals" ECOC 2003, paper Mo3.6.3.

[60] O. Vassilieva, et al, "Non-linear tolerant and spectral efficient 86 Bb/s RZ-DQPSK format for a system upgrade", ThE7, OFC 2003.

[61] B. Konrad, K. Petermann, "Optimum fiber dispersion in high-speed TDM systems", IEEE Photonics Technology Letters, Vol. 13, No. 4, April. 2001, pp. 299-301.

[62] Beate Konrad, Anes Hodzic, Klaus Petermann, “Dispersion compensation schemes for 160 Gb/s TDM-transmission over SSMF and NZDSF,” ECOC 01, paper Tu.L.2.4.

[63] B. Mikkelsen et al.: "160Gbit/s single-channel transmission over 300km nonzero-dispersion fiber with semiconductor based transmitter and demultiplexer", ECOC`1999, Nice, France, PDP2-3.

[64] R. Ludwig et al.: "Unrepeatered 160Gbit/s RZ single-channel transmission over 160km of standard fibre at 1.55um with hybrid MZI optical DEMUX", ECOC`2000, Munich, Germany, Tu 6.1.3

[65] U. Feiste et al.: "160Gbit/s transmission over 116 km field-installed fiber using 160Gbit/s OTDM and 40Gbit/s ETDM", OFC`2001, Anaheim, CA, USA, ThF3.

[66] H. Murai, M. Kagawa, H. Tsuji, K. Fujii, et al, “Single channel 160 Gbit/s 300km transmission using EA modulator based-OTDM module and 40 GHz external-cavity-mode-locked LD” ECOC 2002, paper 2.1.4.

[67] J. Yu et al.: "160Gbit/s single-channel un-repeatered transmission over 200km of non-zero dispersion shifted fiber", ECOC`2001, Amsterdam, Netherlands, PDP.M.1

[68] E. Lach et al.: "Advanced 160Gbit/s OTDM system based on wavelength transparent 4x40Gbit/s ETDM transmitters and receivers", OFC`2002, Anaheim, CA, USA, TuA2

[69] S. Ferber, R. Ludwig, C. Boerner, A. Wietfeld, B. Schmauss, J. Berger, C. Schubert, G. Unterboersch, H.G. Weber: "Comparison of DPSK and OOK modulation format in 160 Gbit/s transmission system", El. Lett. 39, pp. 1458-1459 (2003)

[70] S. Kawanishi et al. "3Tbit/s (160Gbit/s x19channel) optical TDM and WDM transmissionexperiment", Electr. Lett. 35, 826-827, 1999

[71] B. Mikkelsen et al.: "High spectral efficiency (0.53bit/s/Hz) WDM transmission of 160Gbit/s per wavelength over 400km of fiber", OFC`2001, Anaheim, CA, USA, ThF2-1

[72] A.H. Gnauck, G. Raybon, P.G. Bernasconi, J. Leuthold, C.R. Doerr, L.W. Stulz: "1Tb/s (6 X 170,6Gb/s) transmission over 2000 km NZDF using OTDM and RZ-DPSK Format", Photon. Techn. Lett. 15, pp. 1618-1620 (2003)

[73] M. Schmidt, M. Witte,F. Buchalim, E. Lach, E. Le Rouzic, S. Salaun, S. Vorbeck and R. Leppla, "8*170 Gb/s DWDM field transmission experiment over 430 km SSMF using adaptive PMD compensation," ECOC 2003 Paper Mo3.6.5

[74] M. Daikoku, T. Otani, M. Suzuki, "160 Gb/s four WDM quasi-linear transmission over 225 km NZ-DSF with 75 km spacing," IEEE Photonics Technology Letters, Vol.15, No.8, August, 2003, pp. 1165-1167.

[75] R. Leppla, S. Vorbeck, M. Schmidt, M. Witte, E. Buchali and E. Lach, "PMD tolerance of 8*170 Gbit/s field transmission experiment over 430 km SSMF with and without PMDC", OFC 2005, paper OFF2.

[76] B. Cuenot, "Comparison of engineering scenarios for N*160 Gb/s WDM transmission systems," IEEE Photonics Technology Letters, Vol. 15, No. 6, June 2003, pp. 864-866.

[77] A. Hodzic, B. Konrad, S. Randel, K. Petermann, "Performance comparison of 4N×40 Gb/s and N×160 Gb/s transmission systems," ECOC 2002, paper P3.24.

[78] Y. Zhu, K. Cordina, R. Feced, H. Kee, R. Rickard and A. Hadjifotiou,"1.6 bit/s/Hz orthogonally polarized CSRZ-DQPSK transmission of 8×40 Gbit/s over 320 km NZDSF," in Proc. OFC 2004, Los Angels, CA, paper TuF1.

[79] A.Hirano et al. "Novel modulation formats in ultra-high-speed optical transmission systems, and their applications", OFC 2004, paper ThM1.

[80] B. Zhu, "Ultra high density and long haul transmissions," in Proc. OFC 2004, Los Angels, CA, paper ThE1.

[81] C. Xu, X. Liu, L. F. Mollenauer, X. Wei, "Comparison of Return-to-Zero Differential Phase-Shift Keying and ON-OFF Keying in Long-Haul Dispersion Managed Transmission," IEEE Photon. Technol. Lett., vol. 15, pp. 617-619, Apr., 2003.

[82] A. Hodzic, B. Konrad, K. Petermann, "Alternative Modulation Formats in N×40 Gbit/s WDM Standard Fiber RZ-Transmission Systems," J. Lightwave Technol., vol. 20, pp.598-607, Apr., 2002.

[83] R. Ludwig, et al. "160 Gbit/s DPSK-Transmission–Technologies and System Impact", ECOC 2004, paper Symposium Tu1.1.3.

[84] Z. Xu, K. Rottwitt, C. Peucheret, P. Jeppesen, "Optimization of Pumping Schemes for 160-Gbit/s Single-Channel Raman Amplified Systems," IEEE Photon. Technol. Lett., vol. 16, pp. 329-331, Jan. 2004.

[85] S. Randel, B. Konrad, A. Hodzic, K. Petermann, "Comparison of Modulation Format for DWDM Transmission of 160 Gbit/s OTDM-Channel with Spectral Efficiency of 0.8 bit/s/Hz," in Proc ECOC 2003, Rimini, Italy, paper Mo4.2.6.

[86] Chandra Chandrasekhar, Peter Winzer, "Modulation formats and receiver concepts for optical transmission systems," short course in Proc ECOC 2004, Stockholm, Sweden.

[87] Y. Frignac, et al. "Enhanced anakytical engineering rule for fast optimizatoin of disperson map in 40 Gbit/s based transmsison systems", OFC 2004, paper TuN3.

[88] Y. Frignac, J. Antona, S. Bigo, J. Hamaide, "Numerical optimization of pre- and in–line dispersion compensation in dispersion-managed systems at 40 Gbit/s," OFC 2002, paper ThFF5.

[89] R. I. Killey, et al. “Reduction of intrachannel nonlinear distortion in 40 Gb/s based WDM transmisson over standard”, IEEE Photonics. Tech. Lett., Vol. 12, No. 12, Dec. 2000, pp. 1624-1626.

[90] Y. Frignac, H. Bissesur, P. Pecci, S. Bigo, “Dispersion management optimization for 160 Gbit/s transmission systems using RZ or CS-RZ modulation formats”, In Proc ECOC 2002, Copenhagen, Denmark, paper 6.1.6.

[91] Peter J. Winzer, Rene-J. Essiambre and S. Chandrasekhar, “Dispersion-tolerance optical communication systems” ECOC 2004, Paper We2.4.1

[92] Cornelius Furst, Horst Wernz, Jorg-peter Elbers, and Christophe Glingener, “Dispersion tolerance of duobianry long-haul transmission at 10.7 Gb/s and 43 Gb/s with 50 GHz channel grid”, ECOC 2004, Paper We 2.4.2

[93] M. Vaa, E. A. Golovchenko, L. Rahman, G. Mohs, W. Patterson and A. Pilipetskii, “Dense WDM RZ-DPSK transmission over transoceanic distances without use of periodic dispersion management,” ECOC 2004, Paper Th3.5.6

[94] K. Mukasa, K. Imamura, T. Yagi, “Dispersion management line consisted of medial dispersion fiber,” ECOC 2004, Paper We3.3.3.

[95] S. Banerjee, A. Agarwal, D. F. Grosz, D. N. Maywar and A. P. Kung, “Doubly periodic dispersion maps for DWDM transmission at 10 Gb/s an 40 Gb/s,” ECOC 2004, Paper We4.P.096

[96] E. Corbel, G. Charlet, “Tolerance of DPSK formats to dispersion-management parameters in 43 Gb/s system over transatlantic distance,” ECOC 2004, Paper We2.4.5.

[97] P. Pecci, S. Lanne, Y. Frignac, J. Antona, G. Charlet, S. Bigo, “Tolerance to dispersion compensation parameters of six modulation formats in system operating at 43 Gbit/s,” ECOC 2003, paper We 3.5.5.

[98] A. Cauvin, et al, “Single–channel nonlinear impairments at various bit-rate in dispersion managed systems”, ECOC 2003, paper Mo4.2.4.